Spring 5-1-2018

Antimicrobial Materials via Thiol-ene Chemistry

Dahlia Amato
University of Southern Mississippi

ANTIMICROBIAL MATERIALS VIA THIOL-ENE CHEMISTRY

by

Dahlia Ningrum Amato

A Dissertation
Submitted to the Graduate School,
the College of Science and Technology
and the Department/ School of Polymer Science and Engineering
at The University of Southern Mississippi
in Partial Fulfillment of the Requirements
for the Degree of Doctor of Philosophy

Approved by:

Dr. Derek L. Patton, Committee Chair
Dr. Robson F. Storey
Dr. Sarah E. Morgan
Dr. Sergei I. Nazarenko
Dr. Dmitri V. Mavrodi

Dr. Derek L. Patton Committee Chair	Dr. Jeffrey S. Wiggins Department Chair	Dr. Karen S. Coats Dean of the Graduate School

May 2018

Published by the Graduate School

ABSTRACT

With the increasing prevalence of antimicrobial resistance, the escalation of opportunistic/pathogenic infections is a looming global crisis. To avoid the pitfalls of conventional antibiotics, this dissertation focuses on developing macromolecular solutions to develop novel antimicrobial materials based on essential oils (thymol, carvacrol, and aldehydes). It is well established that essential oil derivatives exhibit high potency towards a wide range of pathogenic microbes. The rapid photopolymerization kinetics, limited by-products, and homogeneous network formation afforded by thiol-ene photopolymerization are utilized to either encapsulate essential oil derivatives or convert them into monomers which can subsequently be incorporated into new antimicrobial materials with new structure-function relationships.

The first chapter of this dissertation outlines the need for alternatives to traditional antibiotics and the motivation for developing essential oil-based therapies. In the second chapter, the utilization of thiol-ene chemistry in the design of drug delivery and encapsulation are reviewed. The third chapter of this dissertation focus on the development of one-pot/solvent-free thiol-ene miniemulsion technique to synthesize thymol/carvacrol-loaded nanoparticles with high loading capacity (≈50% w/w), excellent encapsulation efficiencies (>95%), and potent antimicrobial activity. In the following chapters, new pro-antimicrobial networks via degradable acetals (PANDAs) were fabricated as a new paradigm for the sequestration and triggered release of volatile, antimicrobial aldehydes. PANDAs are crosslinked networks in which every crosslink junction contains a degradable acetal linkage. When PANDAs are exposed to neutral to acidic conditions (pH < 8), the PANDAs undergo surface erosion and exhibit sustained

aldehyde release from days to months. Chapter IV details the fabrication of PANDAs with a synthetic aldehyde, chlorobenzaldehyde, while chapter V emphases on the use of the plant-derived, p-anisaldehyde (an extract from star anise). In both chapters, the synthesis of PANDAs, thermal/mechanical properties, aldehyde release kinetics, as well as antimicrobial efficacy and cytotoxicity were elucidated.

ACKNOWLEDGMENTS

The completion of this dissertation could not have been possible without the help of the following individuals which whom I am forever grateful:

My advisor, Dr. Derek Patton, thank you for your mentorship, guidance, and your vote of confidence in me which have helped me to be a better researcher, writer, and mentor to others. Thank you for providing invaluable opportunities and support with research throughout my entire PhD.

My committee members, Dr. Storey, Dr. Morgan, Dr. Nazarenko and Dr. Mavrodi for their tremendous support in research, career, and life advice. I truly appreciate your commitment in my future and your constant motivation for me strive for greatness.

The Patton research group past and present: Dr. Jananee Narayanan, Dr. Emily Hoff, Dr. Li Xiong, Dr. Wei Guo, Dr. Brian Donovan, Dr. Yidan Guan, Douglas Amato, Cassandra Reese, Michelle Vekasy, and William Walker. Thank you for making the lab a fun place to be and thank you for all your feedback/help in research. To my undergraduates: Susan Walley, Blake Martin, Sarah Swilley, and Michael Sandoz – thank you for your hard work, patience, and positive attitude – your stability, accountability, and friendship helped me tremendously.

To my best lab partner and husband, Douglas Amato, thank you for your constant love, support, and laughter to get me through graduate school. Thank you for always believing in me and challenging me to be a better version of myself everyday.

DEDICATION

To my biggest supporter and mother, Mary Ellen Lewis, thank you for your constant love, encouragement, and support. You gave a 16 year-old a chance to pursue her dreams in the world. Thank you.

TABLE OF CONTENTS

LIST OF TABLES

LIST OF ILLUSTRATIONS

LIST OF SCHEMES

LIST OF ABBREVIATIONS

AFM	atomic force microscope
AMR	antimicrobial resistance
AIBN	azobisisobutyronitrile
$CDCl_3$	deuterated chloroform
DI	deionized
Ene	alkene
EO	essential oil
Et_3N	triethylamine
FTIR	fourier transform infrared spectroscopy
H_2O	water
mW	milliwatts
N_2	nitrogen
NH_2	amine
OCH_3	methoxy
OH	hydroxy
pH	potential hydrogen
r.t.	room temperature
SEM	scanning electron microscopy
SH	thiol
THF	tetrahydrofuran
TMS	trimethylsilane
USM	The University of Southern Mississippi

X	halogen or functional group
Yne	alkyne

CHAPTER I – ESSENTIAL OILS AS ANTIMICROBIAL AGENTS: CHALLENGES AND DESIGN STRATEGIES

1.1 Antimicrobial Resistance

With 700,000 annual deaths globally, antimicrobial resistance (AMR) – attributed in part to overuse and misuse of antibiotics in medicine and agriculture – is a global crisis that seriously threatens the sustainability of public health.[1] Without significant steps toward solving AMR, a recent review predicts 10 million deaths annually attributed to AMR in 2050.[1] AMR occurs when pathogenic microbes are able to survive and grow after exposure to antibiotics that would normally kill/inhibit their growth.[2] Infections caused by AMR strains are deadly, difficult to treat with common antibiotics, often require toxic/costly treatments, and create broader infection control problems (spreading infections globally).[3] Compounding the issue of AMR, over 23.5 million Americans are more susceptible to common infections due to weakened immune systems (i.e. elderly or patients with rheumatoid arthritis, HIV, organ transplants, etc.).[4] To mitigate the rapid rise of AMR and protect immunocompromised individuals, new antibiotics and new approaches to control the spread and evolution of AMR pathogens are required. Additionally, a conscious effort to reduce use of antibiotics in medicine and agriculture is critical. The continuous emergence of resistant pathogens, scarcity of new antimicrobial drug scaffolds in the pharmaceutical discovery pipeline, and public demand for antibiotic-free food production have led to growing interest in natural, plant-derived extracts, or essential oils, as alternatives and/or supplements to synthetic antibiotics.

1.2 Essential oils as antimicrobials

Essential oils (EOs) are complex mixtures of bioactive phytochemicals, including aldehydes, terpenes, terpenoids, and phenolics, that are known to exhibit broad spectrum antimicrobial activity and represent an attractive alternative to conventional antibiotics.[5-6] Most EO constituents are selective towards pathogenic bacteria without promoting resistance and the Food and Drug Administration has classified many EOs and individual constituents of EOs with Generally Regarded as Safe (GRAS) status.[3, 7-8] EOs have recently found applications as food preservatives[9], packaging additives[7], textile fragrances[10], pesticides[11], and therapeutic applications[12-13]. Additionally, EOs have been successfully used as an exceptionally potent treatment against biofilm forming bacteria *Pseudomonas aeruginosa* and *Staphylococcus aureus*.[14] EOs as an antimicrobial treatment exhibit fewer adverse effects, have higher patient tolerance, and are relatively inexpensive compared to traditional antibiotics.[3]

Studies have shown that EOs eradicate microbial populations by targeting inner-and-outer membranes, membrane proteins, and intracellular targets.[15] It is important to note that determining the mode of action for each EO constituent is not trivial. EO constituents have shown to affect multiple-connected pathways without specified targets.[15] To complicate matters further, different species of bacteria may exhibit different responses to each EO constituent. For a review of EO mechanisms of action and potential targets, we encourage reading comprehensive reviews by Hyldgaard[7], Burt[15], and Nazzaro[16].

1.3 Essential oil challenges

Despite historical interest in EOs, significant challenges for practical implementation of phytochemicals as antimicrobial agents stem from the hydrophobicity

(poor water solubility), volatility, and instability of many EO constituents.[17] Poor water solubility particularly limits the bioavailability of these compounds and significantly lowers biological and antimicrobial activity, whereas volatility is problematic for achieving sustained release and controlled delivery. Many strategies have been reported to sequester or encapsulate EOs within films or colloidal systems; however, these strategies often suffer deficiencies such as low loading, poor encapsulation efficiencies, necessity of organic processing solvents, and uncontrolled burst release profiles.[18 19] Encapsulation and controlled/sustained release of EO constituents could help to overcome these issues and lead to the wider use of these plant-derived antimicrobials in the food industry and agriculture.

1.4 Encapsulation and release of phytochemicals via the "polyactive" approach.

Many approaches have been reported to encapsulate hydrophobic EO constituents within polymer systems in attempt to address the challenges (poor solubility, volatility, oxidative instability, low bioavailability, uncontrolled delivery) associated with implementation of EOs as alternative antimicrobials.[20-21] Previous studies have shown that encapsulating EOs improves both their aqueous stability and increases their antimicrobial activity.[22 23] These approaches however, predominately focused on physical mixtures and non-covalent interactions resulting in low loading, poor encapsulation efficiency, and burst release profiles. Recent work in the area of polyactives offers a viable solution to these challenges. "Polyactives" refer to polymeric pro-drugs that undergo partial or complete degradation to release active therapeutic agents (e.g., anti-inflammatory, antioxidant, antibiotic).[24] Phytochemical-based polyactives, reported by Lee et al., released vanillin from a linear polyoxalate backbone for antioxidant

properties.[25-26] Similarly, Uhrich et al. demonstrated antioxidant and antimicrobial activities via the release of EDTA/phenolics (carvacrol, thymol, and eugenol)[27] and pinosylvin[28] from linear poly(anhydride esters). These few examples illustrate the ability to effectively sequester phytochemicals as biodegradable polyactives with high loading (50 – 100 wt %) and sustained, tunable release profiles.

1.5 Our approach

The work highlighted in this dissertation focuses on the encapsulation, sequestration, and release of antimicrobial EO derivatives from thiol-ene networks. The second chapter of this dissertation provides a detailed review of how thiol-ene chemistry has been harnessed to design novel encapsulation/delivery platforms of model hydrophobic compounds. The third chapter demonstrates the direct encapsulation of phenolic phytochemicals (carvacrol and thymol) within thiol-ene nanoparticles for sustained delivery. Chapters 4 and 5 present a new paradigm for sequestration and release of EOs within phytochemical-derived polymer systems – an approach that draws inspiration from well-established "pro-drug" and "pro-fragrance" strategies employed successfully in pharma and cosmetic industries.[29-30] We focus on the design of poly(thioether acetal) polymer networks in which aldehydes (e.g., anisaldehyde and chlorobenzaldehyde) are covalently incorporated into the polymer network via an acetal linkage – as an integral part of the polymer backbone. These materials serve as *pro-antimicrobial networks* (PANs) that release active antimicrobial aldehydes upon exposure to conditions conducive to acetal degradation (e.g., change in humidity/pH). The PAN approach enables high loading, highly efficient "encapsulation", solvent-free processing, and rational design of phytochemical release profiles.

CHAPTER II - UTILIZATION OF THIOL-ENE CHEMISTRY IN DRUG DELIVERY APPLICATIONS

2.1 Thiol-ene "click" coupling/polymerization reactions

Thiol-mediated polymerizations, including radical, base, and nucleophile catalyzed reactions, have emerged as valuable tools for the synthesis of a variety of functional materials.[31-35] The thiol-mediated reactions are attractive for developing therapeutic delivery platforms since the reactions proceed under facile reaction conditions (oxygen, water, and room temperature), possess rapid kinetics in high yield, do not require expensive or potentially toxic catalysts, and are highly tolerant toward a wide range of functional groups.[33] The use of thiol-mediated chemistries has enabled the formation of multiple therapeutic matrices exhibiting tunable release properties and triggered responses from external stimuli. In this introduction chapter, we will provide a brief overview of thiol-mediated reactions and their usage within controlled drug delivery – covering topics such as therapeutic encapsulation, prolonged release, and release of drugs from degradeable matrices.

2.1.1 Radical-mediated thiol-ene photopolymerization

The radical mediated thiol-ene reaction, which became popular after the pioneering work of Hoyle [36-38], Khan [39-40], and Bowman[41-43], is the reaction of a thiol across an electron rich alkene in the presence of a radical initiator (thermal, photo, or redox). Thiol-ene networks form via a free-radical step-growth polymerization of multifunctional thiols and enes – facilitated by a rapid, highly efficient chain-transfer reaction as depicted in Figure 2A**.** The initiating species is often generated via hydrogen abstraction between a thiol and an activated initiator. The generated thiol radical then

adds across the double bond of an ene monomer generating a β-thioether carbon-centered radical; the latter radical rapidly undergoes chain transfer with an additional thiol to regenerate the thiol radical species. Termination then occurs via various recombination reactions.[44] Typical thiols that are commonly encountered in radical mediated thiol-ene polymerizations include alkyl thiols, thiol propionates, thiol glycolates, and thiol phenols. For each thiol, electron rich terminal alkenes (vinyl ethers and allyl ethers) and strained alkenes (norbornene) react faster than electron defficient, internal, or substituted alkenes.[33] In drug delivery applications, the use of thiol-ene photopolymerization is particularly attractive as it offers readily available biocompatible monomers with tunable polymerization kinetics simply by controlling intensity or photoinitiator type. [45-46]

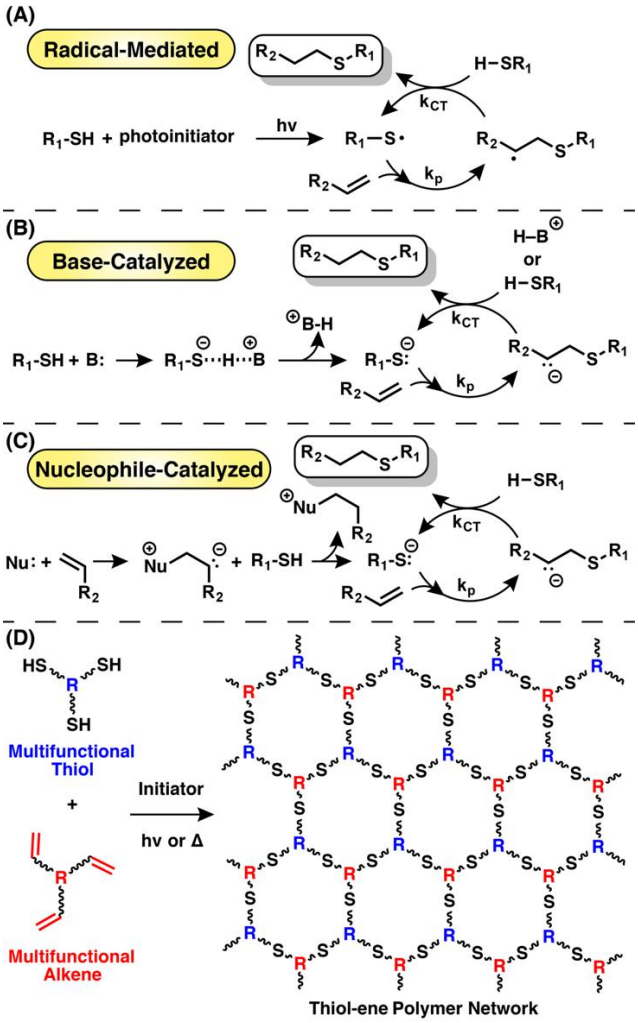

Figure 2.1 Different initiation mechanisms for thiol-ene reactions: (A) radical mediated, (B) base-catalyzed, and (C) nucleophile catalyzed.

2.1.2 Base and nucleophile-catalyzed thiol-ene polymerization

The base-catalyzed thiol-ene addition, or Michael addition, has found wide-spread utility as a mild reaction strategy in both organic and polymer "click" reactions owing to its high selectivity, rapid kinetics, and environmentally friendly reaction conditions (room temperature, oxygen/light tolerant, low catalyst levels).[47] Specifically, the base-catalyzed Michael addition is an 1,4 addition which starts by deprotonation of a thiol by a sterically hindered base (e.g. triethylamine) (Figure 2.1B). The thiolate ion attacks the β-carbon of

an α,β-unsaturated carbonyl/sulfonyl resulting in a negatively charged enolate intermediate, which undergoes chain transfer via the protonated catalyst or other thiol to continue the process. The benefits of the thiol-Michael addtion (as mentioned previously) have been exploited in the synthesis of click hydrogels for theraputic delivery under aqueous conditions.[48-49]

Unlike the base-catalyzed pathway, the nucleophile-catalyzed pathway involves direct reaction of a nucleophile (e.g. dimethylphenylphosphine) with an electron deficient alkene to generate a strong base (Figure 2.1C). The generated base abstracts a hydrogen from a thiol to form a thiolate anion which then follows the same addition and chain transfer reactions as described for the base-catalyzed mechanism. Due to the limited water solubility and high reactivity with metals and organic compounds, phosphine-catalyzed reactions have not been used in the fabrication of hydrogels for cell incapsulation or drug delivery. For a detailed description of the effect of different initiators/catalysts, a thorough review on the advancements on thiol-Michael additions was published recently by Bowman and coworkers.[47]

2.1.3 Thiol-ene step-growth vs. chain growth networks

Thiol-ene monomers can undergo either a step-growth polymerization mechanism or a combination of step and chain growth polymerization. While parameters such as initator type, cure intensity, and oxygen tolerance are critical for curing monomer, it is the monomer structure (e.g. functional groups) and polymerization mechanism which dictate the final macromolecular architecture of the three-dimensional polymer network. It has been well established that networks formed via chain growth polymerization are heteregeneous (with regions of high localized crosslink density – interspersed between

regions of low crosslink density) due to the formation of different kinetic chain lengths, cycles, and dangling chain ends (Figure 2.2A).[50] Importantly, the polymerization of multifunctional monomers such as acrylates, methacrylates, or styrenics, results in repeating -C–C- linkages along the backbone of the crosslinked network rendering the material nondegradable.[51] Cleaveable linkages (ester, anhydride, acetal, ketal, etc.) can be installed within the crosslinker to promote network degradation. Unfortunately, due to chain growth network formation, the cleavage of the degradable linkages often leads to long linear polymer fragments which may trigger an immune response.[52-56]

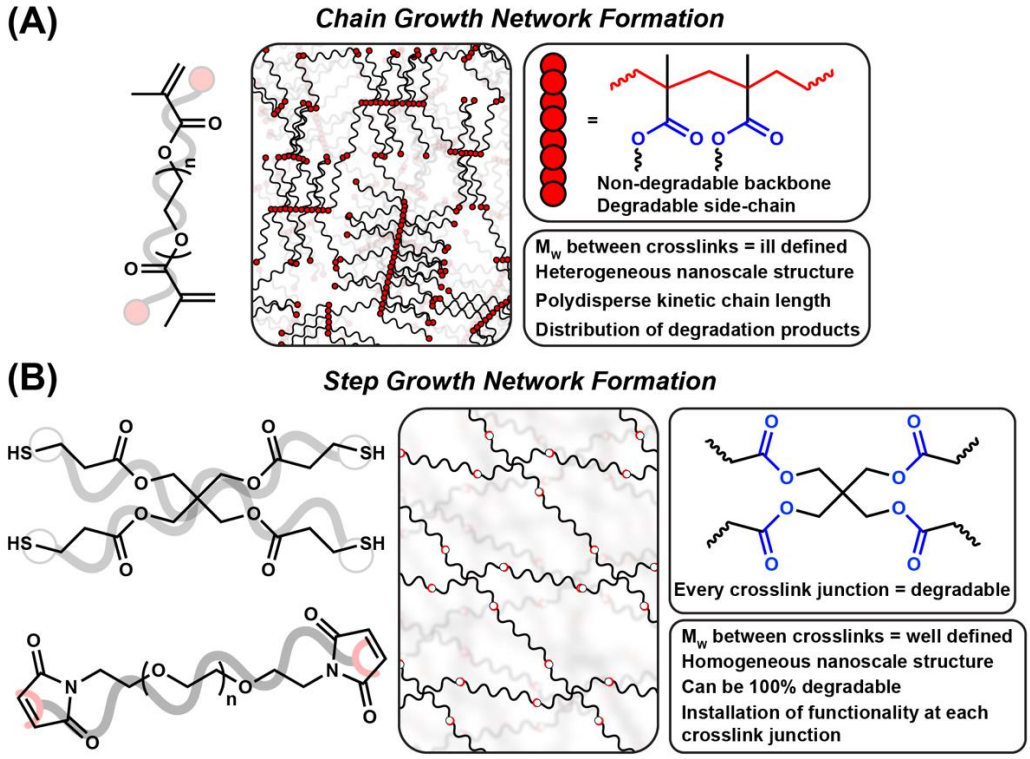

Figure 2.2 Differences between chain-growth (A) and step-growth (B) network formation.

Alternatively, step-growth polymerization provides a superior method for the formation of a homogeneous network. Multifunctional monomers (f > 2) with different functional groups react in a stepwise fashion to form a crosslinked network with well

defined molecular weight between each crosslink junction. The mechanism of step-growth polymerization ensures that any functionality (e.g. degradable linkages) in the monomer will be present within the crosslink junctions of the network (Figure 2.2B). For a step-growth network, exposure to a stimulus will trigger every crosslink junction to cleave allowing for complete network degradation into small molecule constituents as opposed to polymers/oligomers derived from chain-growth networks.

Specific to thiol-ene step-growth polymerizations, the alternating propagation and chain transfer events of the polymerization process proceed rapidly and build molecular weight in a uniform manner, but reach the gel-point only at relatively high functional group conversions yielding defect-free polymer networks.[57] The homogeneity of the network is typically reflected by a narrow glass transition occurring over a range of 30 – 50 °C. Recently, Kim et al. compared the degradation of acetal-based networks prepared via chain-growth (methacrylates) and step-growth (thiol-ene) polymerization.[58] Upon network hydrolysis, the methacrylate network remained intact (long linear polymer fragments did not degrade) while viscous flow was observed for the thiol-ene network due to complete degradation into small molecule byproducts.

2.1.4 Drug delivery design via thiol-ene chemistry

Incorporation of a drug within a polymeric matrix can be classified into one of two strategies: 1) traditional delivery, which relies on dispersing the drug within a degradable or non-degradable polymeric matrix; and 2) poly(actives), in which the drug is polymerized directly into the polymer backbone or covalently tethered to the backbone (pendent) via degradable linkages (Table 2.1). These delivery strategies offer different

release mechanisms, which can be governed by Fickian or non-Fickian diffusion, or a combination of both.

Table 2.1 Thiol-ene based drug delivery platforms (potential and existing).

Delivery platform	Release Parameters	Matrix Fate	References
Traditional delivery platforms			
Dispersed thermoplastic 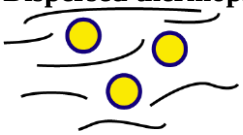	• Drug/polymer: crystallinity, solubility, and miscibility • Water permeability • Polymer MW and T_g	Non-degradable	No examples to date
Dispersed thermoset 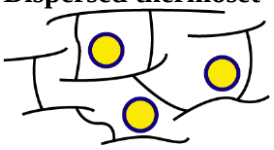	• Drug/polymer: crosslink density, solubility, miscibility • Water permeability • T_g	Non-degradable	Lignin[59], thio-ether ester[60]
Dispersed + degradable thermoplastic 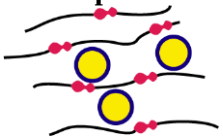	• Drug/polymer: crystallinity, solubility, miscibility • Water permeability • Polymer MW and T_g • Degradation rate of linker in the environment	Degradable	poly(thioether ester)[61-62]
Dispersed + degradable thermoset 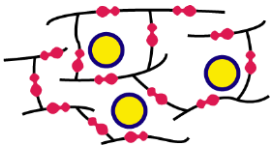	• Drug/polymer: crosslink density, solubility, miscibility • Water permeability • T_g • Degradation rate of linker in the environment	Degradable	Anhydrides[63-64], orthoester[65], chitosan-ester[66]
Poly(actives)			
Covalently attached thermoplastic (pendent) 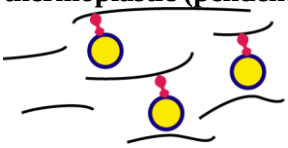	• Drug/polymer: crystallinity, solubility, miscibility • Water permeability • Polymer MW and T_g • Degradation rate of linker in the environment	Non-degradable	No examples to date

Covalently attached thermoplastic (main chain) 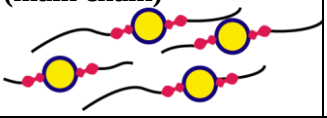	• Drug/polymer: crystallinity, solubility, miscibility • Water permeability • Polymer MW and T_g • Degradation rate of linker in the environment	Degradable	No examples to date
Covalently attached thermoset 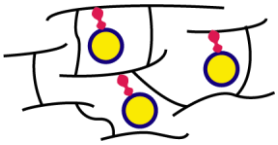	• Drug/polymer: crosslink density, solubility, miscibility • Water permeability • T_g • Degradation rate of linker in the environment	Non-degradable	Disulfides and esters,[67]
Active Networks 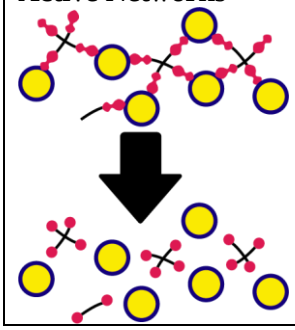	• Drug/polymer: crosslink density, solubility, miscibility • Water permeability • T_g • Degradation rate of linker in the environment	Degradable	acetals[68-69]

In designing effective drug delivery platforms for specific applications – monomer selection, polymerization kinetics, incorporation of degradable/non-degradable linkages, drug hydrophilicity/phobicity, crosslink density, crystallinity, glass transition temperature (T_g), reaction byproducts and relevant degradation stimuli should be carefully considered. In this section, we will discuss the advantages and disadvantages of each strategy, followed by examples of drug delivery utilizing thiol-ene chemistry.

2.1.5 Passive delivery

Passive delivery relies on physically mixing/encapsulation of the drug within either a non-degradable or degradable polymer matrix (thermoset and thermoplastic), which mitigates the need of drug modification and improves the biostability and bioavailability - especially for hydrophobic drugs. Polymeric matrices can be inert, in

which the matrix behaves as a membrane with constant drug release, or swellable, in which drug release is dependent on concentration gradients and degree of swellability.

2.1.5.1 Thermoplastics

Various non-degradable linear polymeric matrices such as poly(urethanes) and poly(dimethylsiloxanes) have been highlighted in the literature and have been widely used as drug-eluting medical implants; however, very few examples of drug eluting poly(thioethers) exist in literature.[61-62] In general, the release profile of drugs dispersed in thermoplastics can be controlled via polymer molecular weight, crystallinity, hydrophilicity/phobicity, swellability, and the presence/absence of degradable linkages.

Multiple papers have reported the synthesis of semicrystalline poly(thioethers) with tunable crystallinity through traditional emulsion polymerization techniques.[70-71] Additionally, direct incorporation of degradable esters and anhydrides have been demonstrated within semicrystalline poly(thioether) backbones.[72-74] These degradable linkages allow the polymer chains to be broken down into di-acids and di-alcohols under mild conditions. For instance, Cardosa et al. have directly polymerized a di-alkene anhydride (1,3-propylene diundec-10-enoate) with 1,4-butanedithiol to yield degradable linear poly(thioether) with number average molecular weights ranging from 5-20 kDa.[75] These semicrystalline polymers have a melting temperature around 70 °C and exhibited no observable cytotoxicity toward red blood cells even at 200 μg L^{-1}.

Recently, Araújo and coworkers developed a linear poly(thioether ester) platform[61-62] based on butanedithiol and a dialkene synthesized via an esterification reaction of 10-undecanoic acid with isosorbide. The monomers were polymerized via radical-initiated miniemulsion polymerization, resulting in semicrystalline polymers with

molecular weights ranging from 2-11 kDa.[62] Coumarin 6, a hydrophobic dye, was encapsulated during the emulsification process with up to 98% efficiency and served as a visual marker for cellular uptake. The nanoparticles displayed no observable cytotoxicity at concentrations ranging from 10-200 μg mL^{-1} and are good candidates for a biomedical nanomaterial. Araújo expanded this platform with the encapsulation of clove oil within the poly(thioether ester) miniemulsion process.[61] The nanoparticles obtained by miniemulsion polymerization were formulated with clove oil varying from 0 to 25% (w/w of monomer) with a ~98% encapsulation efficiency. The antioxidant, or radical scavenging properties of the nanoparticles with only 6% clove oil demonstrated potent antioxidant capabilities while preserving the bioactivity of the antioxidant rich clove oil constituents (e.g. eugenol). The ability to rapidly generate libraries of materials under facile reaction conditions necessitates future investigations into thiol-ene scaffolds as drug delivery matrices. While Cardosa and Araújo have highlighted the use of difunctional thiol and alkene monomers for direct preparation of linear poly(thioethers), additional studies are needed to translate the use of these polymers into clinical studies *in vivo*.

2.1.5.2 Thermosets

Tuning the degradation of and release from linear polymers remains a challenge as degradation/release rates are determined by manipulating coupled parameters such as drug/polymer crystallinity, drug/polymer molecular weight, polymer functionality, swellability, and drug/polymer hydropathy. Alternatively, crosslinked (thermoset) matrices offer unique opportunities to tailor the release of actives via manipulation of

defined parameters such as monomer functionality, crosslink density, monomer concentration, and monomer molecular weight.

Two of the most commonly used crosslinked thiol-ene based drug delivery designs are hydrophilic (e.g. hydrogels) [76] and hydrophobic (e.g. low molecular weight multifunctional thiols and alkenes) crosslinked networks[77]. In a recent review by Kloxin et al., the design parameters for tuning the drug release from thiol-ene based hydrogels, such as tuning mesh size and swellability, are discussed.[76] While hydrophilic networks primarily rely on swelling as a mechanism for drug release, hydrophobic thiol-ene networks depend on either the diffusivity of the drug through the matrix or degradation of cleavable linkages present within the backbone/side chain of the network.

2.1.5.2.1 Non-degradable thermosets

One key advantage to the direct encapsulation of drugs is that challenges such as hydrophobicity, volatility, and chemical instability can be easily overcome. Direct encapsulation via thiol-ene miniemulsion has recently been proven to be an effective encapsulation technique. Tong et al. used a miniemulsion to copolymerize an allyl-functionalized-lignin with a multifunctional thiol in the presence of a hydrophobic dye (to monitor release), hexadecane (hydrophobe), solvent, surfactant, and water (continuous phase).[59] The resulting nano-sized emulsions possessed high encapsulation efficiencies and were able to release 40% of the dye within 48 h at pH 7.4. These nanoparticles served as a primary example of utilizing materials found in nature for the controlled release of hydrophobic molecules such as drugs/dyes. Recently, Amato et al. demonstrated the direct sequestration of essential oil derivatives (carvacrol from oregano and thymol from thyme) into crosslinked poly(thioether) nanoparticles via miniemulsion

polymerization.[60] The nanoparticles were loaded with relatively high efficiencies (>90%) and exhibited a constant drug release (<5%) over a 24 h period. The necessity of a hydrophobic matrix was pronounced, as high loadings, long-term delivery, and high encapsulation efficiencies of essential oils could not be readily attainable within a hydrogel.

Additionally, Shi and coworkers synthesized micron-sized oil-in-water thiol-ene droplets for the sequestration of hydrophobic fragrance oils and dyes.[78] The process showed a remarkable encapsulation efficiency (91-96%), rapid polymerization kinetics (<45 minutes) and the resulting capsules were relatively shelf-stable at 45°C for at least one month. Heating the microcapsules to 100 °C pressurized the capsules, induced rupture of the membrane, and subsequently released the fragrance. Emulsion focused crosslinked thiol-ene platforms highlight the utilities of applying fast reaction kinetics to rapidly encapsulate – and eventually release – hydrophobic drugs. However, these emulsion-based delivery platforms are complicated due to the multiple additives used during polymerization which can affect the release profile as well as biocompatibility. Additionally, the previously mentioned studies have yet to systematically vary parameters such as crosslink density (mesh size and T_g,), network hydrophobicity, or drug solubility to control drug release and these parameters should be studied in the future.

2.1.5.2.2 Degradable Thermosets

One of the most well-characterized hydrophobic drug delivery systems obtained by thiol-ene polymerization is the poly(anhydride), which has been popularized by Shipp et al.[79] Photopolymerized poly(anhydride) thiol-ene networks have been shown to surface

erode as seen in other poly(anhydride) materials.[80-81] The erosion process is due to the rate of anhydride degradation being faster than water ingress into the hydrophobic polymer matrix. Aside from the rate of anhydride hydrolysis, two synergistic parameters work together to limit water ingress: 1) high crosslink density achieved from low molecular weight – multifunctional monomers; and 2) monomer hydrophobicity (e.g., absence of alcohols, amines, carboxylic acids, etc. typically found in hydrogels). It is a common phenomenon within thiol-ene networks that as molecular weight between crosslinks increases, the free volume, hole-size, and diffusivity of molecules through the network increase.[82] Additionally, reducing the number of hydrogen bond donors/acceptors within the polymer structure is known to limit the water uptake of the network and can therefore serve as another parameter to tune the release profile.

Regarding direct polymerization of degradable poly(anhydrides), Shipp and coworkers synthesized a library of linear and crosslinked drug-loaded poly(thioether anhydrides) with varying degrees of hydrophilicity, hydrophobicity, and crosslink density.[63] Shipp's work highlighted that increasing the amount of tetrafunctional crosslinker resulted in a delayed onset of degradation. Other work from Shipp and coworkers involved the direct encapsulation of lidocaine within thiol-ene poly(anhydride) networks of varying crosslink density.[64] Results from the study showed minimal differences in network degradation for networks prepared with 30, 20, and 10% crosslinker, indicating that erosion of the material plays a greater role in the release of lidocaine than drug diffusion out of the hydrophobic network.

The encapsulation and controlled release of other hydrophobic drugs, such as doxorubicin and paclitaxel, are paramount because of the associated high toxicity and

limited pharmacokinetics of the drugs. Tang and coworkers successfully entrapped doxorubicin within a hydrophobic/degradable crosslinked thiol-ene poly(orthoester) via reaction-induced nanoprecipitation.[65] During nanoprecipitation, doxorubicin was loaded into the nanogels with high drug loading efficiency greater than 70%. Release kinetics were performed at pH 7.4 and 5.0 to highlight the rapid degradation of the pH triggered hydrolysis of the orthoester. At pH 5.0, ~75% of doxorubicin was released within 24 h and at pH 7.4, ~15% was released. Cheng et al. also encapsulated doxorubicin via photopolymerization of N-maleoyl-functionalized chitosan and 1,4-butanediol bis(3mercaptopropionate) in miniemulsions.[66] The crosslinked emulsified particles exhibited a doxorubicin encapsulation efficiency and loading level ranging from 76-82% and 5.6-6.1%, respectively. To demonstrate a pH directed release, the doxorubicin-loaded nanoemulsions were subjected to pH 7.4 and 5.5 – leading to ~30-40% and 55-80% release, respectively, within 48 h. Additionally, the results from cellular uptake studies suggested that the doxorubicin-loaded nanoparticles can serve as an extended/controlled release delivery platform in which the particles slowly release doxorubicin outside cells (pH 7.4) and release doxorubicin at higher concentrations when internalized in endosomes/lysosomes (pH 4.5-6.5).

Other processing techniques, such as electrospinning, have also been used to encapsulate/release drugs from crosslinked thiol-ene networks. Heise et al.[83] UV-cured electrospun crosslinked fibers, with poly(globalide), difunctional thiols (crosslinkers), photoinitiators, and indomethacin (an anti-inflammatory drug). The fibers could swell in organic solvents, such as dichloromethane (DCM), without dissolving, and were able to be loaded either by direct incorporation of indomethacin into the resin or swelling neat

fibers in concentrated indomethacin/DCM solutions. They found that the direct incorporation method led to linear release, proportional to fiber degradation, whereas the solvent swelled methods added physiosorbed drug to the surface – causing unwanted burst release followed by gradual and sustained release.

2.1.5.2.3 Poly(active) thiol-ene materials

Poly(actives) are polymeric pro-drugs that undergo partial or complete degradation to release active therapeutic agents (e.g., anti-inflammatory, antioxidant, antibiotic).[84] Direct attachment of a drug to a poly(active) affords many unique advantages such as the alteration and control over the drug's hydropathy, propensity to crystallize, pharmacokinetics, dissolution/release rate, and potential cytotoxicity. The linker between the drug and polymer scaffold can either be cleavable (pH, enzymatic cleavage, temperature, electromagnet radiation, etc.) or highly stable (amides, ethers, thio-ethers, etc.). For systems containing cleavable linkages, the rate of drug release is governed by both the linker chemistry (linker type and hydropathy) and environmental conditions . Additionally, the hydropathy and crosslink density of the polymer network in crosslinked poly(actives) or crystallinity in linear poly(actives) will play a significant role in linker degradation for processes such as hydrolysis and enzymatic degradation. Unlike traditional hydrogels in which hydrolysis events are statistical throughout the gel, hydrophobic networks must rely on the diffusion of water from the outside of the material towards the center – leading to a gradient of hydrolysis events through the material.

Shen and coworkers synthesized a crosslinked poly[oligo(ethylene glycol)fumarate-codithiodiethanol fumarate] micelle with a covalently attached doxorubicin.[67] The system involved a hydrophobic fumarate, a PEG-diol, and a disulfide-

diol, which creates linear hydrophilic/phobic domains interspersed between disulfides and esters allowing for both pH and reduction triggered degradation. The degradable poly[oligo(ethylene glycol)fumarate-codithiodiethanol fumarate] was crosslinked in water via a one pot addition of doxorubicin-SH (synthesized with a hydrolysable hydrazone linkage) and a dithiol crosslinker. During crosslinking, the system self-assembles into a micelle in which the doxorubicin is covalently attached to the core at drug loading concentrations up to as high as 17.5 wt%. Importantly, when the crosslinked particles were placed into pH 7.4 water, only 5% of doxorubicin was released in 48 h, indicative of a high degree of covalent attachment of doxorubicin-SH during the crosslinking reaction. Under pH 7.4 and 10 mM dithiothreitol (a reducing environment to mimic the intracellular environment) only a 5% release of doxorubicin was observed. However, when the particles were subjected to pH 5.8 in the absence of dithiothreitol, ~50% of doxorubicin was released in 48 h. This behavior suggests that the environmental pH controls the rate of hydrazone hydrolysis of the doxorubicin linkage not the scaffold degradation. The combination of dithiothreitol and a pH 5.8 environment resulted in ~70% doxorubicin release and micelle disassociation. In this system, pH was the dominant factor in controlling doxorubicin release and serves as a model for how to design crosslinked-covalently linked poly(actives) for triggered release applications.

Recently, Amato et al. have published on the covalent ligation of two aldehydes, p-chlorobenzaldehyde[68] and p-anisaldehyde[69] into a poly(thioether acetal) network. Both examples relied on the conversion of the aldehyde into a difunctional alkene monomer, which was subsequently photopolymerized into a thiol-ene network. When the network was submerged into acidic environments, the networks rapidly degraded into small

molecule constituents (tetrafunctional alcohol and aldehyde). Similar to Shen's work[67], the rate of acetal hydrolysis controlled the rate of aldehyde released and 100% release occurred when the material completely dissolved into solution. Currently, few examples exist of covalent attachment of drugs into hydrophobic thiol-ene networks; however, unique opportunities exist in high performance sustained release systems in which permanence is not a requirement.

2.1.6 Conclusion

Remarkable progress has been made in the design and characterization of controlled drug-releasing materials prepared via thiol-ene chemistry. Many examples presented in this introduction chapter have shown great promise in the delivery of model hydrophobic drugs; these systems provide formulations for the delivery of application specific cargo moving forward. However, multiple opportunities to tailor drug release within well-defined thiol-ene networks remain unexplored, including monomer design, crosslinker design, monomer functionality, crosslink density, hydrophobicity, and thermal mechanical properties. Additionally, precise control over the release of hydrophobic drugs from thiol-ene matrices remains a constant challenge that needs to be addressed. Finally, the remarkable functional group tolerance and plug-in-play nature of the thiol-ene monomers can lead to new fundamental network structure-drug release relationships within crosslinked hydrophobic thiol-ene networks.

CHAPTER III - DESTRUCTION OF OPPORTUNISTIC PATHOGENS VIA POLYMER NANOPARTICLE-MEDIATED RELEASE OF PLANT-BASED ANTIMICROBIAL PAYLOADS

3.1 Abstract

We report the synthesis of antimicrobial thymol/carvacrol-loaded polythioether nanoparticles (NPs) *via* a one-pot, solvent-free miniemulsion thiol-ene photopolymerization process. The active antimicrobial agents, thymol and carvacrol, were employed as "solvents" for the thiol-ene monomer phase in the miniemulsion to enable facile high capacity loading (~50% w/w), excellent encapsulation efficiencies (> 95%), and elimination of all postpolymerization purification processes. The NPs serve as high capacity reservoirs for slow-release and delivery of thymol/carvacrol-combination payloads that exhibit inhibitory and bactericidal activity (> 99.9% kill efficiency at 24h) against gram-positive and gram-negative bacteria, including both saprophytic (*Bacillus subtilis* ATCC 6633 and *Escherichia coli* ATCC 25922) and pathogenic species (*E. coli* ATCC 43895, *Staphylococcus aureus* RN6390, and *Burkholderia cenocepacia* K56-2). This report is among the first to demonstrate antimicrobial efficacy of essential oil-loaded nanoparticles against *B. cenocepacia* – an innately resistant opportunistic pathogen commonly associated with debilitating respiratory infections in cystic fibrosis. Although a model platform, these results point to promising pathways to particle-based delivery of plant-derived extracts for a range of antimicrobial applications, including active packaging materials, topical antiseptics, and innovative therapeutics.

3.2 Introduction

Microbial threats, particularly multidrug-resistant (MDR) bacterial strains and other emerging pathogens, are greatly impacting public health, burdening healthcare systems, and have potential to disrupt socioeconomic infrastructures in both developing and industrialized nations. In the United States alone, the Center for Disease Control estimates at least two million illnesses and 23,000 deaths are attributed to multidrug-resistant bacterial infections each year. Annually, these cases account for approximately $20 billion in excess health care costs and up to $35 billion in lost productivity due to sick leave and hospitalizations.[85] While *Staphylococcus aureus* and *Pseudomonas aeruginosa* tend to dominate the MDR discussion, other microorganisms, such as *Burkholderia cepacia* complex (Bcc), have emerged as opportunistic pathogens with significant clinical importance in persons with cystic fibrosis (CF).[86] Pulmonary colonization with *Burkholderia cenocepacia*, the most common isolate of the 18 member Bcc, results in severe respiratory infections in persons with CF and is associated with high morbidity and mortality rates.[87] Effective treatments for *B. cenocepacia* infections are rare, as these bacteria exhibit high intrinsic resistance to most antibiotics.[88] In general, the MDR microbial threat extends far beyond the effect on humans, and additionally impacts animal agriculture and veterinary medicine. The continuous emergence of MDR pathogens and scarcity of new antimicrobial drug scaffolds in the pharmaceutical discovery pipeline have led to growing interest in natural, plant-derived extracts as alternatives to synthetic antibiotics.[21] In this direction, essential oils (EOs) – typically complex extracts from aromatic plants comprising mixtures of aldehydes, terpenes and phenols – are well known to exhibit broad spectrum biological and antimicrobial activity.[89-90] With many EOs identified as "Generally Regarded as Safe"

(GRAS), these extracts have been actively explored and continue to garner interest as food preservatives and packaging constituents,[91-92] textile fragrances,[93] pesticides,[94] and other antimicrobial therapeutic applications.[12, 27, 95]

Monoterpene phenol isomers, carvacrol and thymol, are major constituents of EOs extracted from oregano, thyme, and other plants belonging to the *Lamiaceae* family. These isomers show antiviral, antifungal, and broad spectrum antibacterial properties against both gram-negative and gram-positive bacteria, including MDR and biofilm forming microorganisms.[96-97] In one promising example, EO extracts containing carvacrol and thymol as primary constituents were shown to inhibit the growth of several environmental and clinical bacterial strains belonging to the *B. cepacia* complex.[98] The broad spectrum of activity of these isomers has been attributed to multiple modes of toxicity; however, the primary site of toxicity is the cell membrane.[97] In general, these hydrophobic isomers act by partitioning into the cytoplasmic membrane leading to increased permeability, depletion of proton gradients, and subsequent disruption of adenosine triphosphate (ATP) synthesis. The collapse of the proton motive force and depletion of the ATP pool eventually lead to cell death.

A major challenge for the practical application of carvacrol and thymol as antimicrobial agents stems from the hydrophobicity (poor water solubility), volatility, and instability of these EO constituents. Poor water solubility, in particular, limits the bioavailability of these compounds and significantly lowers their biological and antimicrobial activity, whereas volatility is problematic for achieving sustained release and controlled delivery. To address these challenges, a variety of approaches have been reported to encapsulate hydrophobic EO constituents as colloidal systems, including oil-

in-water emulsions, microemulsions, and nanoemulsions; molecular inclusion complexes; lipid-based carriers (e.g. liposomes and solid lipid nanocapsules);[99] and polymer-based carriers (e.g. films, micro/nanocapsules, and nanoparticles).[20-21, 100] Polymer nanoparticles (PNPs) are advantageous in that they offer a highly flexible delivery platform for antimicrobial applications, where nanoparticle properties (e.g. morphology, bulk/surface composition, and size) are readily tunable using a variety of synthetic approaches.[101-104] In turn, these tunable PNP properties dictate important features such as particle stability, surface interactions, and EO loading and release kinetics. In this direction, researchers have successfully incorporated carvacrol, thymol, and other phenolic EO constituents into various PNP matrices (chitosan,[105] poly(lactide-co-glycolide)[23, 106], methylcellulose,[107] and zein[108]) *via* emulsification-evaporation,[23, 106] emulsification-solvent exchange,[107] and nanoprecipitation[108] methods. While these examples demonstrate facile fabrication, encapsulation, and exhibit antimicrobial activity, many suffer several deficiencies such as low EO loading (i.e. 3% w/w carvacrol in chitosan matrix), poor EO encapsulation efficiencies (e.g. 14 – 31% carvacrol-in-water emulsion and ionic gelation of chitosan),[109] use of organic solvents during encapsulation (acetone, ethanol, dichloromethane),[23, 108] and burst release profiles of EO.[23, 106]

Miniemulsion polymerization is ideally suited for encapsulation of hydrophobic payloads (e.g. lipophilic drugs, pigments, fragrances, inorganic nanomaterials, and polymers) with high loading and encapsulation efficiencies,[110-112] but has received little attention for sequestration and delivery of essential oils – particularly towards antimicrobial applications. Miniemulsion polymerizations are described as aqueous dispersions of small, narrowly distributed monomer droplets stabilized against Ostwald

ripening and collisional degradation by addition of an appropriate surfactant and costabilizer. Monomer droplets ranging in size from 50-500 nm are attained *via* high shear mixing – typically either high-pressure homogenization or ultrasonic processing – and subsequently serve as discrete nanoreactors for the formation of polymer nanoparticles upon polymerization. Since mass transport between monomer droplets is suppressed, encapsulation of hydrophobic materials requires a straightforward addition of the desired material to the organic phase prior to shear mixing. Thus, encapsulation of materials miscible with the monomer phase provides polymer nanoparticles with the payload dispersed throughout the polymer matrix (whereas immiscible materials provide a route to nanocapsules).[112] Recently, we and others have reported thiol-ene[113-116] and thiol-alkyne[117-118] polymerization in miniemulsion as a facile platform for the synthesis of crosslinked polythioether nanoparticles with tunable particle sizes, tailorable network properties, and clickable surface functionality. More importantly, we demonstrated the ability to encapsulate hydrophobic inorganic nanoparticles within the polythioether matrix with high efficiency without sacrificing the rapid polymerization kinetics and high conversions provided by the thiol-mediated photopolymerization process.

Herein, we report a facile, one-pot approach to encapsulate monoterpene phenols (carvacrol/thymol) within polythioether nanoparticles as a model, sustained-release antimicrobial platform. We employ thiol-ene photopolymerization in miniemulsion for rapid nanoparticle synthesis, where carvacrol and thymol serve as miscible compatibilizers in the monomer phase enabling solvent-free encapsulation with high loading capacities (33-66% w/w, EO relative to the NP) and excellent encapsulation efficiencies (> 95%). The absence of solvent and use of a polymerizable surfactant

eliminate the need for any post-polymerization purification steps. Release studies reveal the polythioether nanoparticles function as sustained-release reservoirs for carvacrol/thymol – discharging less than 4% of the payload over 24 h. The thymol/carvacrol-loaded (TC_{NPs}) nanoparticles show effective antimicrobial activity (> 99.9% kill efficiency at 24h) against gram-positive (*Bacillus subtilis* and *Staphylococcus aureus*) and gram-negative (*Escherichia coli* and *Burkholderia cenocepacia*) bacteria. Considering the innate resistance of the bacterial strain, the high efficacy of TC_{NPs} against *Burkholderia cenocepacia* is particularly significant, and to our knowledge, represents the first demonstration of antibacterial efficacy against *B. cenocepacia* using thymol/carvacrol-loaded polymer nanoparticles.

3.3 Experimental

3.3.1 Materials

Glycol di(3-mercaptopropionate) (GDMP) and pentaerythritol tetra(3-mercaptopropionate) (PETMP) were provided by Bruno Bock. Hexadecane, ethyl acetate, sodium chloride and thymol were obtained from Fisher Scientific. Diallyl phthalate (DAP), 4-methoxy phenol (MEHQ), and butyl acetate were acquired from Sigma Aldrich. Other reagents were purchased from the following vendors: 1-hydroxycyclohexyl phenyl ketone (Irgacure 184) from CIBA; Hitenol BC-20 from Montello, Inc.; carvacrol from TCI America. Difco Agar, Mueller Hinton II agar (MHA), Mueller Hinton II broth (MHB), and Bacto Tryptone were from Becton, Dickinson and Company. All the materials were obtained at the highest purity available and used without further purification unless otherwise specified.

3.3.2 Characterization Methods.

The size and distribution of the nanoparticles (NPs) were measured by dynamic light scattering (DLS) using a Microtrac Nanotrac Ultra NPA150 particle analyzer. Particle size and distribution were obtained using the Microtrac Flex software (v.10.6.1), which employs non-negatively constrained least-squares (NNLS) and cumulants analysis to obtain the intensity-weighted "z-average" mean particle size as the first cumulant, and the polydispersity index from the second cumulant.[119] Transmission electron micrographs were taken with a Zeiss 900 electron microscope operating at 50 kV and outfitted with a Model 785 Erlangshen ES1000W CCD camera (Gatan). Samples were applied to 200 mesh copper grids (3.05 mm, 200 lines per inch square mesh, EMS) coated with Formvar (5% polyvinyl formal resin). Proton (^{1}H) NMR was recorded on a Bruker Acend™ 600 MHz spectrometer at 30°C in D_2O, using 128 scans and a 4.27 s relaxation delay. Optical density (OD) and fluorescence readings were performed in a BioTek Synergy 2 programmable microplate reader. Confocal images were taken using a Zeiss LSM 510 confocal laser scanning microscope. High-resolution field emission SEM (FE-SEM) was performed with a Zeiss SIGMA variable pressure field emission scanning electron Microscope operating at 10 kV in high vacuum mode. Samples were sputter coated with silver at instrument reported thickness of 5 nm with a Quorum Emitech K550X sputter coater. Raman spectra were acquired using a high-performance portable Raman spectrometer (i-Raman Plus, B&W Tek Inc., Delaware, USA). The samples were analyzed at 100 mW, with a 785 nm diode laser and 150 s accumulation time.

3.3.3 *General nanoparticle sample preparation*.

Each nanoparticle reaction was prepared in a 20 mL scintillation vial with a total volume of 10 mL. The organic stock solutions shown in Table A.1 were added into a vial

containing a stock solution of 70 mM Hitenol BC 20 and deionized water. As we previously reported, MEHQ serves as a radical inhibitor to suppress thermal polymerization during ultrasonication.[113] The samples were placed into an ice bath and sonicated using a Qsonica Q700 probe ultrasonicator at 25% amplitude for 25 min. The resultant miniemulsions were cured for 15 min at intensity of 185 mW cm^{-2} using an OmniCure S1000 UV light source with a 100W mercury lamp (λ_{max} = 365 nm, 320–500 nm filter). All samples were made in triplicate to ensure data reproducibility.

3.3.4 Preparation of essential oil encapsulated nanoparticles.

Carvacrol encapsulated nanoparticles were prepared by replacing butyl acetate with 33% w/w carvacrol as the solvent. For nanoparticles containing a combination of thymol and carvacrol, 20% w/w thymol was added along with 27% w/w carvacrol. The total organic fraction evaluated was 4.5% w/w for all samples.

3.3.5 Determination of nanoparticle number density (particles/mL)

$$V_{total} = \text{organic added} \quad (1)$$

Where organic added is a known volume that can be converted into cubic nanometers.

$$V_{sphere} = \frac{4}{3}\pi(r)^3 \quad (2)$$

Where *r,* is the radius (nm) determined from light scattering.

$$\frac{V_{total}}{V_{sphere}} = \#\ particles \quad (3)$$

The final *# of particles* is determined by dividing the total volume of organic by the volume of the average nanoparticle size (see Table A.2). This number results in

particles/10 mL (10 mL is the total volume of the emulsified solution), multiplication of volume added by this number results in # of particles delivered.

3.3.6 Gas chromatography-mass spectrometry (GC-MS) release study of essentials oil nanoparticles.

Freshly prepared C_{NPs} and TC_{NPs} were transferred into 100 mL volumetric flasks and diluted 1:10 with deionized water. For each diluted suspension, 10-mL aliquots were removed at 0, 4, 8, 12, and 24 h, and NPs were precipitated for 4 h at 40,000 rpm (4°C) in a Beckman Coulter Optima XE ultracentrifuge. 200 µL of the supernatant were removed and extracted by vortexing for 30 s with 800 µL of ethyl acetate. The liquid phases were separated by centrifugation for 15 min at 13,000 rpm, and the organic layer was transferred to a capped 1.5 mL GC-MS vial. To determine the amounts of EOs in the pre-emulsified organic monomer mixture, 450 µL of organic stock solution (carvacrol and combo) was diluted 1:100 in ethyl acetate. All samples were placed into capped GC-MS vials and run using the following protocol.

GC-MS analysis was performed on an Agilent 6890 GC/MSD equipped with an auto sampler and a Restek RTx-1 30 meter column. All samples and standards were analyzed from 1 µL injection volumes. Analysis parameters include an inlet temperature of 200 °C in splitless mode and a helium flow rate of 30 ml/min in gas saver mode. Thermal ramping conditions used include an initial hold at 45 °C for 4 min followed by an increase in temperature at 25 °C/ min. up to 140 °C with a 3 min hold at 140°C. The temperature ramp continued at 2.5 °C/ min up to 150 °C with a 3 min hold followed by a final increase at 50 °C/min to 220 °C with a 7.00 min hold (Figure A8). The method provided unique separation of thymol and carvacrol isomers eluting at 19.41 and 19.58

min respectively (Figure A9). Calibration curves for both isomers were prepared in ethyl acetate at 0, 200, 400, 600, 800 and 1,000 ng μL^{-1} (Figure A10). A representative chromatogram of extracted nanoparticles depicting the elution of thymol, carvacol and hexadecane can be seen in Figure A11.

3.3.7 Evaluation of antibacterial activity of nanoparticles

The antimicrobial activity of NPs was tested against several species of bacteria using a well diffusion method. The indicator microorganisms included *Escherichia coli* ATCC 25922 (serotype O6, biotype 1), *E. coli* ATCC 43895 (serotype O157:H7), *Staphylococcus aureus* RN6390,[120] *Bacillus subtilis* subsp. *spizizenii* ATCC 6633, and *Burkholderia cenocepacia* K56-2 (clinical isolate from Canada)[121]. The testing was done on Mueller Hinton II agar (MHA) plates that have been overlaid with soft agar seeded with individual bacterial strains. The soft agar contained (per liter): 10 g of Bacto Tryptone, 6 g of Difco agar, and 8 g of sodium chloride. To create an overlay, the indicator organisms were grown overnight at 27°C (*B. subtilis*) or 37°C (*E. coli*, *S. aureus,* and *B. cenocepacia*) in Mueller Hinton II broth (MHB). The overnight cultures were diluted 1:5 with fresh MHB, and mixed with molten soft agar to achieve the density of ~10^8 CFU mL^{-1}. From this mixture, 4-mL aliquots were overlaid onto MHA base plates and allowed to completely solidify.

After solidifying of soft agar, 8 mm wells were made, and their bottoms were sealed with 20 µL of MHA. Then, 70 µL of each sample were added to the wells and allowed to freely diffuse into growth medium. Wells containing pure carvacrol or a mixture of carvacrol (1 g) with thymol (0.6 g) were used as a positive control. Negative controls contained 70 mM Hitenol BC 20, or empty NPs suspended in butyl acetate. The

plates were incubated at each bacterium's optimum growth temperature as listed above. The zones of inhibition (ZOI) were measured after 24, 48 and 72 h. Three replicates were carried out for each nanoparticle treatment and bacterial strain. Experiment was repeated three times to ensure data reproducibility.

3.3.8 Determination of Minimum Inhibitory Concentrations (MICs)

MICs of nanoparticles were determined using a modified broth microdilution method[122]. Briefly, overnight bacterial cultures were adjusted to ~10^5 CFU mL^{-1}, and nanoparticles were serially diluted with sterile water to achieve a range of concentrations between 10^{11} to 10^7 particles μL^{-1}. In a 96-well microplate, 150 µL aliquots of adjusted bacterial cultures were mixed with 50 µL aliquots of different NPs. Bacteria suspended in MHB without addition of nanoparticles served as a positive control, while MHB without bacterial inoculum and nanoparticles served as a negative control. The inoculated microplates were incubated at each bacterium's optimum growth temperature, and the susceptibility of microorganisms to different NPs was assessed by measuring optical density at 600 nm. The results were expressed as % viability obtained through equation 4:

$$\%viability = \frac{(OD_{t_{20}}) - (OD_{t_0})}{(OD_{t_{20}})} \times 100 \quad (4)$$

Where OD is the optical density at 600 nm, t_0 is the initial time 0 h, and t_{20} is the time after 20 h of incubation.

For further verification of inhibition of bacterial growth, 10 µL of bacterial cultures treated for 20 h with different nanoparticles were plated on MHA and incubated at each bacterium's optimum growth temperature for additional 20 h. The MIC refers to

the concentration of NPs that completely inhibited bacterial growth. Each treatment had four replications and experiment was repeated twice.

3.3.9 Viability staining assays

Bacterial viability was determined by using a LIVE/DEAD® BacLight™ Bacterial Viability Kit staining kit (Life Technologies). Overnight bacterial cultures were centrifuged at 8,500 rpm for 3 min, supernatants were removed and the bacterial cells were suspended in 0.9 % NaCl at OD_{600} of 0.1 (~10^8 CFU/mL). Freshly prepared nanoparticles were diluted 1:10 with sterile water. The adjusted bacterial cultures were mixed with the diluted nanoparticles at a ratio of 3:1, and incubated at 20°C in the dark. At 0, 2, 4, 6, 8, 12, and 24 h, 100 µL aliquots of the bacteria-NP mixtures were transferred into a black flat bottom microplate, and mixed with 100 µL of the LIVE/DEAD BacLight staining reagent. The samples were incubated in the dark for 15 min, and fluorescence was measured using a 485/20 nm excitation filter (for both SYTO9 and PI) and a 528/20 nm (SYTO9 emission wavelength) and a 620/40 nm (PI emission wavelength) emission filter. For confocal imaging, 5 µL of the stained sample were cast on a microscope slide. Each sample was assayed in triplicate, and the experiment was repeated twice. The results of viability staining were confirmed by plating 10 µL of each bacterial suspension on MHA, and incubating the plates at an appropriate growth temperature for 20 h.

3.3.10 Terminal dilution assays

To compare the rate of bacterial killing by different NPs, the test organisms were exposed to NPs and the decline in numbers of viable bacteria was followed by a modified terminal dilution method.[123] The bacterial cultures were prepared and adjusted to ~10^8 CFU mL^{-1}

as described above. The adjusted bacterial cultures (9 mL) were mixed with nanoparticles (1 mL), and the bacterial populations were determined immediately after the addition of NPs (0 h), and at 2, 4, 8, 12 and 24 h of exposure. At each time point, 100-µL aliquots of the bacteria-NP suspensions were transferred into 96-well microplates prefilled with 200 µL of MHB and serially diluted. The inoculated microplates were incubated for 48 h at appropriate growth temperature, after which the turbidity in each well was measured with a BioTek Synergy 2 microplate reader. An optical density at 600 nm of ≥ 0.05 was considered positive for bacterial growth. Populations of viable bacteria were calculated from the final dilution (terminal dilution, or TD), in which bacterial growth was observed using equation 5:

$$\frac{\mathrm{CFU}}{\mathrm{mL}} = \frac{10\times 3^{\mathrm{TD}}}{1\mathrm{mL}} \quad (5)$$

Where TD is the terminal dilution factor obtained from microplate readings.

3.4 Results and Discussion

3.4.1 Synthesis and characterization of essential oil encapsulated nanoparticles

Polythioether NPs loaded with various ratios of carvacrol/thymol were synthesized *via* thiol-ene photopolymerization in miniemulsion according to Figure 3.1a. NPs were prepared by dispersing the organic phase, comprising diallyl phthalate (DAP), glycol di(3-mercaptopropionate) (GDMP), pentaerythritol tetra(3-mercaptopropionate) (PETMP), and carvacrol/thymol, into deionized water containing surfactant *via* probe ultrasonication for 25 min (Figure 3.1b). The full details for the miniemulsion formulation are given in Table S1. The monomer droplets were then photopolymerized by exposure to UV light (λ_{max} 365nm). Control NPs (without carvacrol/thymol) were similarly prepared using butyl

acetate as a diluent for the organic phase. After ultrasonication and photopolymerization, aliquots were removed and analyzed *via* ^{1}H NMR (Figure A.1) in D_2O. The disappearance of the peaks attributed to the thiol (–CH_2CH_2–SH, 2.62-2.83 ppm) and alkene (5.07-5.45, 5.87-6.10 ppm) from the monomers, and broadening of other peaks indicated the thiol-ene photopolymerization proceeded to high conversion. Additionally, Raman spectroscopy of freshly emulsified nanoparticles prior to and after UV polymerization showed the disappearance of SH (2580 cm^{-1}) and alkene stretches (1640-1680 cm^{-1}) (Figure A.2). The ability to achieve high thiol-ene monomer conversion in the presence of phenolic functional groups is in good agreement with our previous work.[117, 124-125] At near quantitative conversions, crosslink density (0.168×10^{-3} mol/cm^3) of the polythioether NPs was estimated from the rubbery plateau storage modulus (1.25 MPa, Tg -12.1 °C, Figure A.3) of the base thiol-ene resin (i.e. GDMP+PETMP+diallyl phthalate prepared at identical stoichiometric ratios used in the miniemulsions) at T_g + 40 °C according to the theory of rubber elasticity.[126] To eliminate surfactant leaching, Hitenol BC-20 was employed as a polymerizable surfactant to covalently incorporate the surfactant into the thiol-ene network (discussed further in the antimicrobial section). A series of exploratory NP syntheses were conducted, in which the concentration of Hitenol BC-20 (Figure A.4a) and organic weight fraction (Figure A.4b) were independently varied, to identify conditions to provide acceptable NP size and size distributions. A 4.5 wt.% organic phase and 70 mM Hitenol BC-20 were identified as optimum parameters; these conditions provided pure carvacrol-loaded NPs (C_{NPs}), thymol/carvacrol-loaded NPs (TC_{NPs}), and control NPs with mean particle sizes of 148 ± 24 nm (PDI: 0.560), 147 ± 19 nm (PDI: 0.387), and 183 ± 19 nm (PDI: 0.473), respectively, as determined by DLS (Figure A.3). We note that the reported

std. dev. values represent the deviation in the average particle size obtained from a minimum of three separate syntheses. A representative transmission electron microscopy (TEM) image for TC_{NPs} loaded with a 0.75:1 T/C ratio (Figure 3.1c) showed spherical particles with sizes in good agreement with DLS analysis. TEM for the control NPs and C_{NPs} are shown in Figure A.5a and A.5b, respectively. The salient feature of this synthetic approach is that the carvacrol/thymol constituents serve as the "solvent" for the organic phase in the miniemulsion process. This route enabled a high loading capacity of thymol/carvacrol within the NPs (between 33 – 66% w/w, EO/NP) with high encapsulation efficiencies (>95% by GC-MS), eliminated the need for an organic solvent during NP synthesis, and provided a one-pot approach to EO encapsulation without any post-polymerization purification processes (e.g. no freeze drying, evaporation, extraction processes were required). Thus, the NP dispersions obtained from the previously described synthetic approach were used directly for the antimicrobial studies detailed below.

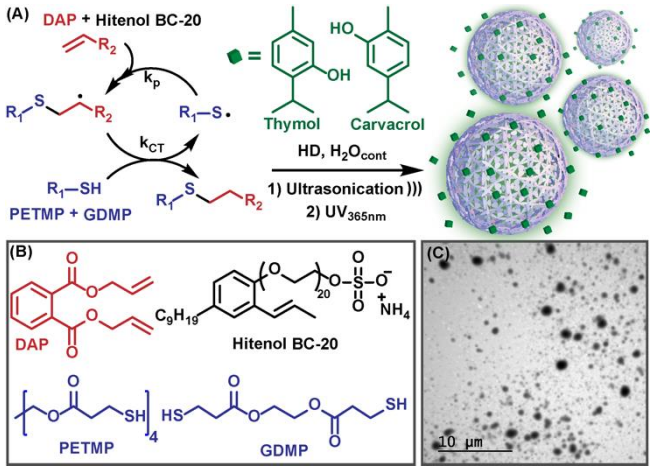

Figure 3.1 (A) The thiol-ene reaction involves alternating chain transfer and propagation (B) with various multifunctional monomers used to generate polythioether nanoparticles via thiol-alkene photopolymerization in miniemulsion. (C) Representative TEM of thymol/carvacrol-loaded nanoparticles.

3.4.2 Loading and Release of Thymol and Carvacrol

Next, we investigated the release kinetics of carvacrol and carvacrol/thymol mixtures released from polythioether NPs into water. The amount of essential oil released was quantified by measuring the concentration of carvacrol/thymol available in water via GC-MS at 0, 4, 8, and 12 h. Figure 3.2a shows the release data for CNPs (synthesized at 33% w/w C/NP) and TC_{NPs} (synthesized with 47% w/w TC/NP, 0.75:1 T:C). The EO_{load} data points represent the total amount of carvacrol (16 ± 0.7 mg/mL) and thymol/carvacrol (25 ± 5 mg/mL) loaded into the NPs during miniemulsion photopolymerization, and are in good agreement with initial formulations for each type of NP. The ratio of the time 0 and EO_{load} concentrations represents the encapsulation efficiency for the miniemulsion process, i.e. ~96.9% for TC_{NPs} and 96.8% for C_{NPs}. Thus, the concentration of EO within the nanoparticles is up to 20 times higher than the reported solubility limits for thymol (0.85 mg/mL) and carvacrol (1.25 mg/mL) at 20 °C.[127] As shown in Figure 3.2a, the concentration of EO released from the NPs in water was relatively constant over 24 h, where TC_{NPs} and C_{NPs} reached plateau concentrations between 0.7-0.9 mg/mL and 0.5–0.6 mg/mL, respectively. These concentrations correspond to less than 4% release of the total EO payload over 24 h, (Figure 3.2b) and approach the solubility limit of thymol and carvacrol in water at 20 °C. These results suggest that the polythioether nanoparticles effectively serve as a reservoir for the hydrophobic carvacrol and thymol compounds. This "reservoir effect" enables extended delivery of EO constituents into the bulk aqueous phase, where the solubility limit of the relatively insoluble compounds ultimately dictates the aqueous-phase equilibrium concentration.

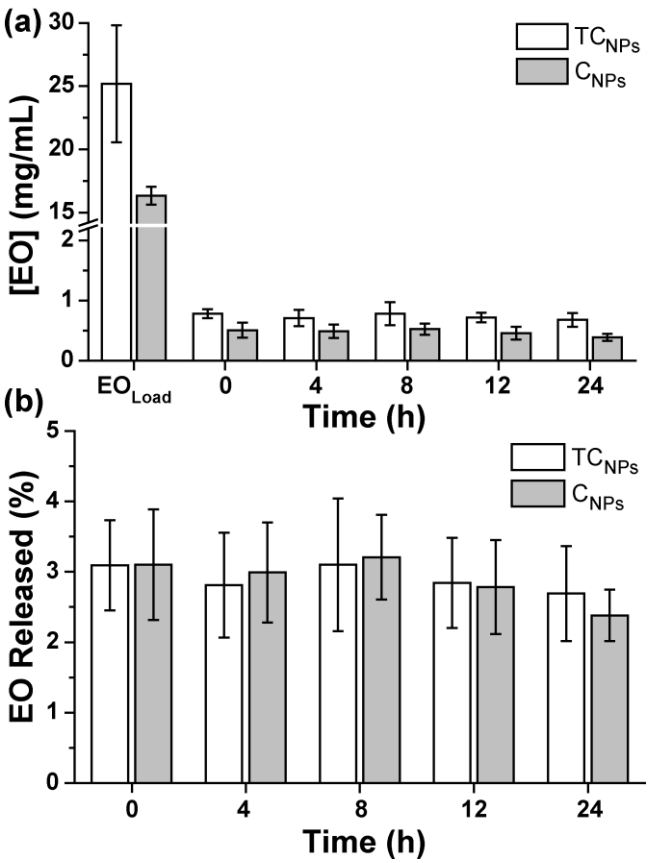

Figure 3.2 (a) Amounts of essential oils extracted from the supernatant after pelleting NPs by ultracentrifugation. (b) Calculated release profiles for both C_{NPs} and TC_{NPs} over 24 h.

3.4.3 Antimicrobial properties

Antimicrobial activity of the EO-containing NPs was evaluated against a panel of gram-positive and gram-negative bacteria that included both saprophytic (*B. subtilis* ATCC 6633 and *E. coli* ATCC 25922) and pathogenic species (*E. coli* ATCC 43895 [serotype O157:H7], *S. aureus* RN6390, and *B. cenocepacia* K56-2). Our preliminary experiments revealed that control NPs prepared using either sodium dodecyl sulfate or cetyltrimethylammonium bromide as surfactant exhibited antimicrobial activity, presumably due to surfactant leaching. Thus, we chose Hitenol BC-20 – a commercially available polymerizable surfactant – for further experiments, as it exhibited no measurable

antimicrobial activity in zone of inhibition (ZOI) experiments at the concentration used in NP synthesis (70 mM Figure 3.3a; 140 mM Figure A.6). More importantly, control NPs prepared with Hitenol BC-20 showed no measureable ZOI against all five bacteria (Figure 3.3b).

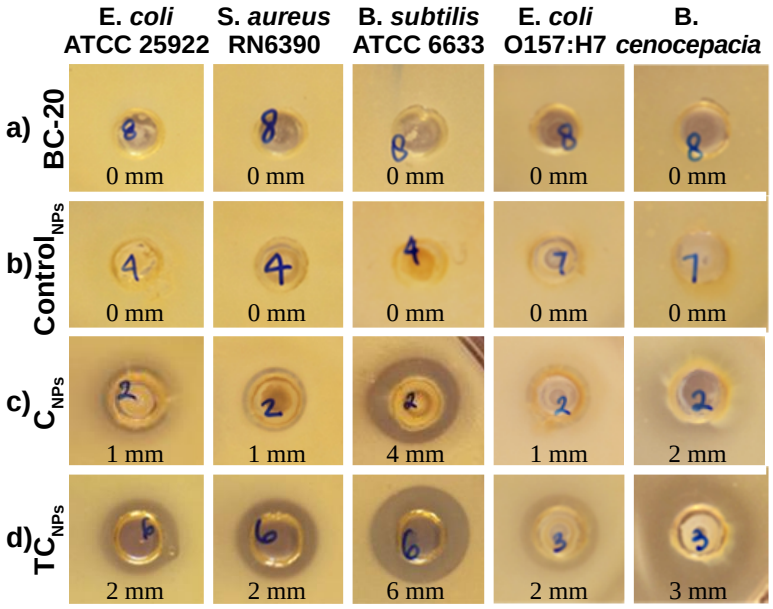

Figure 3.3 Well diffusion assay identifies treatments with antimicrobial activity. Bacteria were incubated with 70 mM Hitenol BC-20 (a), $Control_{NPs}$ (b), C_{NPs} (c), and TC_{NPs} (d) at 10^{13} NPs mL^{-1}. Zones of inhibition (ZOI, mm) are reported below each image.

Initially, we evaluated the antimicrobial activity of NPs containing pure carvacrol (33% w/w, carvacrol relative to NP) and various ratios of thymol:carvacrol (Treatment I – 66% w/w, 3:1 T:C; Treatment II – 55% w/w, 1.5:1 T:C; and Treatment III – 47% w/w, 0.75:1) against *E. coli* ATCC 25922, *S. aureus* RN6390, and *B. subtilis* ATCC 6633 (Figure A.7). Since thymol is a solid at room temperature (mp 49-51 °C), thymol-loaded NPs were difficult to synthesize using a solvent-free approach and were not actively pursued in this work. Previous reports have shown that combinations of thymol and carvacrol exhibit higher antimicrobial activity than each individual constituent,[97] thus,

carvacrol-loaded NPs were evaluated *via* ZOI only as a comparison to NPs loaded with combinations of thymol/carvacrol. Interestingly, all treatments with NPs containing thymol/carvacrol showed similar zones of inhibition (Figure A.7), thus treatment III, with the lowest overall thymol/carvacrol loading, was chosen for the experiments discussed hereafter. From this point forward, the acronym TC_{NP} will refer to nanoparticles loaded with 47% w/w, 0.75:1 T:C (treatment III). Figure 3.3c and 3.3d show the results of well diffusion assays for C_{NPs} and TC_{NPs} against the full panel of bacteria. As shown in Figure 3.3c, C_{NPs} exhibited moderate activity against all bacteria (ZOI 1 – 2 mm). As expected, TC_{NPs} were consistently more effective than C_{NPs}, as indicated by the larger ZOIs shown in Figure 3.3d. TC_{NPs} inhibited the growth of all five bacteria, including *S. aureus* (2 mm ZOI) and *B. cenocepacia* (3 mm ZOI) that are known to exhibit high intrinsic resistance to conventional antibiotics. *Bacillus subtilis* (6 mm ZOI) was the most susceptible species to the TC_{NP} treatment.

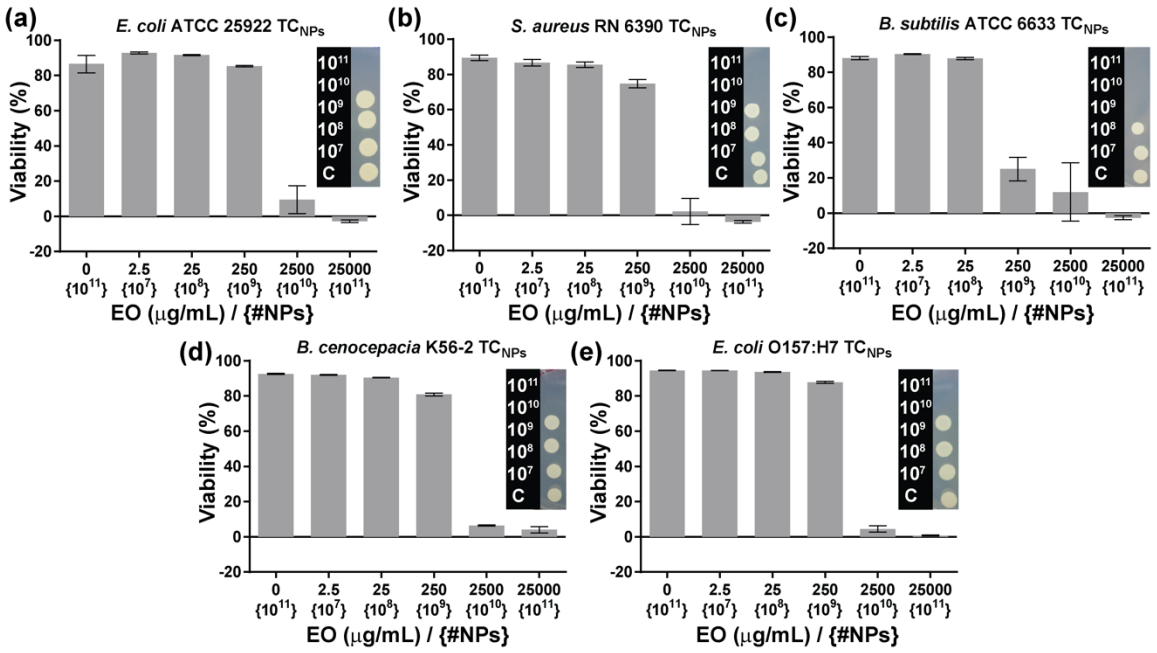

Figure 3.4 Percent viability of various bacteria upon treatment with TC_{NPs}. Inset images show the corresponding spot tests for the presence of live bacteria.

The antimicrobial activity of TC_{NPs} was further evaluated *via* determination of the minimum inhibitory concentration (MIC). The MIC is defined as the lowest concentration of an antimicrobial agent that inhibits the growth of a microorganism following an overnight incubation period. We adopted a modified broth microdilution method to determine MICs for NP-loaded thymol/carvacrol.[122] We also spot-plated bacteria that were incubated with NPs to check for possible bacteriostatic effects. While MIC assays are reputable for accuracy and standardized comparison across numerous antibiotics, the conventional MIC output presents a challenge for hydrophobic antibiotics encapsulated in polymer nanoparticles – and is particularly problematic for NP delivery systems that function *via* the "reservoir effect". As a result of the "reservoir effect", the concentration loaded in the nanoparticle may be orders of magnitude greater than the concentration delivered to the bacteria during the timeframe of the MIC assay. For example, the loaded concentration of thymol/carvacrol in TC_{NPs} was determined to be 25,000 μg/mL by GC-MS. These thymol/carvacrol loading levels are up to 100-fold higher than reported MIC values for *E. coli* 25922 ($MIC_{carvacrol}$: 225 μg/mL, MIC_{thymol}: 225μg/mL) and *S. aureus* ($MIC_{carvacrol}$: 450 μg/mL, MIC_{thymol}: 225 μg/mL);[128] however, our release studies show that carvacrol and thymol are delivered to the bulk aqueous phase at a relatively constant concentration of 500 – 900 μg/mL over 24 h. Following the precedent of Langer *et al.*,[129] who previously noted the difficulty in defining the MIC for antibiotic-loaded nanoparticles, we report concentrations as the total EO concentration within the NP at the beginning of the treatment to identify the MIC. While the loaded concentrations grossly overestimate the MIC value relative to a conventional definition, we reasoned this route of reporting was

the most useful and conservative measure of NP-loaded antimicrobial efficacy. Additionally, we calculated the nanoparticle number density (#particles/mL) to estimate the number of NPs delivered in each experiment as an alternate MIC output value, with the caveat that the number density is based on the average particle diameter of a polydisperse nanoparticle population. Nonetheless, number density MIC provides a point of comparison among the various bacteria investigated in this paper. Figure 3.4 shows the results from the viability assays used to determine the MICs for TC_{NPs}. In general, the growth of all five bacteria included in this study was completely inhibited upon exposure to TC_{NPs} loaded at 25,000 μg/mL (10^{10} nanoparticles) in a 50 μL broth volume, which translated to approximately 10^5 NPs per bacterial cell. *B. subtilis* was the most susceptible species, and was completely inhibited at TC_{NPs} loaded at 2,500 μg/mL (10^9 nanoparticles, ~10^4 NPs per cell). The MIC values are in good agreement with the previously described results of agar well diffusion tests.

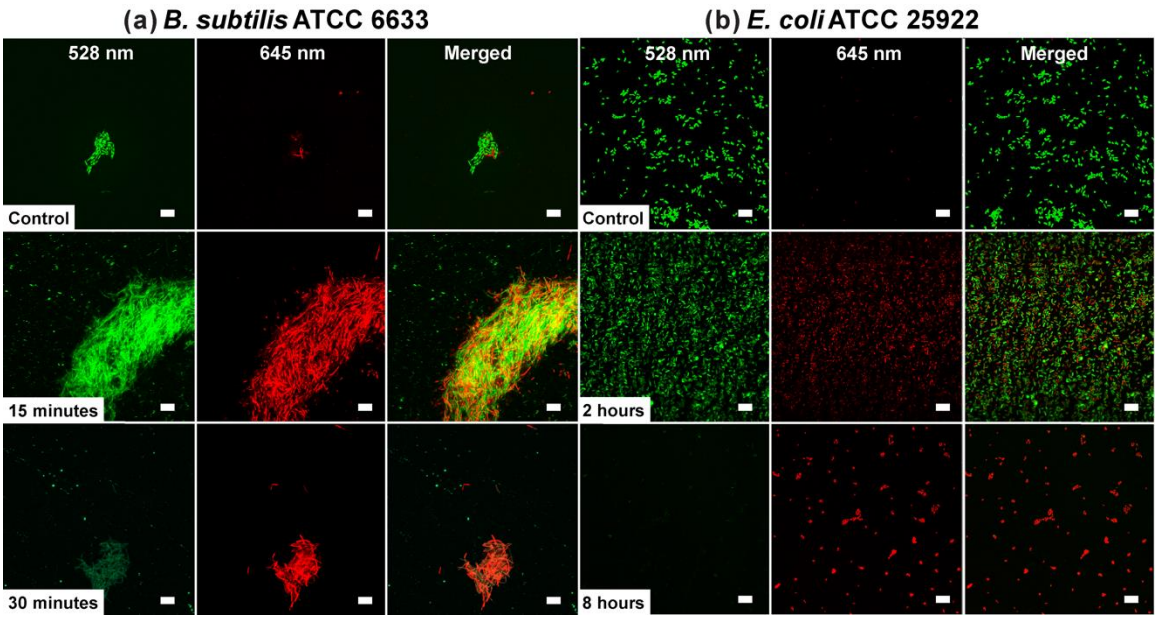

Figure 3.5 Effect of TC_{NPs} on the viability of (a) *B. subtilis* ATCC 6633 and (b) *E. coli* ATCC 25922, as monitored by confocal laser scanning microscopy. Representative images of control cultures (top row), and cultures treated with 10^{11} TC_{NPs} (middle and bottom row) at the indicated time points. The green signal (SYTO 9) indicates viable live cells, whereas red signal (propidium iodide) indicates damaged or dead cells. Scale bars = 10 μm.

We also investigated the kill kinetics for the panel of bacteria incubated with TC_{NPs} using live/dead and terminal dilution assays. Initially, the kill kinetics of TC_{NPs} against *B. subtilis* ATCC 6633 and *E. coli* ATCC 25922 were probed using a live/dead cell viability assay, which stains "dead" bacteria red upon cell membrane damage and uptake of propidium iodide. As shown in Figure 3.5a and 3.5b, a large number of viable bacterial cells (stained green) were observed for the *B. subtilis* and *E. coli* control samples, respectively. Incubation of TC_{NPs} with *B. subtilis* for 15 min yielded an apparent 50:50 live/dead ratio, whereas 30 min resulted in mostly dead bacteria (Figure 3.5a). For *E. coli* ATCC 25922, the 50:50 live/dead ratio was observed after two hours of incubation with TC_{NPs}, and most bacteria stained dead after 8 h of incubation (Figure 3.5b). To quantify the kill kinetics for all five bacteria, we used a terminal dilution assay. Figure

3.6a shows the log reduction in the bacteria count as a function of incubation time with ~10^{11} TC_{NPs}. The log CFU reductions at 48 h are reported as % kill values in Figure 3.6b. In agreement with our previous ZOI data, *B. subtilis* ATCC 6633 showed the highest susceptibility to the TC_{NP} treatment with 4.3 and 7.1 log reductions observed at 12 and 24 h, respectively. The log reductions for *E. coli* O157:H7 (ATCC 43895) were 3.5 at 12 h and 7 at 24 h – results that translate into a kill efficacy of > 99.99%. The viability of *E. coli* ATCC 25922 declined at a slower rate than *E. coli* O157:H7, however, the 48-hour exposure to TC_{NPs} ultimately killed > 99.99% of the bacteria. Incubation of TC_{NPs} with *B. cenocepacia* K56-2 produced 3.9 and 6.2 log reductions at 12 and 24 h, respectively. The kill kinetics and high susceptibility (over 99.99% efficacy at 24 h) of *B. cenocepacia* to the TC_{NPs} is of particular interest, as these bacteria have very high innate resistance to a wide range of antibiotics and biocides.[130] With a 3.6 log reduction, *S. aureus* RN6390 was the only species that maintained viability after 24 h incubation with TC_{NPs}. However, a 6.3 log reduction, or > 99.99 % kill efficacy for *S. aureus* was ultimately attained at 48 h.

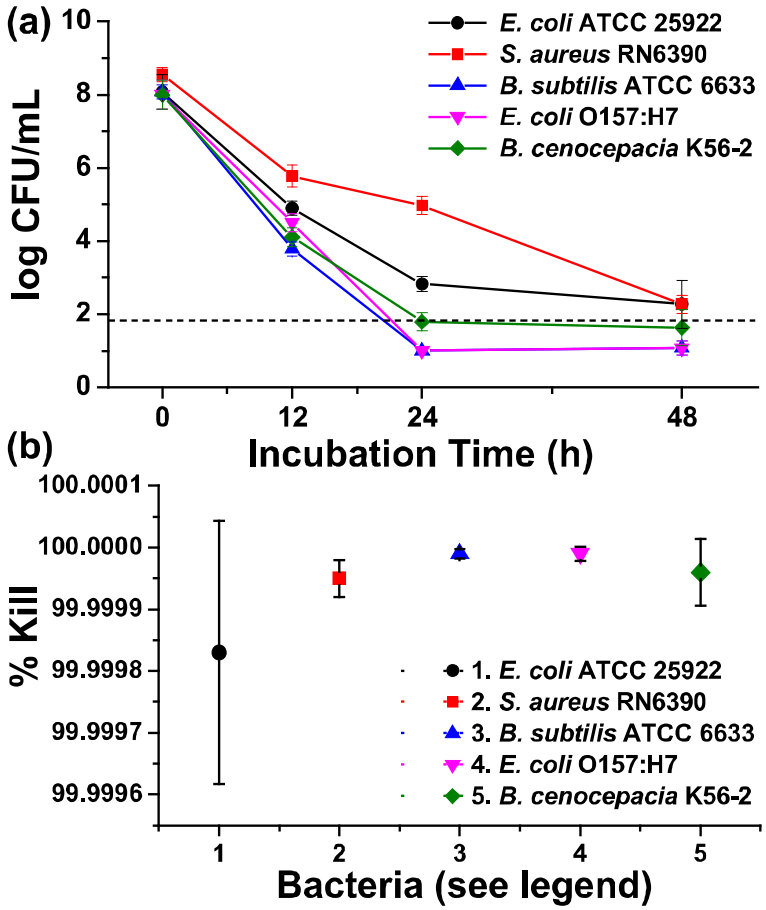

Figure 3.6 Evaluation of antimicrobial activity for 1011 TCNPs/mL on the viability of (●) E. coli ATCC 25922, (■) S. aureus RN6390, (▲) B. subtilis ATCC 6633, (▼) E. coli ATCC 43895 (serotype O157:H7), and (◆) B. cenocepacia K56-2 via (a) a kinetic terminal dilution and (b) percentage of bacteria killed and over 48 h. *Dashed line represents the limit of quantitation.

Finally, insight into the antimicrobial mechanism was investigated by visualizing the microbial structure of *B. subtilis* ATCC 6633 and *E. coli* ATCC 25922 before and after prolonged contact with TC_{NPs} using electron microscopy. Prior to exposure to TC_{NPs}, TEM of both microbes showed intact cell structure (Figure 3.7, control). After exposure with TC_{NPs}, distinct indication of damage to the cell envelope (diffuse membrane, cellular debris) and loss of flagella were visible in both *E. coli* ATCC 25922 (Figure 3.7a) and *B. subtilis* ATCC 6633 (Figure 3.7b). Additionally, the scanning electron microscopy (SEM)

image of *B. subtilis* after 24 h exposure to inhibitory concentrations of TC_{NPs} showed bacteria with crumpled cell envelopes and pore-like lesions, which is consistent with the collapse of the cell structure (Figure 3.7c). These results are consistent with previously reported postulates that identify the cell membrane as the primary site of toxicity for carvacrol/thymol.[97]

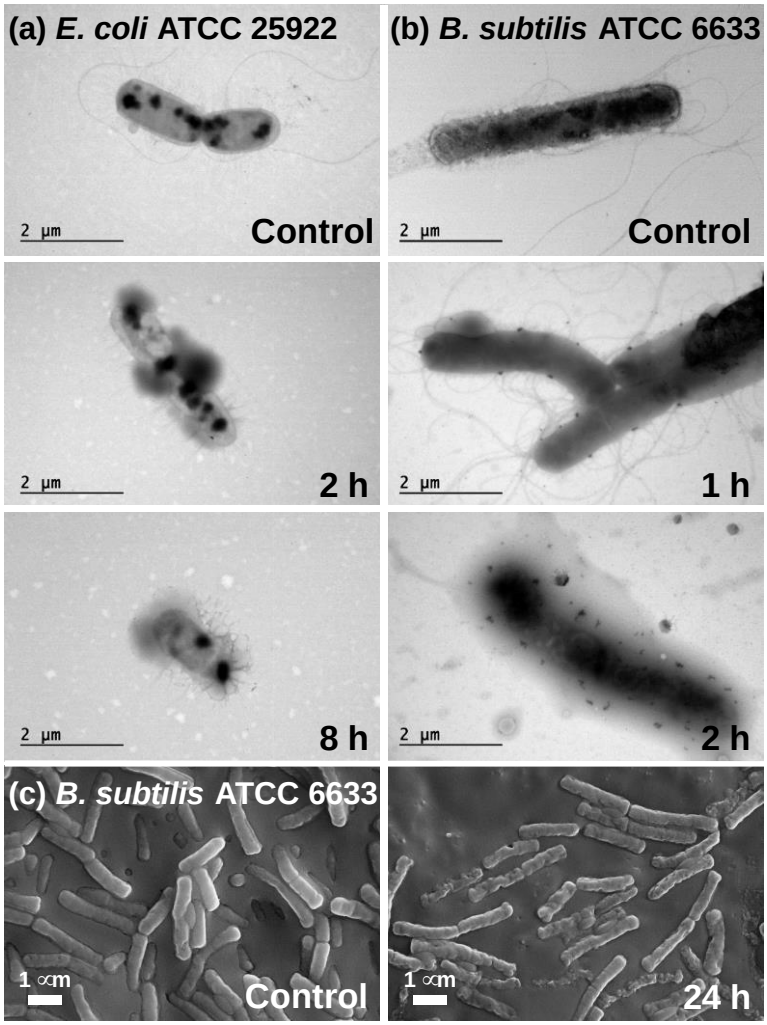

Figure 3.7 (a) TEM of *E. coli* ATCC 25922 and (b) *B. subtilis* ATCC 6633 control cultures and cultures that were challenged with 10^{11} TC_{NPs} for various times. (c) High resolution SEM of the control culture of *B. subtilis* ATCC 6633 and the culture treated for 24 h with 10^{11} TC_{NPs}.

3.5 Conclusions

We have reported a one-pot, solvent-free miniemulsion photopolymerization process for the synthesis of thymol/carvacrol-loaded polythioether nanoparticles. Using the thymol/carvacrol payload directly as a diluent for the monomer phase in the presence of a polymerizable surfactant provided the active NPs without any post-synthetic purification. The NPs serve as high capacity reservoirs for slow-release and delivery of thymol/carvacrol-combination payloads that exhibit inhibitory and bactericidal activity (> 99.9% kill efficiency at 24h) against gram-positive (*Bacillus subtilis* and *Staphylococcus aureus*) and gram-negative (*Escherichia coli* and *Burkholderia cenocepacia*) bacteria. The simplicity, modularity, and efficacy of the essential oil encapsulation platform may combat bacteria with intrinsic resistance to conventional antibiotics, and is potentially adaptable for delivery of EOs as active packaging materials and topical antiseptics. The antimicrobial activity of TC_{NPs} against inherently resistant *Burkholderia cenocepacia* may provide a route to innovative pulmonary therapeutics by appropriately engineering the nanoparticle properties; investigations of thymol/carvacrol-loaded NPs against *B. cepacia* complex biofilms – a challenging form of the bacteria commonly associated with cystic fibrosis – are currently underway. In this direction, we are particularly interested to exploit the simple synthetic modularity of this process for the design of EO-loaded biodegradable nanoparticles with specific surface chemistries to serve as multimode (e.g. contact biocidal, targeted NP-bacteria interactions) antimicrobial platforms.

CHAPTER IV - PRO-ANTIMICROBIAL NETWORKS VIA DEGRADABLE ACETALS (PANDAS) USING THIOL-ENE PHOTOPOLYMERIZATION

4.1 Abstract

We describe the synthesis of pro-antimicrobial networks via degradable acetals (PANDAs) as a new paradigm for sequestration and triggered release of volatile, bioactive aldehydes. PANDAs derived from diallyl p-chlorobenzaldehyde acetal degrade and release p-chlorobenzaldehyde as an antibacterial and antifungal agent under mild conditions (pH 7.4/high humidity). We show that PANDAs enable facile access to materials with tunable release profiles, potent antimicrobial activity without triggering antimicrobial resistance, and minimal cytotoxicity.

4.2 Introduction

With 700,000 annual deaths globally, antimicrobial resistance is an escalating crisis that threatens the sustainability of public health and agricultural ecosystems.[131] As the effectiveness of antibiotics has precipitously declined, a growing interest in alternative antibiotic scaffolds has proliferated. In this direction, aromatic terpene aldehydes – major phytochemical constituents of plant derived essential oils (EOs) − are known to exhibit potent and broad spectrum antibacterial and antifungal activities in both liquid and gaseous states.[132-133] However, practical application of terpenes remains a challenge stemming from their poor water solubility, volatility, and chemical instability. Many strategies have been reported to sequester or encapsulate terpenes within films or colloidal systems;[134-135] however, these strategies often suffer deficiencies such as low loading, poor encapsulation efficiencies, necessity of organic processing solvents, and uncontrolled burst release profiles.[136]

"Polyactives" − polymeric pro-drugs that undergo degradation to release active therapeutic agents − address the deficiencies in sequestering EO constituents by providing high loading, chemical stability, and tailored release kinetics.[84] Recently, linear polyactives of phytochemicals and other synthetic analogs have been used for the extended delivery of antimicrobials,[27, 137] antioxidants,[26, 138] anti-inflammatories,[25] hormones,[139] and anti-cancer therapeutics.[140-141] While successfully demonstrated, tuning the degradation of linear polyactives remains a challenge as degradation rates are determined by manipulating coupled parameters such as crystallinity, polymer molecular weight, functionality, and hydropathy.[142] Alternatively, crosslinked polyactives (i.e. thermosets) offer unique opportunities to tailor release profiles by simple manipulation of crosslink density, monomer concentration, or monomer molecular weight.[143] Recently, Matras and Chatterjee developed biodegradable crosslinked polyactive esters that challenge the performance of traditional linear polymers by offering greater control over degradation rates, mechanical properties, and release kinetics.[144] Although these crosslinked polyesters showed high biocompatibility and are capable of releasing anticancer, anti-inflammatory, or antimicrobial compounds,[145-147] the lengthy polymerization times (>1 day) at elevated temperatures (>130 °C) preclude polymerization in the presence of cells, *in vivo*, or in 3D printing applications. Furthermore, polyesters with sustained degradation typically exhibit localized accumulation of acidic byproducts leading to inflammatory response.[148] Polyactive acetals are promising alternatives as acetals readily hydrolyze under mild aqueous conditions into pH neutral byproducts (alcohols and aldehydes).[149]

Inspired by polyacetal hydrogels,[150-151] the work herein describes the synthesis of pro-antimicrobial networks via degradable acetals (PANDAs) derived from p-chlorobenzaldehyde (pCB) using thiol-ene photopolymerization – an approach designed to address many of the aforementioned challenges with sequestration of terpene aldehydes. Thiol-ene photopolymerization offers rapid cure kinetics at room temperature, low oxygen inhibition, homogeneous network formation, and high monomer conversion.[152] Thiol-ene – as a step-addition polymerization – ensures that nearly every crosslink junction contains a degradable, pCB-derived acetal. Therefore, PANDAs are molecularly designed to undergo complete degradation upon hydrolysis resulting in the release of pCB as an active antimicrobial and antifungal agent, and the generation of inactive low molecular weight degradation byproducts (Figure 4.1).

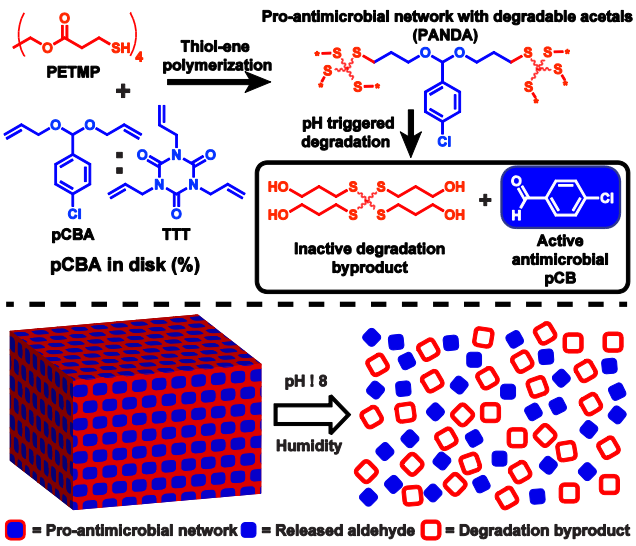

Figure 4.1 Synthesis of PANDAs and major degradation byproducts.

4.3 Experimental

4.3.1 Materials

Allyl alcohol, triethylamine (TEA), 4-chlorobenzaldehyde (pCB), 1,3,5-triallyl-1,3,5-triazine-2,4,6 (1H, 3H, 5H) trione (TTT), 2-hydroxy-2-methyl-1-phenyl-propan-1-one (Darocure 1173), p-toluenesulfonic acid (pTSOH), molecular sieves (3Å), dry tetrahydrofuran (THF), hexane and ethyl acetate were acquired from Fisher Scientific. Pentaerythritol tetra(3-mercaptopropionate) (PETMP) was provided by Bruno Bock. Difco Agar, Mueller Hinton II agar (MHA), Mueller Hinton II broth (MHB), and Bacto Tryptone were from Becton, Dickinson and Company. All the materials were obtained at the highest purity available and used without further purification unless otherwise specified.

4.3.2 Characterization Methods.

^{1}H NMR was recorded on a Varian Mercury Plus 300 MHz NMR spectrometer in chloroform-d. Dynamic mechanical analysis (DMA) was performed using a TA Instruments Q800 dynamic mechanical analyzer in tension mode equipped with a gas cooling accessory. Samples were clamped and tested at a strain of 1 %. Samples were heated from -80 °C to 90 °C at a ramp rate of 3 °C $min^{-1.}$ Kinetic data were obtained using real-time FTIR (RT-FTIR) spectroscopy by determining the conversions of the thiol and ene functional groups. The RT-FTIR studies were conducted using a Nicolet 8700 FTIR spectrometer with a KBr beam splitter and a MCT/A detector with a 320–500 nm filtered ultraviolet light source. Each sample was exposed to a UV light with an intensity of 200 mW cm^{-2}. Series scans were recorded, where spectra were taken approximately 2 scan/s with a resolution of 4 cm^{-1}. Thiol conversions was monitored with integrating the SH conversion peak between 2500-2620 cm^{-1} while the conversion of the allyl group was monitored with conversion peak between 3050-3125 cm^{-1}. Optical

density (OD) and fluorescence readings were performed in a BioTek Synergy 2 programmable microplate reader.

4.3.3 Synthesis of p-chlorobenzaldehyde diallylacetal (pCBA)

pCB (10 g, 71.14 mmol, 1 equiv), pTSOH (4.3 g, 24.97 mmol, 0.35 equiv), 3Å molecular sieves (15 g), and allyl alcohol (16.52 g, 284.6 mmol, 4 equiv) were dissolved in dry THF (50 mL). The yellow reaction mixture was left to stir overnight and then quenched with addition of TEA (19.8 mL, 142.3 mmol, 2 equiv), filtered and rotovapped before adding to a silica gel column. The column was eluted with a 10:90 (v:v) ethyl acetate/hexane mixture to afford 8.3 g (48.9%) of the acetal. ^{1}H NMR (300 MHz, Chloroform-*d*) δ 7.46 (d, *J* = 8.4 Hz, 1H), 7.36 (d, *J* = 8.4 Hz, 1H), 5.95 (ddt, *J* = 16.2, 10.8, 5.6 Hz, 1H), 5.63 (d, *J* = 2.7 Hz, 1H), 5.33 (dt, *J* = 17.2, 1.8 Hz, 1H), 5.20 (dd, *J* = 10.5, 2.1 Hz, 1H), 4.06 (d, *J* = 5.1 Hz, 2H). ^{13}C NMR (75 MHz, $CDCl_3$) δ 136.97, 134.27, 128.41, 128.21, 116.96, 99.63, 66.06. GC-MS observed: 238; calculated: 238.

4.3.4 General preparation of PANDA disks

The 100% pCBA disks were prepared by adding PETMP and pCBA at 1:1 ratio of SH:alkene, along with 4 wt % of Darocure 1173. The 90% pCBA disks were prepared by adding pCBA and TTT as another source of alkene (TTT is 10% of total alkene while maintaining an overall 1:1 ratio of alkene:SH) with PETMP, and Darocure 1173. The mixtures were well mixed and 25 μL of monomer formulations were aliquoted onto a glass slide and covered with another glass slide spaced with Teflon spacers (0.76 ± 0.02 mm in thickness). The samples were then cured using an Omnicure S1000-1B with a 100W mercury lamp (λmax = 365 nm, 320–500 nm filter) at an intensity of 200 mW cm^{-2} for 20 minutes.

4.3.5 Degradation of PANDAs in Phosphate Buffer Saline (PBS)

The hydrolysis of PANDA disks was done using a slight modification of a method reported by Carter and coworkers.[151] In general, the degradation study was performed in aqueous media (PBS) at pH 7.4 with a large excess of octanol to partition the aldehyde from the aqueous environment. Concentration was determined by measuring the absorbance of pCB released at 275 nm over 120 hours and extrapolated from a standard calibration curve. Experiments were done with n=5, with the mean and standard deviation reported. The 25 mm^3 disks were placed at the bottom of 20 mL scintillation vials filled with 3 mL of PBS and 15 mL of octanol. Immediately, 100 µL octanol aliquots were taken out form the vial and measured for t=0. After the measurement, aliquots were placed back to the scintillation vials to maintain the same concentration throughout the kinetic study. Aliquots were analyzed at t = 0, 20, 24, 30, 48, 54, 72, 78, 96, 102, 120 h.

4.3.6 Degradation of PANDAs in HCl, H_2O, and NH_4OH chambers

Humidity chambers were made via bubbling nitrogen gas into a vial containing either 12 M HCl, 30 wt% NH_4OH, or deionized H_2O. A cannula in the head space of the pressurized vial allowed transport into a secondary vial containing a 90% pCBA PANDA disk on a glass slide.

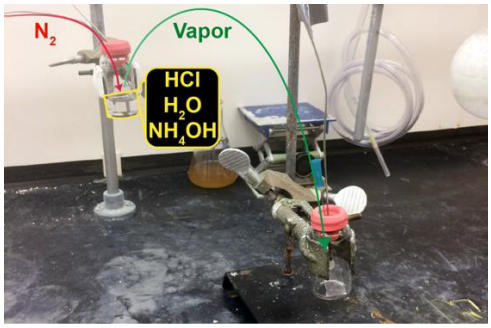

4.3.7 Evaluation of antibacterial activity of PANDAs

The antimicrobial activity of PANDA disks was evaluated against several species of bacteria via the zone of inhibition method. The indicator microorganisms included E. coli ATCC 43895 (serotype O157:H7), Staphylococcus aureus RN6390, Burkholderia cenocepacia K56-2 (clinical isolate from Canada), and Pseudomonas aeruginosa PA-01. The testing was done on Mueller Hinton II agar (MHA) plates that were overlaid with soft agar seeded with individual bacterial strains. The soft agar contained (per liter): 10 g of Bacto Tryptone, 6 g of Difco agar, and 8 g of sodium chloride. To create an overlay, the indicator organisms were grown overnight at 37°C in Mueller Hinton II broth (MHB). The overnight cultures were diluted 1:5 with fresh MHB, and mixed with molten soft agar to achieve the density of ~10^8 CFU mL^{-1}. From this mixture, 4-mL aliquots were overlaid onto MHA base plates and allowed to completely solidify. After solidifying of soft agar, 25 mm^3 disks were overlaid on the plates and incubated at 37°C. The zones of inhibition (ZOI) were measured after 30 h and reported as the radius from the edge of the disk to the edge of the zone. Five replicates were carried out for each disk treatment and bacterial strain with the mean and standard deviation reported.

4.3.8 Determination of Minimum Inhibitory Concentrations (MICs)

MICs of the PANDA disks were determined using a modified broth macrodilution method. Briefly, overnight bacterial cultures in MHB were adjusted to ~10^5 CFU mL^{-1}. Various disks of different sizes (5-50 mm^3) containing pCB at concentrations ranging from 0.5 - 3 mg/mL of were added to 3 mL of bacterial solutions. The tubes then were incubated at 37 °C at 200 rpm for 30 hours. Bacteria suspended in MHB served as a positive control, while MHB without bacterial inoculum served as a negative control. The

inoculated tubes were assessed by measuring optical density at 600 nm where OD < 0.05 considered negative for bacterial growth.

4.3.9 Kill kinetics via terminal dilution assays

To compare the rate of bacterial killing by 90% pCBA PANDA disks, the test organisms were exposed to disks and change of viable bacteria was determined by a modified terminal dilution method. The bacterial cultures were prepared and adjusted to ~10^5 CFU mL^{-1} as described above. The adjusted bacterial cultures (3 mL) were mixed with (2 x 25 mm^3) 90% pCBA PANDA disks. The inoculated tubes were incubated at 37°C with shaking (200 rpm) and bacterial populations were determined immediately after the addition of disks (0 h), and at 2, 4, 8, 12, 24, and 30 hours of exposure. At each time point, six 100 µL aliquots of the bacterial suspensions exposed to PANDAs were transferred into 96-well microplates prefilled with 200 µL of MHB and serially diluted. The inoculated microplates were incubated for 48 h at appropriate growth temperature, after which the turbidity was measured with a BioTek Synergy 2 microplate reader. An optical density at 600 nm of ≥ 0.05 was considered positive for bacterial growth. Populations of viable bacteria were calculated from the final dilution (terminal dilution, or TD), in which bacterial growth was observed using equation 1:

$$\frac{\mathrm{CFU}}{\mathrm{mL}} = \frac{10 \times 3^{\mathrm{TD}}}{1\mathrm{mL}} \quad (1)$$

Where TD is the terminal dilution factor obtained from microplate readings. The calculated CFU/mL was taken as the average of the 6 replicates and the experiment was repeated 3 times for each bacteria.

4.3.10 Evaluation of antifungal activity of PANDA disks

The antifungal activity of 90% pCBA PANDA disks was tested against several species of fungus using zone of inhibition method. The indicator microorganisms included Candida albicans and Trichoderma harzianum. Fungus cultures were adjusted to OD_{600} 0.1 for C. albicans and 10^5 ppg/mL for T. harzianum. Mueller Hinton II agar (MHA) plates have been spread with 100 μL of fungus culture and 25 mm^3 disks were placed on the plates. Zone of inhibition was measured after 72 hours of incubation at 30°C.

4.3.11 Resistance Development Study

This study was done using a slight modification of a method reported by Haldar and coworkers.[153] MIC values for 90% pCBA PANDA disks were determined for P. aeruginosa PAO-1 as described above. For the subsequent MIC determination, bacteria solutions were made by using bacteria from sub-MIC concentrations of the disks (at MIC/2). The bacteria solution was readjusted to ~10^5 via OD_{600} readings. Into 3 separate vials, 3 mL of adjusted bacteria solution was added along with disks of various sizes. After another 24 h incubation period, bacteria solutions again were made by using bacteria from sub-MIC concentrations of the disks (at MIC/2). The resistance development study was repeated twice, each with 20 total passages. The fold increase of MIC was reported.

4.3.12 MTT [3-(4,5-dimethylthiazol-2-yl)-2,5-diphenyltetrazolium bromide] cytotoxicity assay

The anti-proliferative activities of pCB and 90% pCBA PANDA degradation products in 3% DMSO solution were determined following a standard literature procedure.[154] Briefly, 48 hours prior to treatment, KB cells (100,000 cells/mL, 100 μL)

were seeded in a 96 well plate (Corning Inc.). Cells were treated with 50 μL of pCB and 50 μL of PANDA byproducts (media from 7 days incubation at pH 7.4). KB cells treated with 3% DMSO solution served as control. Cell proliferation was determined via a standard MTT assay (Vybrant MTT Cell Proliferation Assay Kit; Invitrogen). Cells were incubated for 30 h before adding 10 μL of a 12 mM MTT reagent to each well. The cells were further incubated for an additional 4 h, followed by removal of the media and addition of 50 μL of DMSO. The absorbance was then determined utilizing a Biotek Synergy2 MultiMode Microplate Reader, experiment was performed in quadruplicate.

4.4 Results and Discussion

Initially, we synthesized an acyclic diallyl p-chlorobenzaldehyde acetal (pCBA) derived from pCB. For proof-of-concept, pCB was selected from several possible benzaldehyde derivatives with known antimicrobial activity.[155-156] Benzylic aldehyde derivatives are known to exert antimicrobial activity through a variety of mechanisms, specifically, inhibition of H^+-ATPase-mediated proton pumping activity, Schiff base/thiazolidine formation with proteins/peptides, and membrane disruption.[157-158] We synthesized pCBA in acceptable yields *via* acid-catalyzed condensation of pCB with allyl alcohol ($^1H/^{13}C$ NMR Figure B.1-B.2). The antimicrobial activity of pCBA and pCB were evaluated via a zone of inhibition (ZOI) assay with clinically isolated strains of *E. coli* ATCC 43895 [serotype O157:H7], *S. aureus* RN6390, *B. cenocepacia* K56-2, and *P. aeruginosa* PAO1 (Figure B.3). At the highest tested concentration (10 mg mL^{-1}), pCBA exhibited no apparent antimicrobial activity. In contrast, pCB showed significant inhibition at 0.5 mg mL^{-1} – results that indicate the acyclic acetal functions as a pro-antimicrobial compound with antimicrobial efficacy only upon hydrolysis to the aldehyde.

UV-curable PANDA resins were then formulated with a photoinitiator, pentaerythritol tetramercaptopropionate (PETMP), and varied concentrations of pCBA relative to non-degradable 1,3,5-triallyl-1,3,5-triazine-2,4,6-trione (TTT) with 1:1 alkene:thiol mole stoichiometry (Figure 4.1). Following exploratory experiments, we focused primarily on PANDAs synthesized from a 90:10 pCBA:TTT monomer feed as proof-of-principle. This composition results in PANDA materials comprised of ~45 wt.% pCBA. PANDAs were photopolymerized in the absence of solvent under a medium-pressure UV light (200 mW cm^{-2}). Polymerization kinetics, investigated using real-time FTIR, were rapid with near quantitative conversions (>95%) observed for both thiol and alkene functional groups within 5 min (Figure 4.2a). The resulting PANDAs are transparent, low modulus thermosets with a glass transition temperature (T_g) at 0.5 °C (Figure 4.2b). Although not presented in detail here, the concentration of TTT can be used to facilely tune the physical properties of the network (i.e., T_g, flexibility, degradation, etc.).

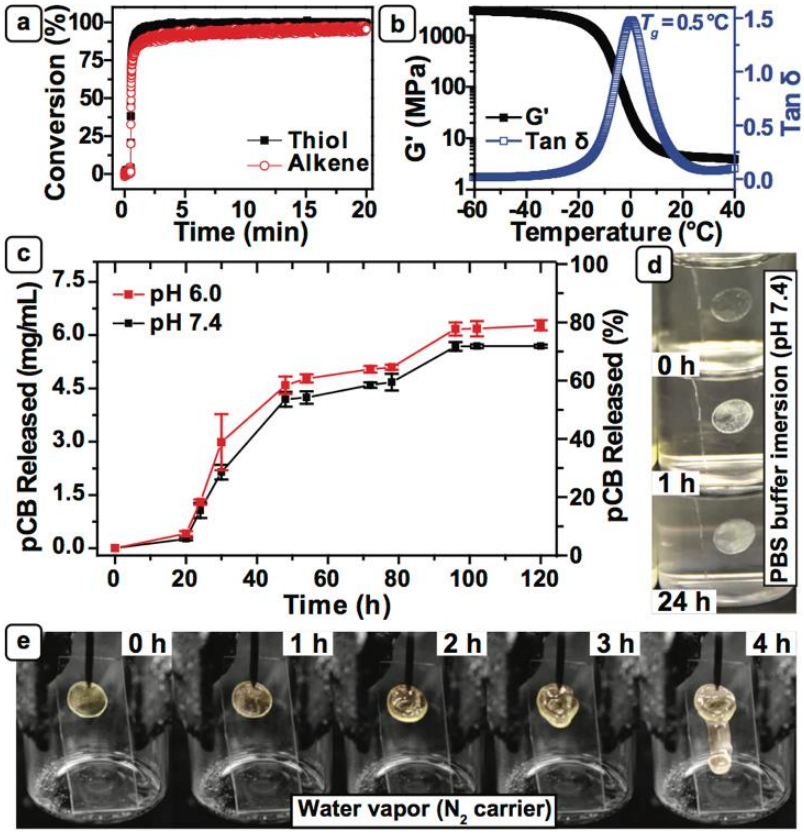

Figure 4.2 Cure kinetics, thermomechanical properties, release kinetics and degradation behavior of PANDAs. (a) Conversion kinetics for 90% pCBA resins cured at 200 mW cm^{-2} UV light. (b) Representative thermomechanical plot of the 90% pCBA PANDA. (c) Correlation between pCB released and incubation time at pH 6.0 and pH 7.4. (d) Time-lapse macroscopic images of degradation of 90% pCBA disks submerged in PBS (pH 7.4) and (e) placed within a 90% humidity chamber under N_2 at 25 °C. (Image contrast enhanced for visibility). Error bars indicate the SD (n=5).

PANDA degradation and subsequent release of pCB were investigated at pH 7.4 and 6.0 by submerging sample disks (25 mm^3) in phosphate buffer solution (PBS) containing octanol to partition the aldehyde. Aliquots from the octanol phase were analyzed via UV-vis spectroscopy to determine the concentration of pCB released over time. Figure 4.2c shows the pCB release profile at pH 7.4 and 6.0. At physiological pH, a 20 h lag time was observed before pCB was slowly released from the polymer network, with 14% (1.07 mg mL^{-1}) and 53% (4.19 mg mL^{-1}) pCB release observed at 24 h and 48 h, respectively.

Similar trends were observed at pH 6 with faster release kinetics, as expected, given the rate of acetal hydrolysis is proportional to the H_3O^+ concentration.[159] After 120 h, 72% and 80% pCB release was observed for pH 7.4 and pH 6.0, respectively. The photo series in Figure 4.2d shows the sample disks immersed in PBS buffer solution (pH 7.4) as a function of time. Shortly after immersion, the samples change from transparent to opaque white, but retain their shape with receding dimensions over time. The observed release and degradation behavior are consistent with a surface erosion process (typical of polyacetals), and may be expected given that these materials are relatively hydrophobic (static water contact angle $\approx$ 90°).[160-161] The degradation behavior of these materials becomes exceedingly more interesting when exposed to water vapor (rather than bulk immersion). Figure 4.2e shows a photo series of PANDA disks subjected to a gentle flow of 90% humidity within a scintillation vial (using N_2 as a carrier for water vapor to avoid acidification from CO_2). Within 2 h, the PANDA disk hydrolyzed to a point where viscous flow of the sample was observed. At 4 h, the degradation byproducts are shown flowing down the supporting substrate. The rapid progression from an infinite polymer network to viscous flow of low molecular weight degradation products is a consequence of the thiol-ene step polyaddition mechanism – a process that ensures most crosslink junctions contain a degradable linkage and precludes the formation of high MW linear degradation products found in chain growth networks.[162-163] Notably, these observations point to a rapid bulk degradation process and suggest a vast difference in water vapor permeability (under high humidity) and liquid water permeability (under immersion) that may be exploited in the synthetic design of humidity-triggered degradable materials. The increased permeability towards water vapor is a phenomenon commonly observed in crosslinked

poly(dimethylsiloxane) microfluidic chips which gradually lose water due to evaporation.[164] Furthermore, qualitative retarded degradation (Figure B.4). Experiments are underway to quantify the degradation behavior under vapor conditions.

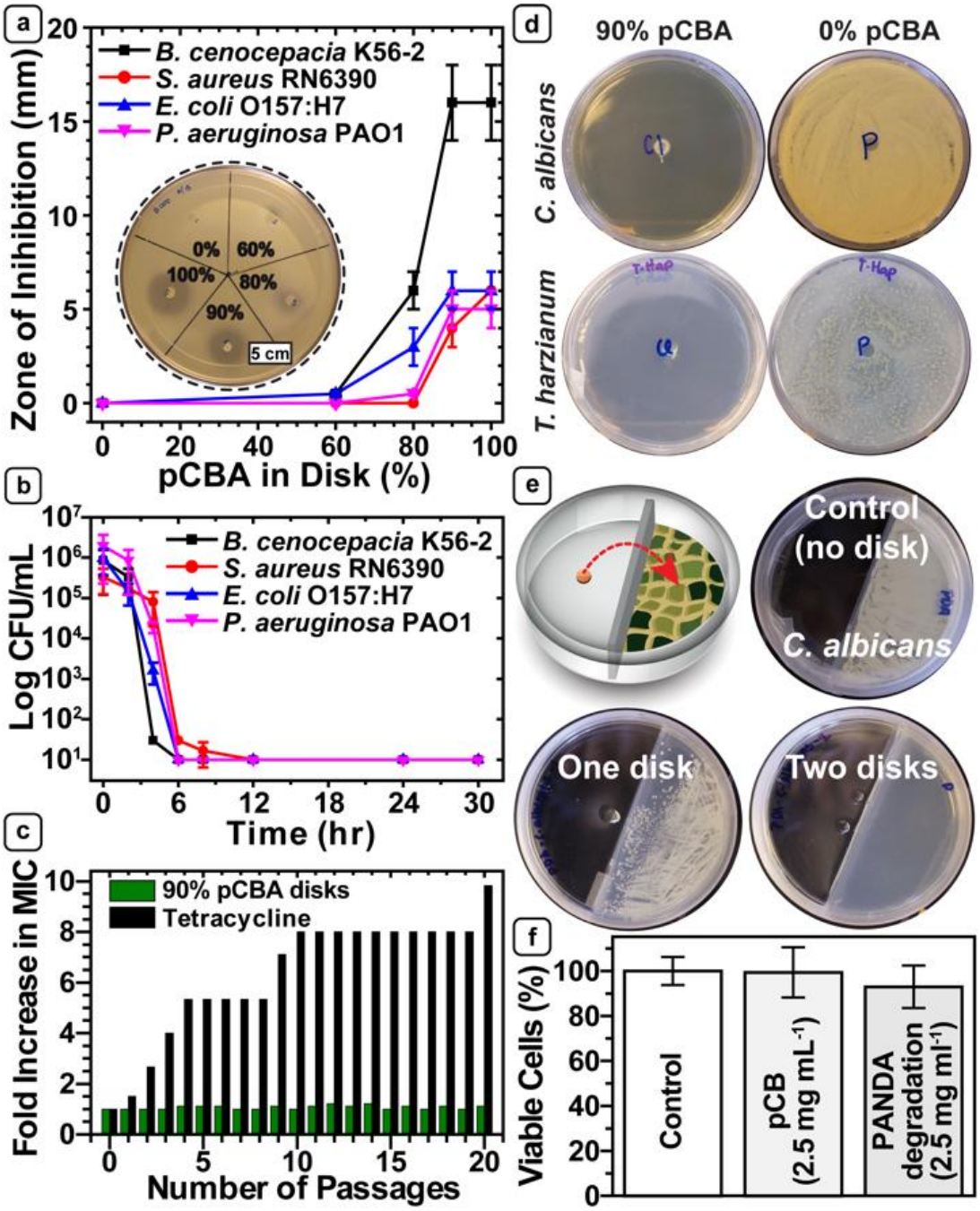

Figure 4.3 Antimicrobial activity and cytocompatibility assays. Error bars indicate the SD (n=5). (a) Correlation between zone of inhibition and % pCBA in disk after 24 h

incubation. (b) Kill kinetics of four bacteria in the presence of 90% pCBA PANDA via terminal dilution assay. (c) Bacterial resistance study of the 90% pCBA PANDA and tetracycline against P. aeruginosa. (d) Zone of inhibition diffusion assay of 0% and 90% pCBA PANDAs against C. albicans and T. harzianum. (e) Split plate diffusion assay of 90% pCBA PANDA disks against C. albicans after 30 days. (f) Cell viability assay for control (DMSO), pCB, and degraded 90% pCBA PANDA.

The synthetic design of PANDAs is motivated by the potential use of these materials in antimicrobial/ antifungal applications. The antimicrobial activity of PANDAs was initially evaluated via a ZOI assay with clinically isolated strains of *E. coli* ATCC 43895 [serotype O157:H7], *S. aureus* RN6390, *B. cenocepacia* K56-2, and *P. aeruginosa* PAO1. As shown in Figure 4.3a, PANDAs containing 0% pCBA showed no ZOI, as expected, and serve as a control for the assay. PANDAs containing >60% pCBA exhibited ZOIs, with larger ZOIs observed for all bacteria with increasing concentration of pCBA (relative to TTT) in the polymer network. The antimicrobial efficacy of the 90% pCBA PANDA material was further investigated using a terminal dilution assay to quantify kill kinetics. Two 25 mm^3 90% pCBA PANDA disks (3.6 mg mL^{-1} pCBA released within 24 h) exhibited more than a 5 log reduction in bacteria count in < 12 h against *E. coli*, *S. aureus*, and other pathogens (Figure 4.3b), which translates into kill efficiencies of >99.999%. In interest of developing strategies and materials to mitigate the development of antimicrobial resistance, we evaluated the potential emergence of bacterial resistance of *P. aeruginosa* against pCBA-based PANDAs using a serial passage mutagenesis assay. For comparison, the same assay was performed using tetracycline. Figure 4.3c shows the inability of *P. aeruginosa* to develop resistance toward pCB released from PANDA disks after 20 serial passages as indicated by the absence of an increase in the MIC (25 mm^3 disk $\approx$ 1.3 mg mL^{-1} pCB released within 24 h). We note that the concentration of pCB released

from the disk after 24 h is comparable to the small molecule MIC at 1.25 mg mL^{-1}. In contrast, the MIC value for tetracycline increased after only two passages, with a 10-fold increase in MIC after 20 passages. The results suggest that *P. aeruginosa* has less propensity to develop resistance against the pCB released from pCBA-based PANDAs, which highlights the potential of PANDAs for use as part of a broader strategy to slow or mitigate the development of antimicrobial resistance.

To further probe the broad-spectrum activity of pCBA PANDAs, we performed zone of inhibition experiments against two opportunistic pathogenic fungi (*C. albicans* and *T. harzianum*).[165-166] Placement of a 25 mm^3 90% pCBA PANDA disk resulted in complete inhibition of both fungi whereas the same size disks containing 0% pCBA exhibited no measurable antimicrobial activity (Figure 4.3d). Borrowing from the known inhibitory activity of volatile EOs, we exploited the inherent volatility of pCB to inhibit *C. albicans* – a pathogenic fungus responsible for up to 65% of all candidiasis cases in humans – via a split plate inhibition volatility assay.[166] As shown in Figure 4.3e, 25 mm^3 90% pCBA PANDA disks were placed on one side of a 9 cm split Petri dish with *C. albicans* plated on agar on the opposite side. The dish was sealed and incubated for 30 days. In the absence of PANDA disks (control), zero inhibition was observed. Partial inhibition was observed with one disk, while the growth of *C. albicans* was completely inhibited by two disks for up to 30 days. These experiments exploit the humidity-triggered degradation and volatility of pCB for non-contact control of fungus. Finally, KB cells (a type of HeLa cells), derived from a glandular cancer of the cervix were used as a model cell line for cytotoxicity.[167] Incubation of the KB cells with a degraded 90% pCBA disk (e.g. media containing PANDA degradation products after 7 days at pH 7.4, equivalent to 2.5 mg mL^{-1} pCB) and

small molecule pCB at the same concentration showed no significant toxicity (>90% viability) to KB cells (Figure 4.3f).

In summary, we have demonstrated the proof-of-principle for pro-antimicrobial networks via degradable acetals. PANDAs undergo degradation under mild conditions to release pCB – a small molecule active that serves as a potent antimicrobial agent against a broad spectrum of microbes. The humidity triggered degradation and volatile release of pCB was exploited to inhibit the growth of *C. albicans* without the need for direct contact. Importantly, the broad spectrum antimicrobial efficacy was achieved with minimal cytotoxicity towards KB HeLa cells. Solvent-free, room temperature photopolymerization provides a rapid, one-pot approach to crosslinked polyactives with excellent potential for advanced processing techniques, including 3D printing. The PANDA approach presented here is readily applicable to other bioactive aldehydes pointing to the potential use of these materials within pharmaceutical, biomedical, and agricultural industries.

4.5 Conclusions

We have reported that PANDAs, building upon linear "polyactives", represent a new paradigm for sequestration and triggered release of volatile, bioactive aldehydes. As proof-of-concept, we showed that PANDAs derived from diallyl p-chlorobenzaldehyde acetal and pentaerythritol tetramercaptopropionate degrade and release p-chlorobenzaldehyde (pCB) as an antibacterial and antifungal agent under mild conditions (pH 7.4/high humidity). Notably, the thiol-ene step polyaddition process ensured that most crosslink junctions contain a degradable acetal linkage enabling rapid progression from an infinite polymer network to low molecular weight degradation products. We showed that PANDAs enable facile access to materials sequestering up to 50 wt% pCB with tunable

release profiles, potent antimicrobial activity against Gram positive and Gram negative bacteria without triggering antimicrobial resistance, and minimal cytotoxicity. We also demonstrated the utility of PANDA materials by exploiting humidity-triggered degradation and volatile release of pCB from the polymer network for vapor-phase inhibition of *Candida albicans* – where a 50 µL PANDA disk provided 30 days of inhibition. To our knowledge, this represents a first example of the pro-antimicrobial approach manifested in the form of crosslinked polymer networks exhibiting broad spectrum antimicrobial activity. Significantly, the PANDA approach is readily applicable to sequestration and release of other bioactive aldehydes and is translatable to various material geometries (e.g., particles, thin films, printable scaffolds) pointing to potential use of these materials within pharmaceutical, biomedical, and agricultural applications.

CHAPTER V – A BIO-BASED PRO-ANTIMICROBIAL POLYMER NETWORK VIA DEGRADABLE ACETAL LINKAGES

5.1 Abstract

The synthesis of a fully degradable, bio-based, sustained release, pro-antimicrobial polymer network comprised of degradable acetals (PANDA) is reported. The active antimicrobial agent – p-anisaldehyde (pA) (an extract from star anise) – was converted into a UV curable acetal containing pro-antimicrobial monomer and subsequently photopolymerized into a homogenous thiol-ene network. Under neutral to acidic conditions (pH < 8), the PANDAs undergo surface erosion and exhibit sustained release of pA over 38 days. The release of pA from PANDAs was shown to be effective against both bacterial and fungal pathogens. From a combination of confocal microscopy and transmission electron microscopy, we observed that the released pA disrupts the cell membrane. Additionally, we demonstrated that PANDAs have minimal cytotoxicity towards both epithelial cells and macrophages. Although a model platform, these results point to promising pathways for the design of fully degradable sustained-release antimicrobial systems with potential applications in agriculture, pharmaceuticals, cosmetics, household/personal care, and food industries.

5.2 Introduction

With the increasing prevalence of antimicrobial resistance (AMR), opportunistic pathogens pose a significant global crisis. Compounding the issue, over 23.5 million immunocompromised patients (i.e. patients with rheumatoid arthritis, HIV, organ transplants, etc.) are prescribed immunosuppressants, making them more prone to both fungal and bacterial infections [168]. For instance, the fungus *Histoplasma capsulatum*

aggressively infects immunocompromised patients with over 500,000 cases annually in the United States, 300,000 of which are HIV-related infections resulting in 10,000 deaths per year [169]. Additionally, exposure to other common pathogens such as *Pseudomonas aeruginosa*, *Escherichia coli*, *Salmonella* Typhi, and *Staphylococcus aureus* can escalate into life threating infections resulting in sepsis and death [170-171]. To combat AMR, new antimicrobial strategies with low propensity to trigger resistance have been developed including quorum sensing inhibitors [172], synergistic pairing to induce sensitivity [173-174], antibiotic adjuvants [175], antibiotic cycling [176], and multimodal antibiotics [177-178]. Of the aforementioned methods, essential oils (EOs) – a unique class of naturally occurring, plant-derived extracts – hold promise in eradicating resistant microbial populations via the multimodal approach. EOs exhibit broad spectrum antimicrobial activity by interfering with membrane integrity, ATP synthesis, protein stability, and quorum sensing pathways [3, 16]. Despite positive results, the use of EOs is still restricted due to their limited water solubility, high volatility, and chemical instability [17]. Many approaches have been reported to sequester EO derivatives within polymeric materials; however, these strategies often utilize slow or non-degradable linkages which slowly release or permanently entrap EOs.

Poly(actives), or polymeric pro-drugs that rely on degradable linkages for the release of therapeutic agents, can improve chemical stability, enable tunable release profiles, and reduce volatility [24]. Multiple linear poly(actives) have been reported including poly(esters) [179-180], poly(anhydride-esters) [138, 181-187], poly(anhydride-amides) [188], poly(carbonate-amides) [189], poly(carbonate esters) [190], poly(ketals) [191], and poly(oxalate-acetals) [25]. While linear poly(actives) successfully entrap drugs and allow

for tunable release profiles, crosslinked poly(actives) represent a relatively unexplored class of degradable drug-releasing materials where opportunities for greater control over degradation profiles, thermomechanical properties, and sample geometry (particles, thin films, or coatings) are available. Recently, crosslinked poly(actives) including poly(esters) [144, 192-193], poly(β-amino esters) [194], and poly(acetals) [68] have utilized degradation rates, crosslink density, and hydropathy as mechanisms to control the release of actives. Of the degradable linkages available, both acetals and ketals have gained recent attention because of their charge-neutral and potentially nontoxic byproducts (alcohols and ketones/aldehydes) upon cleavage [195].

We have recently demonstrated the sequestration of p-chlorobenzaldehyde within a pro-antimicrobial network via degradable acetals (PANDA) [68]. While p-chlorobenzaldehyde is a relatively potent antimicrobial drug, we wanted to shift focus away from oil derived compounds and towards bio-based aldehydes found in nature to offer a fully degradable antimicrobial system based on essential oils. In this work, we turned towards p-anisaldehyde (pA), an extract from star anise (*Pimpinella anisum)* seeds, to fabricate a new class of antimicrobial PANDAs. We demonstrate that incorporation and subsequent release of pA from a PANDA exhibits potent antimicrobial activity against a variety of clinically relevant pathogens with minimal cytotoxicity.

5.3 Experimental

5.3.1 Materials

The chemicals p-anisaldehyde (pA), trimethylol propane diallyl ether, 2-hydroxy-2-methylpropiophenone (Darocur 1173), trimethylsilyl trifluoromethanesulfonate (TMSOTf), dichloromethane (DCM), allyloxytrimethylsilane, pyridine, sodium

bicarbonate, diethyl ether, magnesium sulfate ($MgSO_4$), dextrose, 2,3,5,6-tetrachloronitrobenzene, 3-(4,5-dimethylthiazol-2-yl)-2,5-diphenyltetrazolium bromide (MTT), hexane, 0.5 M Tris-HCl in H_2O, acetonitrile-d_3, Aqua Dead Cell Stain™, LIVE/DEAD BacLight Bacterial Viability Kit staining kit, BacLight RedoxSensor CTC Vitality Kit and ethyl acetate were acquired from Thermo Fisher Scientific. Pentaerythritol tetra(3-mercaptopropionate) (PETMP) was provided by Bruno Bock. Difco Agar, yeast extract, Bacto Tryptone, Mueller Hinton broth and agar, were from Becton, Dickinson and Company. Ham's F-12 and trypsin-EDTA were obtained from GIBCO. Hemin chloride (type II), protoporphyrin IX, histidine (free base), proline, 37% formaldehyde in H_2O, dimethyl sulfoxide (DMSO), fluconazole, fetal bovine serum (FBS), Dulbecco's Modified Eagle's Medium (DMEM) and N-2-hydroxyethylpiperazine-N'-2-ethanesulfonic acid (HEPES) was purchased from Sigma Aldrich. All the materials were obtained at the highest purity available and used without further purification unless otherwise specified.

5.3.2 Characterization Methods.

A Bruker Ascend 600 MHz (TopSpin 3.5) spectrometer was used to record $^{1}H/^{13}C$ NMR spectra with either chloroform-*d* or acetonitrile-d_3. High resolution mass spectroscopy (HRMS) was performed with positive electrospray ionization on a Bruker 12 Tesla APEX-Qe FTICR-MS with an Apollo II ion source. Dynamic mechanical analysis (DMA) was performed using a TA Instruments Q800 dynamic mechanical analyzer in tension mode equipped with a gas cooling accessory. Samples were clamped, evaluated at a strain of 1 %, and heated from -80 °C to 80 °C at a ramp rate of 3 °C min^{-1}. Kinetic data was obtained using real-time FTIR (RT-FTIR) spectroscopy by determining

the conversions of the thiol and ene functional groups. The RT-FTIR studies were conducted using a Nicolet 8700 FTIR spectrometer with a KBr beam splitter and a MCT/A detector with a 320–500 nm filtered ultraviolet light source. Each sample was exposed to a UV light with an intensity of 400 mW cm^{-2}. Series scans were recorded, where spectra were taken approximately 2 scan s^{-1} with a resolution of 4 cm^{-1}. Thiol conversion was monitored via integration of the SH peak between 2500-2620 cm^{-1} while the conversion of the alkene was monitored between 3050-3125 cm^{-1}. Optical density (OD) and fluorescence readings were performed in a BioTek Synergy 2 programmable microplate reader (BioTek Instruments).

5.3.3 Synthesis of p-anisaldehyde diallylacetal (pAA)

The synthesis of pAA was done using a slightly modified procedure from Noyori and coworkers [196]. To a flame dried 250 mL round bottom equipped with a stirbar, TMSOTf (200 µL, 1.1 mmol) was added along with 30 mL dry DCM under nitrogen at -84 °C. While maintaining the same temperature, a mixture of allyloxytrimethylsilane (37 mL, 208 mmol) and pA (12 g, 88 mmol) in 25 mL of dry DCM was added dropwise into the round bottom. The reaction turned yellow and stirred for 3 h. After, the reaction was warmed to -30 °C and stirred for 1 h (reaction turned red). The deep red mixture was then quenched with the addition of pyridine (15 mL, 74.5 mmol) and poured into 100 mL of saturated sodium bicarbonate prior to extraction with (3 x 100 mL) of diethyl ether. The organic layer was dried over anhydrous $MgSO_4$, then the excess solvent was removed under reduced pressure. The yellow oil was then purified via column chromatography using a mixture of hexane: ethyl acetate (9:1) and yielded a clear oil (13.6 g, 65.9 % yield). ^{1}H NMR ($CDCl_3$) δ 7.45 (dd), 6.93 (dd), 5.97 (m), 5.62 (s), 5.35 (dd), 5.17 (dd),

4.07 (d), 3.82 (s). ^{13}C NMR ($CDCl_3$) δ 159.66, 134.16, 130.68, 127.97, 116.67, 113.52, 100.29, 66.00, and 55.22. HRMS (ESI^+) m/z calculated for $C_{14}H_{18}O_3$ $[M+Na]^+$ 257.114816; Found 257.114817.

5.3.4 General preparation of PANDA disks

The PANDA disks were prepared by adding PETMP and pAA at 1:1 ratio of SH:alkene, along with 4 wt.% of Darocur 1173. The mixtures were well mixed and 25 μL of the monomer formulations were aliquoted onto a glass slide and covered with another glass slide spaced with Teflon spacers (0.76 ± 0.02 mm in thickness). The samples were then cured using an Omnicure S1000-1B with a 100W mercury lamp (λmax = 365 nm, 320–500 nm filter) at an intensity of 400 mW cm^{-2} for 40 seconds. Control disks were prepared following the same procedure by using PETMP and trimethylol propane diallyl ether at 1:1 ratio of SH to alkene with addition of 4 wt.% of Darocur 1173..

5.3.5 Degradation of PANDAs

The hydrolysis of PANDA disks was analyzed via ^1H NMR under a pH 7.4 Tris-HCl buffered water:acetonitrile-d_3 solution. First 2,3,5,6-tetrachloronitrobenzene (internal standard) was weighed into a vial along with 500 μL of acetonitrile-d_3. Then 125 μL of 100 mM Tris-HCl in deionized water was added and mixed. A 5 mm^3 disk and 500 μL of the acetonitrile:buffer solution was added to an NMR tube and sealed. Three replicates were prepared for each data point (with mean and standard deviation reported) and NMR spectra were taken over 38 days. To calculate the concentration released of different sized PANDA disks (5-100 mm^3), the grams of pA released (at 24 and 48 h from a 5 mm^3 disk) were multiplied by a factor to equal the desired PANDA disk size (e.g. x10 for a 50 mm^3 disk) and divided by the total volume the disk was placed into. Since the thickness of the

PANDA disks does not change, this assumption is valid, however the degradation profile in the presence of microbes may not be the same as pH 7.4 PBS, yet remains our best estimate.

5.3.6 Evaluation of antibacterial activity of PANDAs

5.3.6.1 Zone of inhibition (ZOI) assay

The antimicrobial activity of PANDA disks was tested against several species of bacteria via the zone of inhibition method. The indicator microorganisms included Escherichia coli ATCC 43895 (serotype O157:H7), Staphylococcus aureus RN6390, Salmonella enterica serovar Typhi ATCC 6539 (S. Typhi), and Pseudomonas aeruginosa PAO1. The testing was done on Mueller Hinton II agar (MHA) plates that have been overlaid with soft agar seeded with individual bacterial strains. The soft agar contained (per liter): 10 g of Bacto Tryptone, 6 g of Difco agar, and 8 g of sodium chloride. To create an overlay, the indicator organisms were grown overnight at 37 °C in Mueller Hinton II broth (MHB). The overnight cultures were diluted 1:5 with fresh MHB, and mixed with molten soft agar to achieve a ~10^8 CFU mL^{-1} density. From this mixture, 4 mL aliquots were overlaid onto MHA base plates and allowed to completely solidify. After solidification of the soft agar, 50 mm^3 disks were overlaid on the plates and incubated at 37 °C. The zones of inhibition (ZOI) were measured after 24 h and reported as the distance from the edge of the disk to the edge of the zone. Three replicates were carried out for each disk/bacterial strain. with the mean and standard deviation reported (experiment was repeated twice).

5.3.6.2 Minimum inhibitory assay

Minimum size of PANDA disks required to inhibit bacterial growth were determined using a modified broth macrodilution method. Briefly, overnight bacterial cultures in MHB were adjusted to ~10^5 CFU mL^{-1}. PANDA disks of different sizes (5-100 mm^3) were added to 4 mL of bacterial solutions. The tubes were then incubated at 37 °C and shaken at 200 rpm for 24 h. Bacteria suspended in MHB served as a positive control, while MHB without bacterial inoculum served as a negative control. The inoculated tubes were assessed by measuring optical density at 600 nm after 24 h where OD < 0.05 considered negative for bacterial growth. Three replicates were carried out for each disk size and bacterial strain. with the mean and standard deviation reported (experiment repeated twice).

5.3.6.3 Kill kinetics via track dilution assays

To compare the rate of bacterial killing by PANDA disks, the test organisms were exposed to 100 mm^3 PANDA disk and the number of viable bacteria was determined by a modified kinetic track dilution method [197]. Individual disks were submerged in 4 mL aliquots of bacterial cultures adjusted to ~10^5 CFU mL^{-1} as described above and incubated at 37 °C with shaking (200 rpm). Bacterial populations were determined immediately after the addition of disks (0 h), and at 4, 8, 16, 24, 30, and 48 h of exposure. For the track-dilution technique, Falcon 15-mm square plates with 13-mm grids (Becton Dickinson Labware) were used. At each time point, six 20 µL aliquots of the bacterial suspensions exposed to PANDAs were transferred into 96-well microplates prefilled with 200 µL of MHB and serially diluted 1 to 10 to reach a final dilution of 10^{-8}. From inoculated samples, 10 µL were spotted on the agar surface along one side of the square plate using a multichannel micropipette. The plate was tipped onto its side (at a 45°–90°

angle), to allow inoculum to migrate in parallel tracks across the agar and to dry for 1 min. The plate was then inverted and incubated for 24 h at 37 °C prior to colony counting. Bacteria suspended in 4 mL MHB served as a positive control, while MHB without bacterial inoculum served as a negative control. Three replicates were carried out for each time point and bacterial strain with the mean and standard deviation reported (experiment repeated twice).

5.3.6.4 Determination of respiratory activity

A BacLight RedoxSensor CTC Vitality Kit was used to evaluate respiratory activity of bacteria (adjusted to ~10^5 CFU mL^{-1}) exposed to either PANDA disks or control disks (100 mm^3) after a 24 h incubation at 37°C at 200 rpm. According to the manufacturer's protocol, 5-cyano-2,3-ditolyl tetrazolium chloride (CTC) (15 mg) was dissolved in 1 mL of sterile deionized water. Next, 180 µL of each sample was mixed with 20 µL of the CTC solution in a Corning™ 96-well solid black microplate and incubated at 37 °C for 30 min prior to reading with a BioTek reader equipped with a monochromator at 450 nm excitation and 630 nm emission.

5.3.6.5 Assessment of cell membrane integrity

Bacterial cell membrane integrity was evaluated using a LIVE/DEAD BacLight Bacterial Viability Kit. A 4 mL of ~10^5 CFU mL^{-1} *P. aeruginosa* was prepared and exposed to a 100 mm^3 PANDA disk, prior to incubation at 37 °C with constant shaking (200 rpm). From each inoculated sample, 100 µL aliquots of the bacteria from the PANDA treatment were transferred into a Corning™ 96-well solid black microplate, and mixed with 100 µL of the LIVE/ DEAD BacLight staining reagent. The samples were taken at 0 and 30 h and incubated in the dark for 15 min. The fluorescence was measured

using a 485/20 nm excitation filter (for both SYTO9 and propidium iodide) and two separate emission filters: 528/20 nm (SYTO9 emission wavelength) and a 620/40 nm (PI emission wavelength). For confocal imaging, 5 µL of the stained samples were cast onto separate microscope slides. Each sample was assayed in triplicate, and the experiment was repeated twice. From the inoculated sample, transmission electron micrographs were taken with a Zeiss 900 electron microscope operating at 50 kV and outfitted with a Model 785 Erlangshen ES1000 WCCD camera (Gatan). Samples were applied to 200 mesh copper grids (3.05 mm, 200 lines per inch square mesh, Electron Microscopy Sciences) coated with Formvar (5% polyvinyl formal resin).

5.3.7 Determination of antifungal activity

5.3.7.1 Zone of inhibition assay

The wild-type *Histoplasma capsulatum* G217B (ATCC 26032) strain was used in this study. Liquid *H. capsulatum* yeast cultures were grown to mid-log (OD_{600} ~1.4-1.9) in Histoplasma macrophage medium (HMM) [198] and enumerated using a hemocytometer (Incyto C-Chip). Once quantified, 1.0×10^7 cells were spread in triplicate onto pre-warmed solid HMM plates and allowed to dry for 1 h before PANDA disks (50 mm^3) were overlaid in the center of each plate. After 4 days of incubation at 37 °C in 5% CO_2 / 95% room air, images were captured using a DinoLite microscope camera and zones of inhibition were measured using the DinoLite software. For a negative control, a control disk was added, whereas, the positive control contained 4 mg fluconazole. Three biological replicates were used to calculate mean and standard deviation (experiment repeated twice).

5.3.7.2 Determination of minimum inhibitory concentration (MIC)

Four-day-old H. capsulatum yeast cultures were diluted 1:5 and grown overnight at 37 °C in 5% CO_2 / 95% room air with shaking (200 rpm). Cells were then diluted with pre-aerated, pre-warmed HMM to a final OD_{600} of 0.1. Various sizes of PANDA disks (0-45 mm^3) were added to 50 mL aliquots of the diluted yeasts as described above. The cultures were then incubated for a total of 7 days. Every 24 h, 1 mL aliquots of each culture were transferred to disposable plastic cuvettes and OD_{600} was measured using a BioTek reader. After 7 days, a growth curve of OD_{600} vs. time was generated to determine MICs. The experiment was repeated twice.

5.3.7.3 Fungal viability

For LIVE/DEAD staining of H. capsulatum yeast-phase cells, 1 mL aliquots of a mid-log phase culture of H. capsulatum challenged with either 45 mm^3 control or PANDA disks was centrifuged at 1000 × g for 5 min, washed once with PBS, and re-suspended in PBS. Next, cells were enumerated via hemocytometry and diluted to 1 x 10^6 cells per mL. At this point Aqua Dead Cell Stain™ was added to the cell suspension in a final dilution of 1:1000 and incubated for 30 min at room temperature in the dark. Once labelled, the cells were washed with PBS and fixed with 37% formaldehyde for 15 min at room temperature. Flow cytometry was performed on a BD Accuri C6 Flow Cytometer using an excitation wavelength of 405 nm with emission capture at ~525 nm. A gate was then applied and viability assessed by analyzing the shift in fluorescent intensity. To qualitatively assess fungal viability, the same labelled cells were analyzed on a Zeiss LSM 510 Meta confocal microscope at 40x magnification using both differential interference contrast and 405 nm laser excitation.

5.3.7.4 Direct contact mammalian cell viability

To assess the effects of the PANDAs directly on host cells, a direct contact assay based on ISO 10993-5 with MTT was used to quantify viability of RAW 264.7 murine macrophages and VERO epithelial cells (isolated from kidney) after the addition of either control (1.5 mm^3) or PANDA disks (0.5, 1.0, and 1.5 mm^3) [199]. Cells with no additional supplementations were used as a control. Six replicates were measured to calculate percent survival and standard deviation. The MTT assay was carried out per the manufacturer's protocol (Thermo Fisher) with modifications to adapt the assay from the standard 96-well plate to a 24-well cell culture plate. Both RAW 264.7 and VERO cell lines were maintained in 20 mL DMEM supplemented with 10% FBS, 50 µg mL^{-1} ampicillin, 4.5 mg mL^{-1} glucose, 584 µg mL^{-1} L-glutamine, and 100 µg mL^{-1} streptomycin in T-150 culture flasks (Sigma). Cells were incubated at 37 °C in 5% CO_2. Briefly, cells were grown to confluence and detached from the culture flask with trypsin-EDTA and centrifuged briefly at 200 × g for 5 min. They were then re-suspended in 1 mL DMEM and enumerated using a hemocytometer. The cells were diluted to 5.0 x 10^4 cells mL^{-1} and 1 mL aliquots were added to each well of a 24-well cell culture plate (Sigma). Once the culture reached subconfluency (~80% confluency) in the 24-well plate, 1.5 mm^3 disks were overlayed on the cells and allowed to incubate for 24 h at 37 °C in 5% CO_2. After the incubation, all media were removed from the wells and replaced with 500 µL of Dulbecco's phosphate-buffered saline (DPBS), pH 7.5. 50 µL of 12 mM MTT was then added to each well and incubated at 37 °C for 2 h. After labelling the cultures with MTT, all but 250 µL of DPBS/MTT mixture was removed from the wells. To solubilize the MTT dye, 500 µL of DMSO was added to each well and mixed thoroughly before

incubating at 37°C for 10 min. Lastly, each 24-well plate was mixed and absorbance was read at 540 nm. Experiment was repeated twice.

5.3.7.5 Statistical Analysis

All measurements were made in triplicate unless otherwise stated and each experiment was performed on at least two separate occasions; the results are expressed as the average of the parallel assays with error bars representing a standard deviation from the mean."

5.4 Results and Discussion

5.4.1 Monomer synthesis and PANDA fabrication/properties

As shown in Scheme 5.1A, the acyclic diallyl p-anisaldehyde acetal (pAA) was synthesized in modest yields (66% after column) through Noyori's acetal forming procedure by the reaction of allyloxytrimethylsilane with pA in the presence of TMSOTf (^{1}H NMR, Fig. 5.1A) [196]. To assess the pro-antimicrobial nature of pAA, 10 µL of pure pAA and pA were placed on plates overlayed with *S.* Typhi (Scheme 5.1A). After 24 h of incubation, pAA showed no apparent zone of inhibition indicating no antimicrobial activity. In contrast, pA showed a 1 cm zone of inhibition indicating that pAA functions as a pro-antimicrobial compound only exhibiting antimicrobial activity upon hydrolysis back to pA.

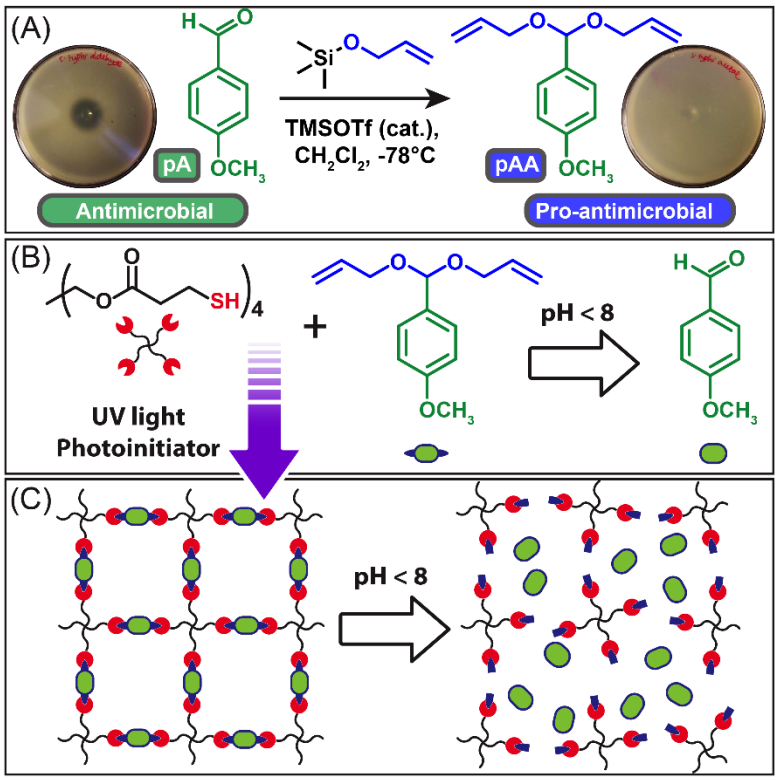

Scheme 5.1 Overview of monomer synthesis and PANDA fabrication. (A) Synthesis of pro-antimicrobial pAA from antimicrobial pA. Antimicrobial properties of pAA/pA are indicated by a zone of inhibition assay against *S.* Typhi. (B) Monomers used to synthesize the PANDAs via thiol-ene photopolymerization and acid mediated transformation of pAA to pA. (C) Schematic depiction of PANDA degradation mechanism.

To fabricate PANDAs, pentaerythritol tetrakis(3-mercaptopropionate) (PETMP), photoinitiator and pAA were copolymerized with 1:1 alkene/thiol mole stoichiometry via radically mediated step-growth thiol-ene photopolymerization (Scheme 5.1B). The fabricated PANDAs are comprised of 47 wt.% pAA which corresponds to 27 wt.% pA loading. The polymerization kinetics are rapid and exhibit nearly quantitative monomer conversion (>95%, Fig. 5.1B) for both thiol and alkene functional groups within seconds under a medium pressure UV light (400 mW cm^{-2}). The step-growth polymerization ensures that each crosslink junction contains a hydrolytically cleavable acetal linkage for the release of pA from the network (Scheme 5.1C). Additionally, the resulting PANDAs

possess a narrow tan δ (indicative of a homogenous network), a glass transition temperature of -0.5 °C (Fig. 5.1C), and are optically transparent – typical of thiol-ene materials [33].

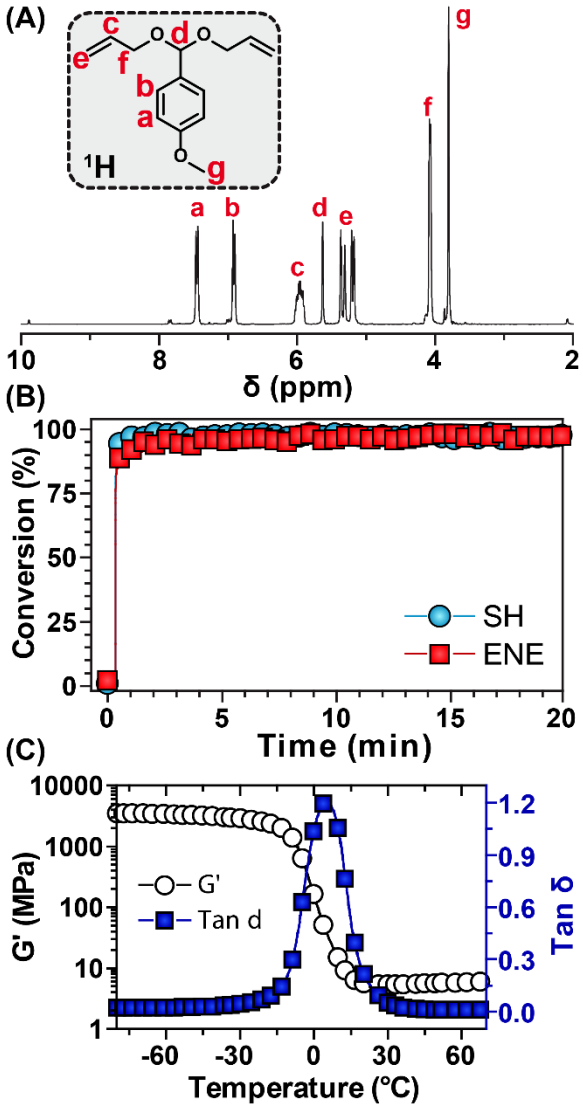

Figure 5.1 Monomer structure, cure kinetics, and final network properties. (A) ^{1}H NMR spectra of pAA. (B) Real-time FT-IR of SH and ene conversion during photopolymerization. (C) Dynamic mechanical analysis of the resulting PANDA.

5.4.2 PANDA release kinetics

The release kinetics of pA from the PANDAs were monitored via ^{1}H NMR spectroscopy over 38 days at pH 7.4 by submerging disks in buffered solutions in acetonitrile-d_3 within

sealed NMR tubes. An internal standard, 2,3,5,6-tetrachloronitrobenzene (δ = 7.75 ppm), was added to the buffered solution and integrated relative to the benzylic aldehyde proton (δ = 9.85 ppm) to determine the concentration of pA over time (Fig. 5.2A). Figure 5.2B shows the release profile of pA from the integrated ^{1}H NMR results. At physiological pH, no burst release was observed and 90% pA was released after 38 days. The release profile was then fit to the cylindrical Hopfenberg model [200] described as:

$$\frac{M_t}{M_\infty} = 1 - \left[1 - \frac{k_0 t}{C_0 a}\right]^2$$

where, M_t is the concentration of released pA at time *t*, M_∞ is the theoretical maximum of pA released, k_0 is the erosion rate constant, C_0 is the initial concentration of drug in the matrix, and *a* is the initial radius of the cylinder. From the Hopfenberg model, the half-life was determined to be 14.9 days and the fit was in good agreement with the release data as indicated by an r^2 value of 0.989. To verify the surface erosion of the PANDAs, control (PETMP and trimethylolpropane diallyl ether) and PANDA disks were fabricated, immediately submerged in a 1N aqueous HCl solution, and imaged over time. Within 1 h, significant surface erosion was visually observed as noted by the degradation front highlighted by the green arrows in Figure 5.2C. Due to the immiscibility of the degradation byproducts in water, the solid disk gradually transitions to an oil-like residue within 3 h.

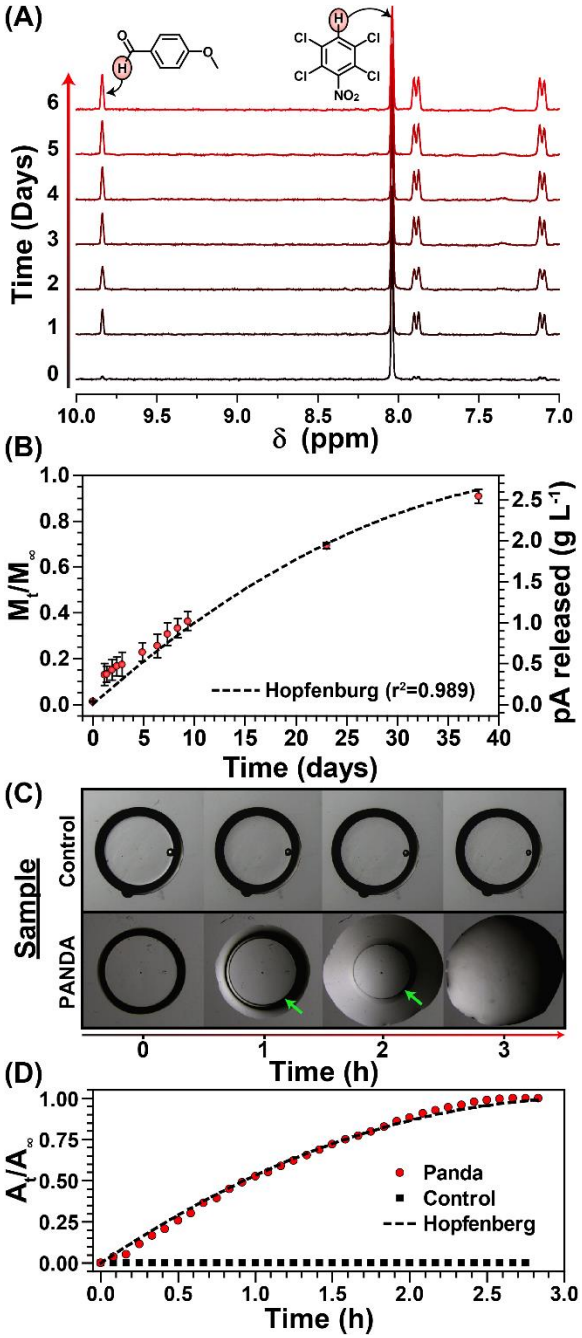

Figure 5.2 Degradation of PANDAs. (A) ^{1}H NMR degradation kinetics of PANDA at pH 7.4. (B) Cumulative release of pA from PANDA subjected to pH 7.4. (C) Kinetic optical microscopy images of a PANDA disk submerged in 1 N HCl. Green arrows indicate remaining PANDA disk. (D) Calculated cumulative area from 1N HCl degradation kinetics determined by imageJ analysis.

A plot of the remaining disk area at time *t* (A_t) relative to the initial area (A_∞) was plotted overtime and then fit by the Hopfenberg model, where M_t/M_∞ were replaced by A_t/A_∞ (Fig. 5.2D). In comparison to the degradation at pH 7.4, the degradation at pH 0.1 was 380x faster (half-life = 0.04 days), indicating that PANDA degradation is acid sensitive. While small molecule model studies show that acetal degradation is generally 10 times faster with each unit of pH decrease[201], Liu *et al*. reported that crosslinked acetal network degradation follows small molecule degradation kinetics qualitatively[195]. Moreover, Garripelli and coworkers showed that acetal-based material degradation does not follow first order kinetics relative to the hydronium ion concentration[202]. The differences between network and small molecule degradation are likely attributed to differences in accessibility of the acid to each acetal as well as the hydropathy of the crosslinked network.

5.4.3 PANDA antibacterial activity

5.4.3.1 Bacterial inhibitory assays

The use of pA was motivated by its potent activity exhibited in screening experiments against pathogenic bacteria. The antimicrobial activity of 50 mm^3 PANDAs and control disks was initially evaluated via a ZOI assay with clinically isolated strains: *S. aureus* RN6390 and *P. aeruginosa* PAO1, and foodborne pathogens: *E. coli* ATCC 43895 (serotype O157:H7) and *S.* Typhi ATCC 6539 (Fig. 5.3A). In all cases, the control disks showed no inherent antimicrobial activity towards any bacteria, whereas zones of inhibition (>1 cm) were present for the PANDA disks. The ZOI assay showed that the order of antimicrobial inhibition was *S.* Typhi > *S. aureus* > *E. coli* O157:H7 > *P. aeruginosa*.

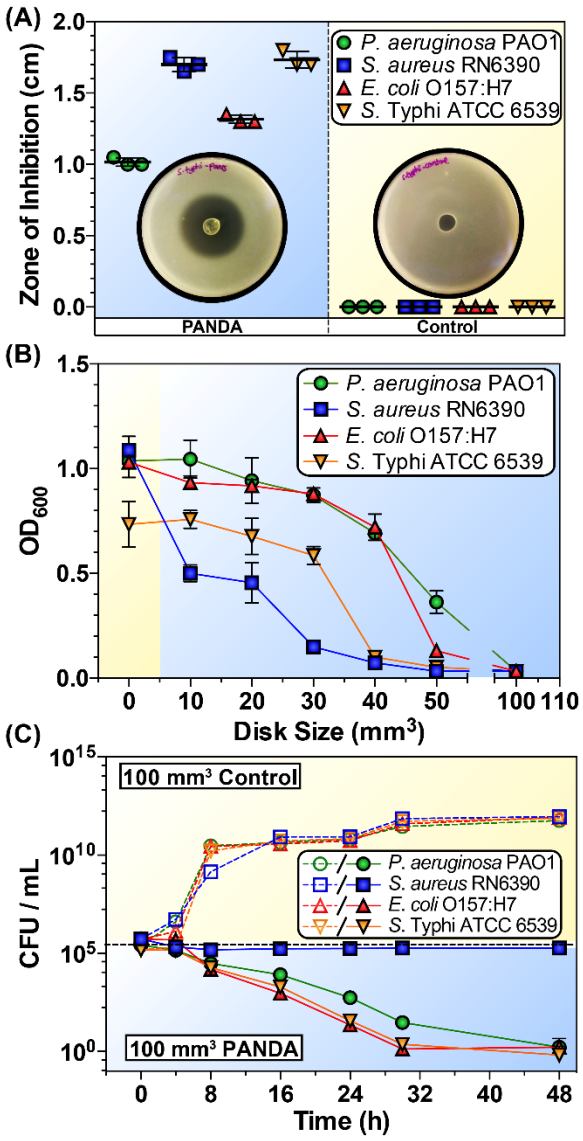

Figure 5.3 Antibacterial activity of PANDAs. (A) ZOI of PANDA and control disks. Plotted data points represent individual measurements. (B) Minimum inhibition assay of different sized PANDA disks. (C) Time-dependent killing of pathogens by 100 mm^3 PANDA disks. Data are representative of 2 independent experiments ± s.d.

To determine the PANDA disk size required to inhibit bacterial growth, a minimum inhibitory disk size assay was performed with exponentially grown bacteria (10^5 CFU mL^{-1} in 4 mL media) challenged with PANDA disks (0-100 mm^3). As shown in Figure 5.3b, an increase in disk size correlates with an increase in bacterial inhibition with a 100 mm^3 PANDA disk [910 µg mL^{-1} released after 24 h (determined from Fig. 5.2B)] completely

inhibiting the growth of all bacteria. The trend in bacterial susceptibility from the ZOI assay was also observed in the minimum inhibition assay with *E. coli* O157:H7 and *P. aeruginosa* requiring the largest PANDA disk (100 mm^3), while *S.* Typhi and *S. aureus* were inhibited by a 50 mm^3 PANDA disk [455 µg mL^{-1} released after 24 h (determined from Fig. 5.2B). These determined MICs are in good agreement with other inhibition studies involving pA [8].

5.4.3.2 Determination of bacteriostatic/bactericidal activity of PANDA disks

To examine the bactericidal activity of 100 mm^3 PANDA disks, the number of viable bacteria was quantified via a kinetic track dilution assay at 0, 4, 8, 16, 24, 30, and 48 h (Fig. 5.3C). The PANDA disk (1085 µg mL^{-1} pA released within 48 h) exhibited bactericidal activity with a >4 log reduction in bacteria count (>99.99% elimination) against *P. aeruginosa, E. coli*, and *S.* Typhi. However, the concentration of gram-positive *S. aureus* remained constant at 10^5 CFU mL^{-1}, indicating a bacteriostatic effect. Our results are in agreement with previous studies which have shown that the bactericidal/bacteriostatic activity is dependent on both EO concentration and bacterial species [203-204].

5.4.3.3 Evaluation of bacterial respiratory activity and membrane integrity

To investigate the antibacterial efficacy of PANDA disks (100 mm^3), a series of physiological assays along with micrographs were performed. The fluorogenic probe, 5-cyano-2,3-ditolyl tetrazolium chloride (CTC) was used to measure bacterial respiratory activity. Bacteria capable of respiration reduce CTC into CTC-formazan (CTF), an insoluble, fluorescent product that can be quantified via fluorescence readings. As shown in Figure 5.4A, in comparison to the control disks, bacteria treated with PANDAs showed

a 90-95% loss of fluorescence indicating a significant decrease in respiratory activity. Interestingly, with *S. aureus*, PANDAs had a bacteriostatic effect and the population remained unchanged despite the significant decrease in metabolic activity. The different response of bacteria to pA is not unprecedented as some antibiotics can act as both bactericidal or bacteriostatic agents [205]. Lobritz et al. [205] attributed the differences between the bactericidal or bacteriostatic modes of actions to the interference with cellular respiration. Bactericidal antibiotics cause an acceleration in respiration and basal metabolism that ultimately lead to cell death. In contrast, bacteriostatic antibiotics suppress cellular respiration and translation thus interfering with killing. It is plausible that the altered responses of *S. aureus* and the tested gram-negative species to pA are caused by the different effect of pA on metabolism in these microorganisms. We also investigated the effect of PANDA disks (100 mm^3) on membrane integrity of *P. aeruginosa* stained with SYTO9 and propidium iodide at 0 h and 30 h by confocal imaging. Green-fluorescing SYTO9 can penetrate intact and damaged bacterial membranes, whereas red propidium iodide enters only cells with damaged cytoplasmic membranes and displaces SYTO9, leading to red fluorescence when both dyes are present [206]. Prior to PANDA exposure (0 h), a majority of cells fluoresce green indicating intact membranes while after 30 h, a large number of cells fluoresce red denoting damage of the cytoplasmic membranes (Fig. 5.4B & 5.4C). To compliment the membrane integrity assay, transmission electron microscopy (TEM) was also used to image *P. aeruginosa* after 0 and 30 h of incubation with a PANDA disk. At 0 h, an intact membrane is clearly observed (Fig. 5.4D), however after 30 h, TEM shows the complete destruction of the cell membrane with crumpled cell envelopes (Fig. 5.4E). These results show that PANDAs lead to a loss of respiratory activity and damage

of cell membrane integrity, indicating that the pA released from PANDAs, can disrupt membrane and damage other metabolic functions as previously reported in literature [207-208]. Additionally, other labs have begun to elucidate the specific antimicrobial mechanism of pA with evidence demonstrating up/down regulation of genes critical for cellular survival [209], and rapid shiff-base formation with amines potentially present in peptides, proteins, and DNA/RNA [210].

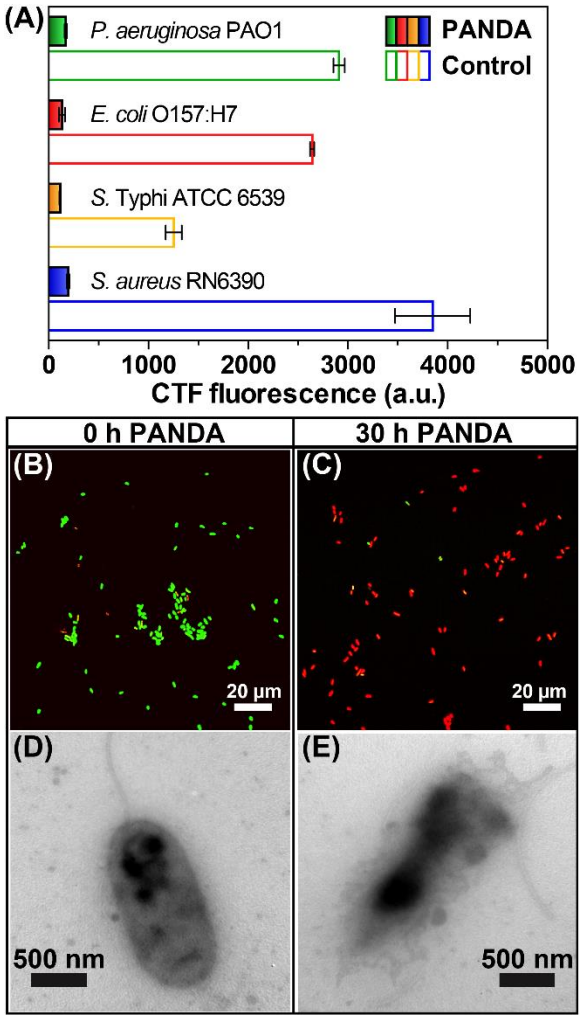

Figure 5.4 Antibacterial activity of PANDAs. (A) ZOI of PANDA and control disks. Plotted data points represent individual measurements. (B) Minimum inhibition assay of different sized PANDA disks. (C) Time-dependent killing of pathogens by 100 mm^3 PANDA disks. Data are representative of 2 independent experiments ± s.d.

5.4.4 Antifungal activity of PANDAs.

5.4.4.1 Fungal inhibitory assays

To further probe the broad spectrum antimicrobial activity of PANDAs, we performed a series of assays against the pathogenic fungus *H. capsulatum*. The invasive nature of *H. capsulatum* coupled with its resistance to most azole-based antifungal treatments makes the highly pathogenic *H. capsulatum* strain G217B, a model fungal system to assess PANDA activity.[211] As a preliminary experiment, a ZOI assay was performed with a 50 mm^3 PANDA and control disk on yeast-phase *H. capsulatum*. Complete inhibition of growth was observed with the PANDA treatment, whereas no measureable antifungal activity was detected for the control disk (Fig. 5.5A). To determine the minimum PANDA disk size required to inhibit *H. capsulatum*, PANDAs of various disk sizes (0-45 mm^3) were added to freshly passed cells, incubated, and every 24 h, optical density measurements were recorded to assess the growth kinetics (Fig. 5.5B). As the size of the PANDA disk increased, a reduction in *H. capsulatum* growth rate was observed, with 45 mm^3 disks (32.8 $\mu g\ mL^{-1}$ released in 24 h) completely inhibiting growth. In contrast, the control disk, as expected, displayed a normal growth pattern with initial log phase (1-3 days) followed by lag phase (3-7 days), which is consistent with healthy *H. capsulatum* growth. Interestingly, the MIC for the fungus (32.8 $\mu g\ mL^{-1}$) was significantly less than the MIC for the bacteria (910 $\mu g\ mL^{-1}$) indicating that the fungus is more sensitive to the PANDA disks than the pathogenic bacteria tested.

5.4.4.2 Fungicidal activity of PANDAs

To examine the fungicidal activity of the PANDA disks, we utilized an Aqua live/dead cell stain and flow cytometry. In brief, an exponential-growing culture of *H. capsulatum* was

split in half where one half of the culture received a control disk and the other half received a 50 mm^3 PANDA disk. At 24 h and 48 h after PANDA addition, aliquots were taken and subjected to staining, fixation (37% formaldehyde), confocal microscopy, and flow cytometry to assess viability. Once complete gating was performed on the sample data, the viability was determined as a percent of the survived cells. The Aqua fluorescent dye reacts with amines yielding fluorescence, but is unable to penetrate living cells leading to weakly fluorescent cells. However, compromised cellular membranes allow the dye to permeate the cell, reacting with both cell-wall bound amines and intracellular amines, leading to intense fluorescence. As shown in Figure 5.5C, at 48 h post addition the control disk cells showed very little, if any fluorescence, indicating that the cell walls are functional and intact. In contrast, treatment with the PANDA disks resulted in intense fluorescence from all cells, indicating membrane destabilization and cell death (Fig. 5.5D). The difference in fluorescence intensity is sufficient to quantify living from non-living cells using flow cytometry (Fig. 5.5E). As shown in Figure 4.5F, roughly 25% of the *H. capsulatum* population were viable within 24 h for the PANDA treatment, whereas virtually no change in viability was observed for the control disk. After 48 h only 15% of PANDA treated *H. capsulatum* cells remained viable whereas there was again no significant change in viability in the control disk. We can conclude from this assay that the release of pA from PANDAs results in potent membrane disruption and that the PANDA disk is not only bactericidal but also fungicidal.

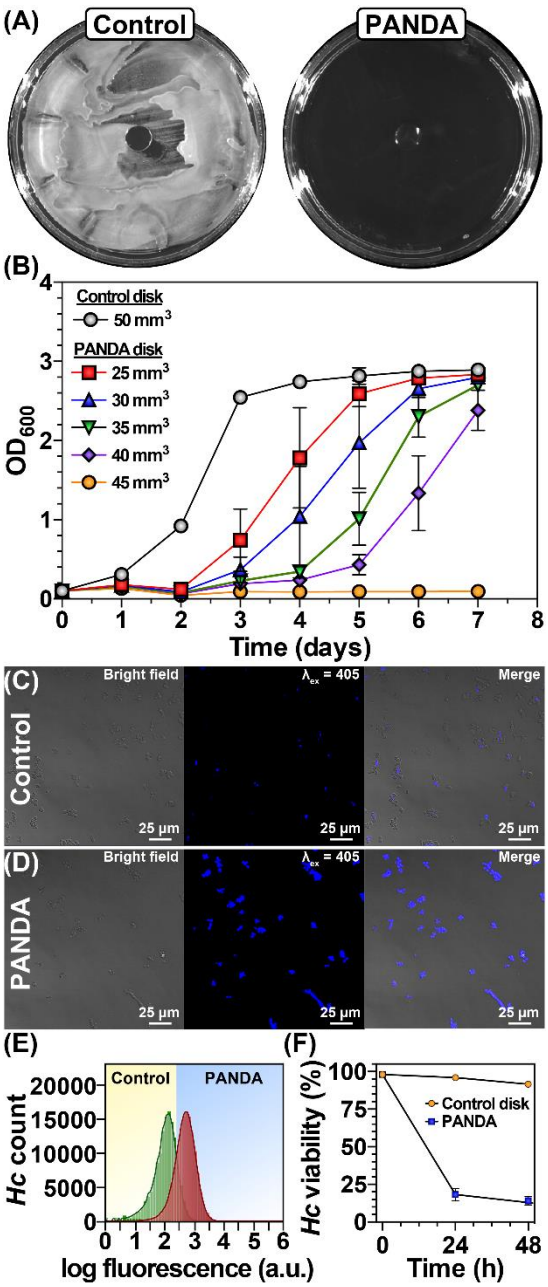

Figure 5.5 Antifungal activity of PANDAs. (A) ZOI of PANDA and control disks. (B) Minimum inhibition assay of different sized PANDA disks. Confocal microscopy images of H. capsulatum challenged with control (C) and PANDA disks (D) after 48 h. (E) Flow cytometry data of control and PANDA disks after 48 h incubation F) Time-dependent killing of pathogens by PANDA. Data are representative of 3 independent experiments ± s.d.

5.4.5 Cytotoxicity analysis

Successful antimicrobial agents should possess both potency against pathogens as well as low cytotoxicity to host cells. Clinically speaking, pathogens like *H. capsulatum* are difficult to treat because they sequester themselves inside alveolar macrophages, one of the most valuable immune cell needed to eradicate them. To evaluate PANDA cytotoxicity, two cell lines, including RAW 264.7 murine macrophages and VERO epithelial cells (isolated from kidney), were analyzed by directly exposing cells to multiple sizes of PANDA disks [0.5 mm^3 (18.2 µg mL^{-1}), 1.0 mm^3 (36.4 µg mL^{-1}), and 1.5 mm^3 (54.6 µg mL^{-1})], 1.5 mm^3 control disks, and a native control (blank). Cell viabilities were determined using a MTT assay over a 24 h period. MTT is a colorimetric dye that assesses cellular metabolic activity. In brief, live viable cells can reduce MTT to an insoluble formazan by their native oxidase system, which is accompanied by a change in color to purple that can be observed via spectrophotometry. As shown in Figure 5.6A, both cell lines showed no significant decrease in viability (90-100 % viable compared to the native control) after exposure to PANDA disks of various sizes (0.5-1.5 mm^3), indicating minimal cytotoxicity towards host cells. We also qualitatively investigated cell morphologies to ensure no changes were observed after PANDA treatments. After 24 h, the cells treated with the PANDA disk exhibited indistinguishable morphologies and confluency compared to the control disk and native control. Macrophage cells displayed a dominant spherical morphology with minimal pseudopodia (Figure 5.6B) whereas epithelial cells displayed a spindle like morphology of closely aggregated cells (Figure 5.6C), both without any signs of cytoplasmic vacuolation or granularity around the nucleus. Of significance, the low cytotoxicity of PANDAs against macrophages at a concentration that is shown to eradicate *H. capsulatum* holds great promise for clinical applications moving forward.

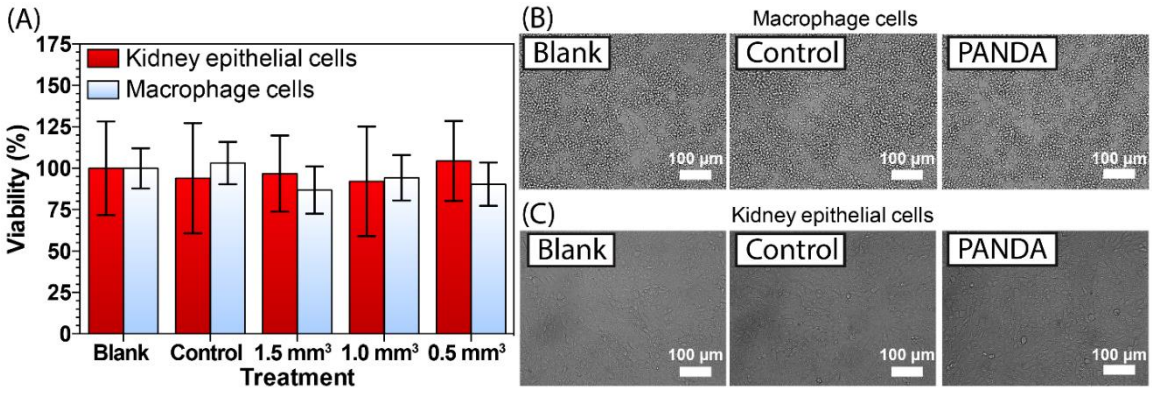

Figure 5.6 Cytocompatability of PANDAs. (A) MTT assay of PANDAs incubated with VERO kidney epithelial and RAW 264.7 macrophage cells. (B) Bright-field images of macrophage and epithelial cells (C), incubated with either nothing (blank), a 1.5 mm^3 control disk, or a 1.5 mm^3 PANDA disk.

5.5 Conclusion

In summary, we have demonstrated a potent bio-based PANDA that has the versatility to treat both prokaryotic and eukaryotic pathogens through the sustained release of pA over time. The sustained release of pA allows many generations of the microbes to be exposed, thus successfully clearing even slow growing pathogens such as *H. capsulatum*. Both inhibitory and biocidal activity was measured against bacteria and fungi and found that the fungi were significantly more susceptible to the PANDA treatment. Through a combination of confocal microscopy and transmission electron microscopy, we showed PANDAs primary mode of action is via membrane disruption. Additionally, we demonstrated that PANDAs have minimal cytotoxicity towards both epithelial and macrophages which are both relevant in immunosuppressed patient response. The PANDA network design coupled with the potency of pA has the potential to be a streamline target to add to the arsenal of defenses against a broad spectrum of pathogens and bares potential for future *in vivo* experiments.

APPENDIX A – Supporting Information for Chapter III

Table A.1 General formulation of organic stock solutions for thiol-ene photopolymerization in miniemulsion.

Organic Components	Mass [g]	Moles [mmol]	wt. %
Diallyl phthalate	2.57	10.44	23.53
GDMP	2.00	8.39	18.32
PETMP	0.50	1.02	4.58
Carvacrol	2.90	19.31	26.56
p-methoxyphenol	0.05	0.40	0.46
Irgacure 184	0.10	0.49	0.92
Hexadecane	0.60	2.65	5.49
Thymol	2.20	14.65	20.15

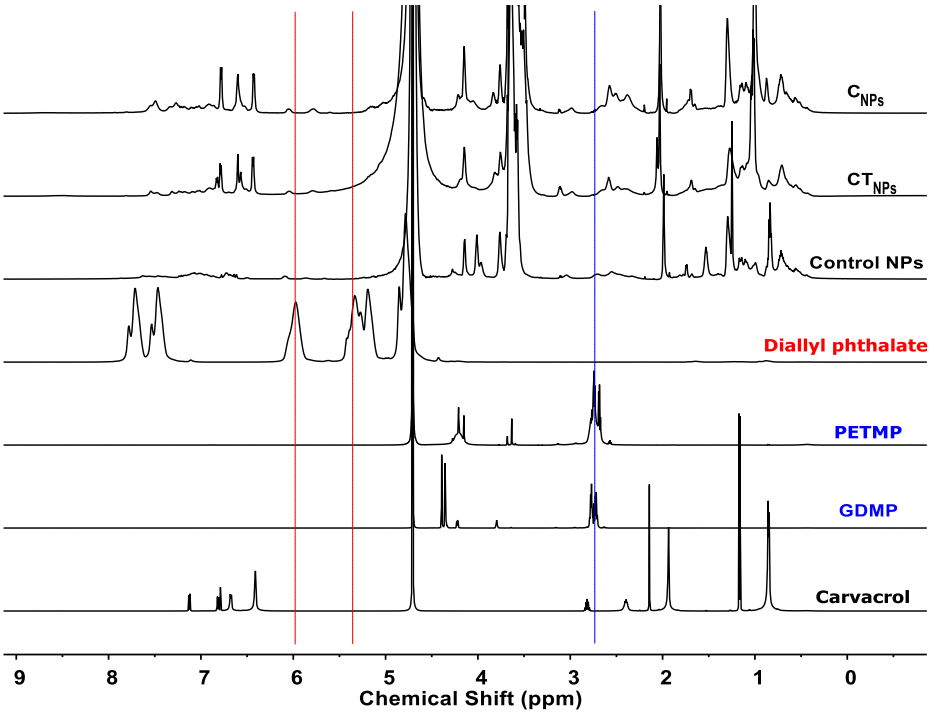

Figure A.1 ^{1}H NMR of starting materials and cured NPs.

^{1}H NMR of the starting materials: diallyl phthalate, PETMP, GDMP, carvacrol, and all three types of NPs after UV polymerization. ^{1}H spectrum confirmed the disappearance of both mercaptopriopionate (2.62-2.83 ppm) and alkene (5.07-5.45 ppm and 5.87-6.10 ppm) peaks after UV exposure.

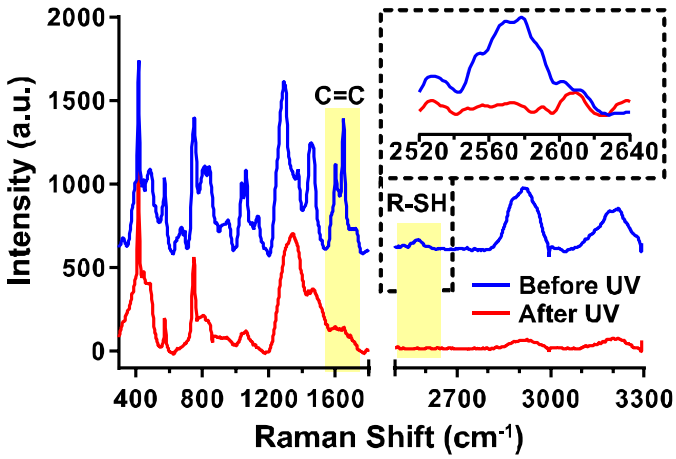

Figure A.2 Raman spectra of TC_{NPs} after ultrasonication (top, blue) and after exposure to UV light (λ_{365} nm).

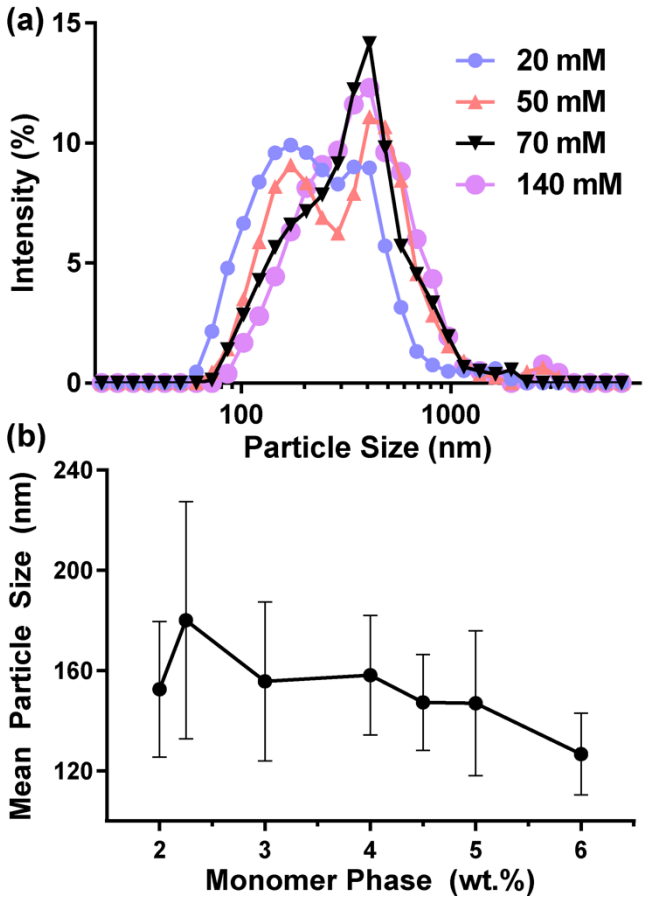

Figure A.3 A) Surfactant concentration sweep of Hitenol BC-20 and B) Effect of weight fraction of the organic monomer phase on particle size for TC_{NPs}.

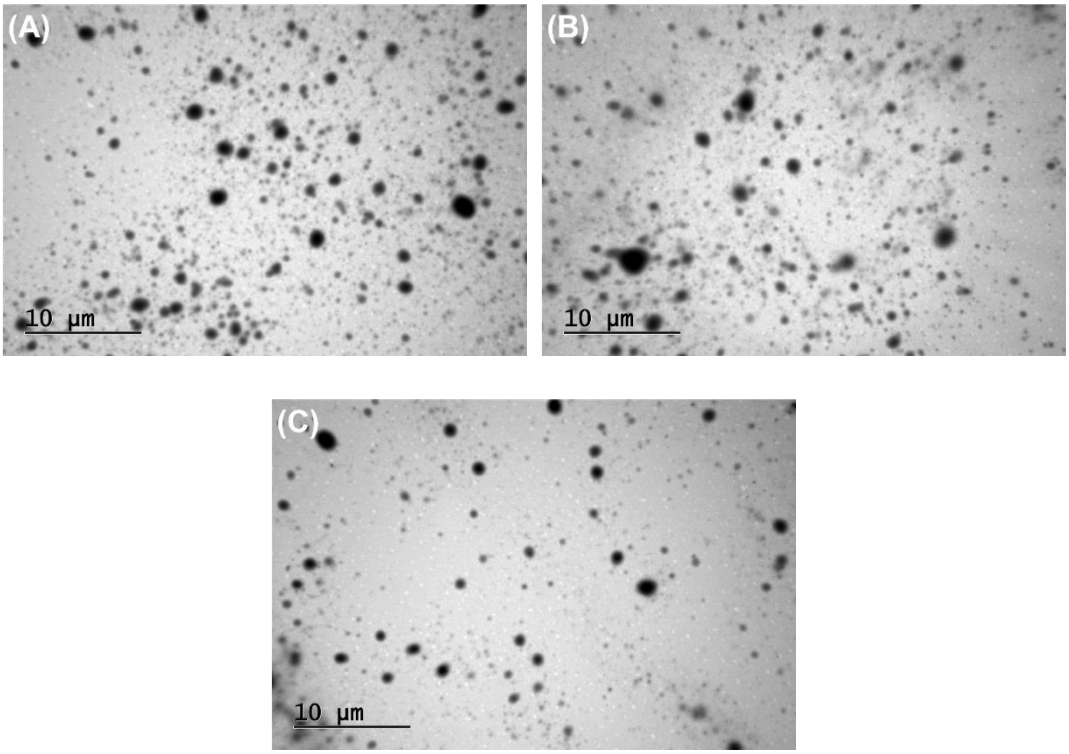

Figure A.4 Transmission electron microscopy of (A) c NPs, (B) C_{NPs}, and (C) TC_{NPs}.

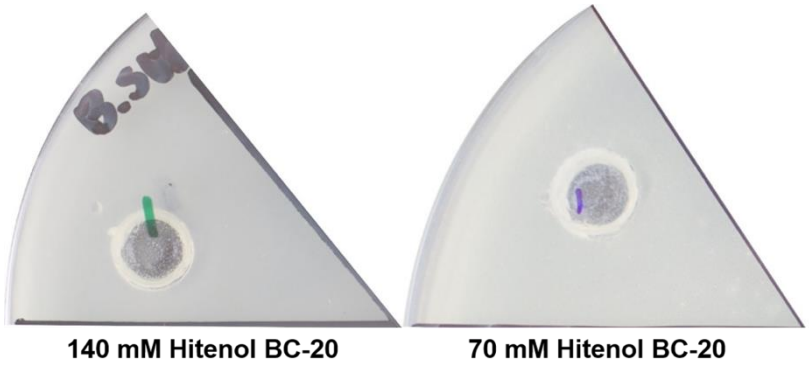

Figure A.5 Absence of antimicrobial activity of B. subtilis by Hitenol BC-20 at 140 and 70 mM.

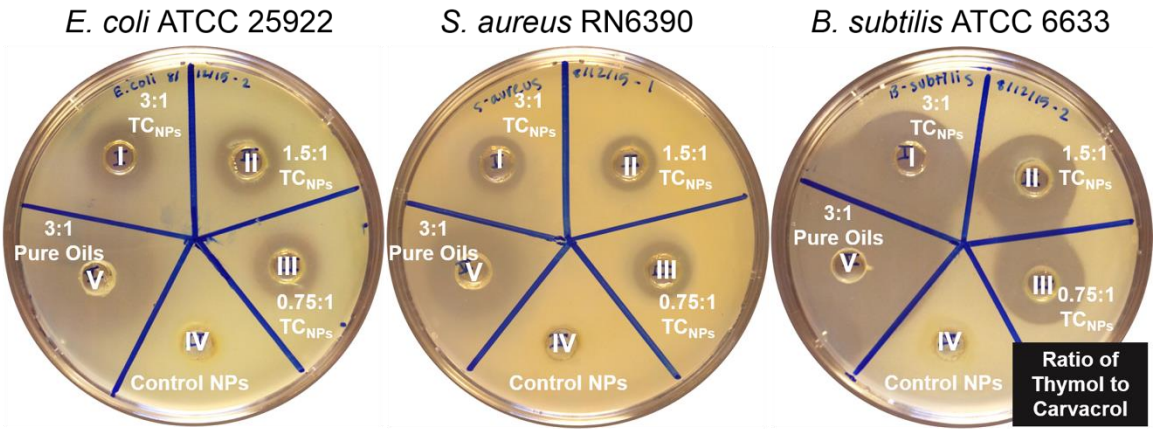

Figure A.6 Antimicrobial activity of nanoparticles loaded with different ratios of carvacrol and thymol (treatments I, II, and III). Controls included empty NPs (IV) and a 12:4 mixture of pure carvacrol and thymol (V).

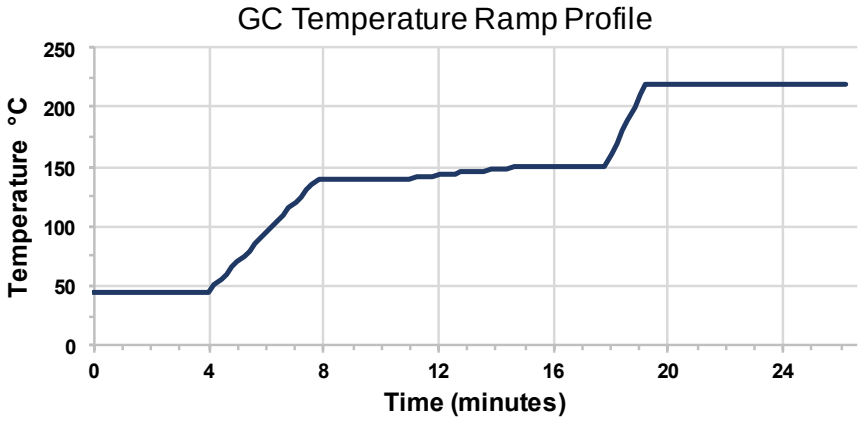

Figure A.7 Ramping conditions used for GC-MS separation of thymol and carvacrol isomers.

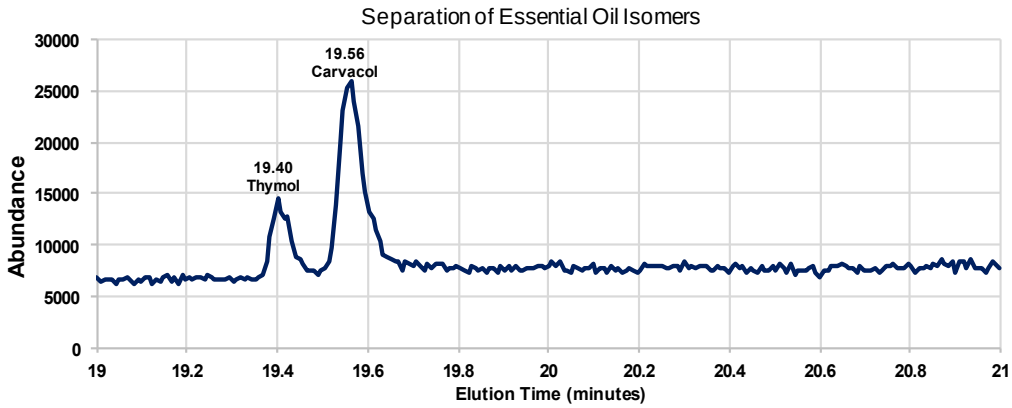

Figure A.8 Example separation of thymol and carvacol isomers eluting at 19.40 and 19.56 min respectively.

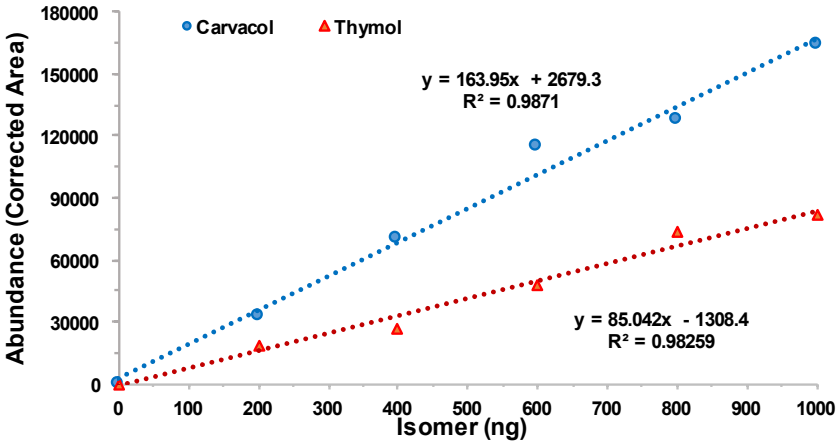

Figure A.9 Calibration curves for thymol and carvacrol isomers.

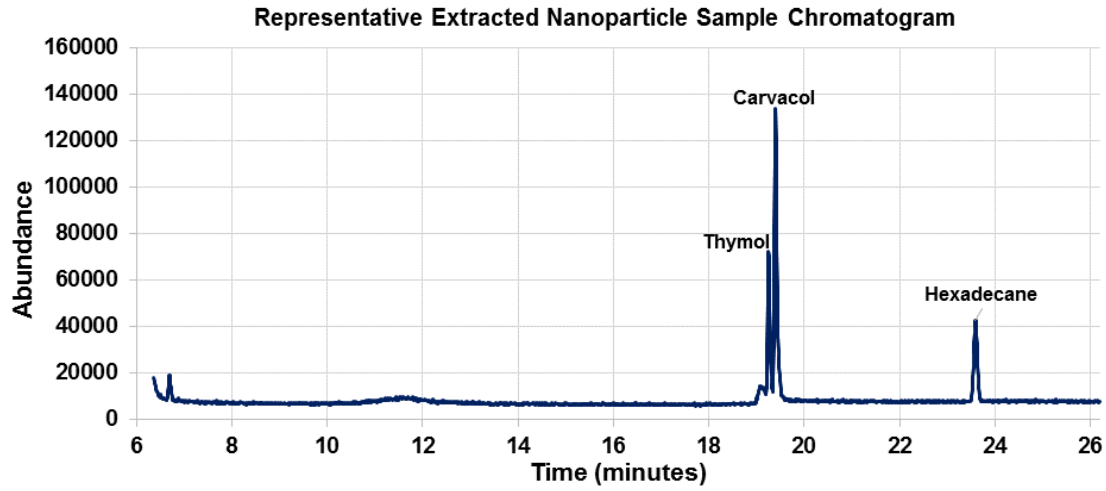

Table A.2 Nanoparticle size and concentration for different formulations.

Sample	Particle size (nm)	[NP] (particles mL^{-1})
Control NPs (Butyl acetate)	183 ± 19	1.4×10^{13}
C_{NPs} (Carvacrol)	148 ± 24	2.7×10^{13}
TC_{NPs} (Thymol and Carvacrol)	147 ± 19	2.7×10^{13}

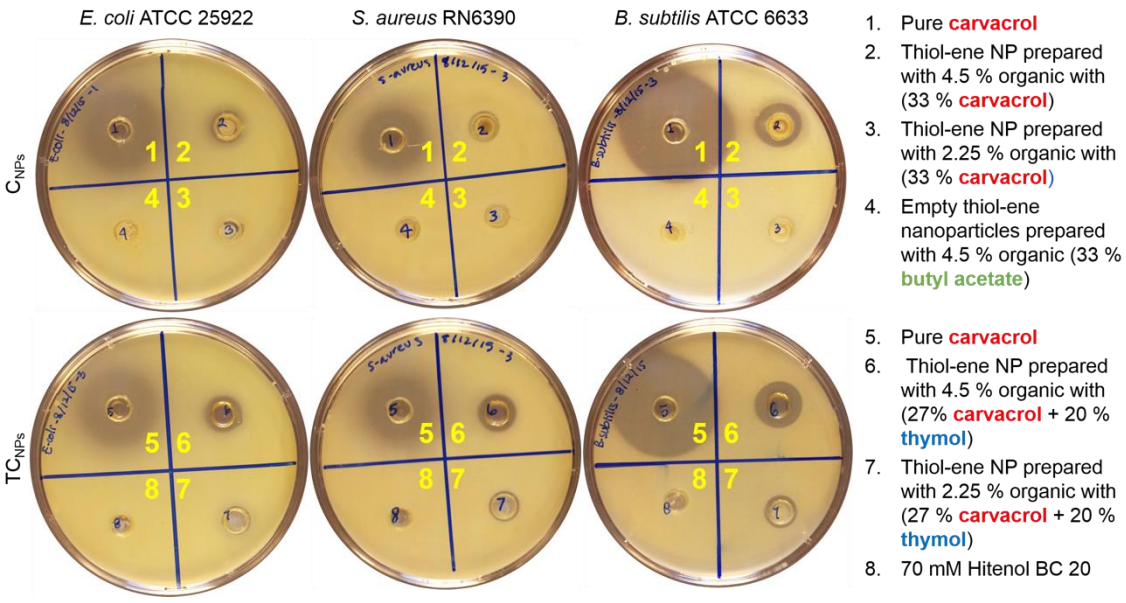

Figure A.10 Additional data with controls: inhibition of *B. subtilis* ATCC 6633, *E. coli* ATCC 25922, and *S. aureus* RN6390 with thiol-ene nanoparticles containing different ratios of essential oils (shown in Table S5).

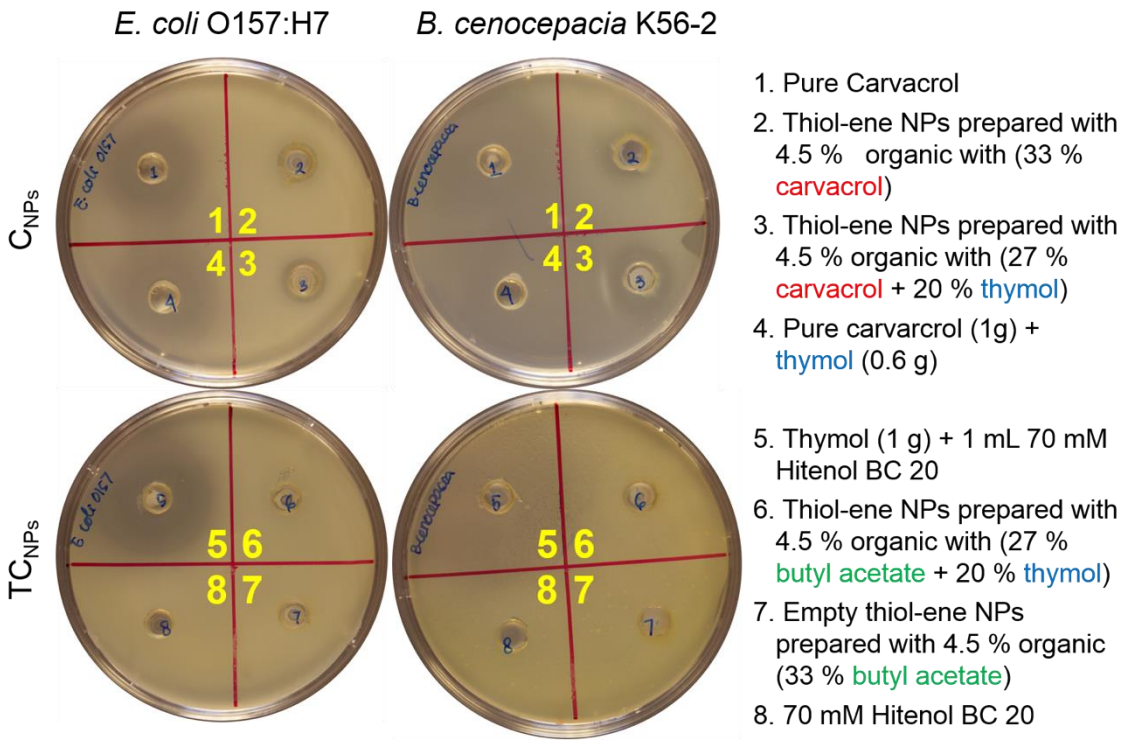

Figure A.11 Additional data with controls: Inhibition of *E. coli* O157:H7 and *B. cenocepacia* K56-2 with different types of NPs.

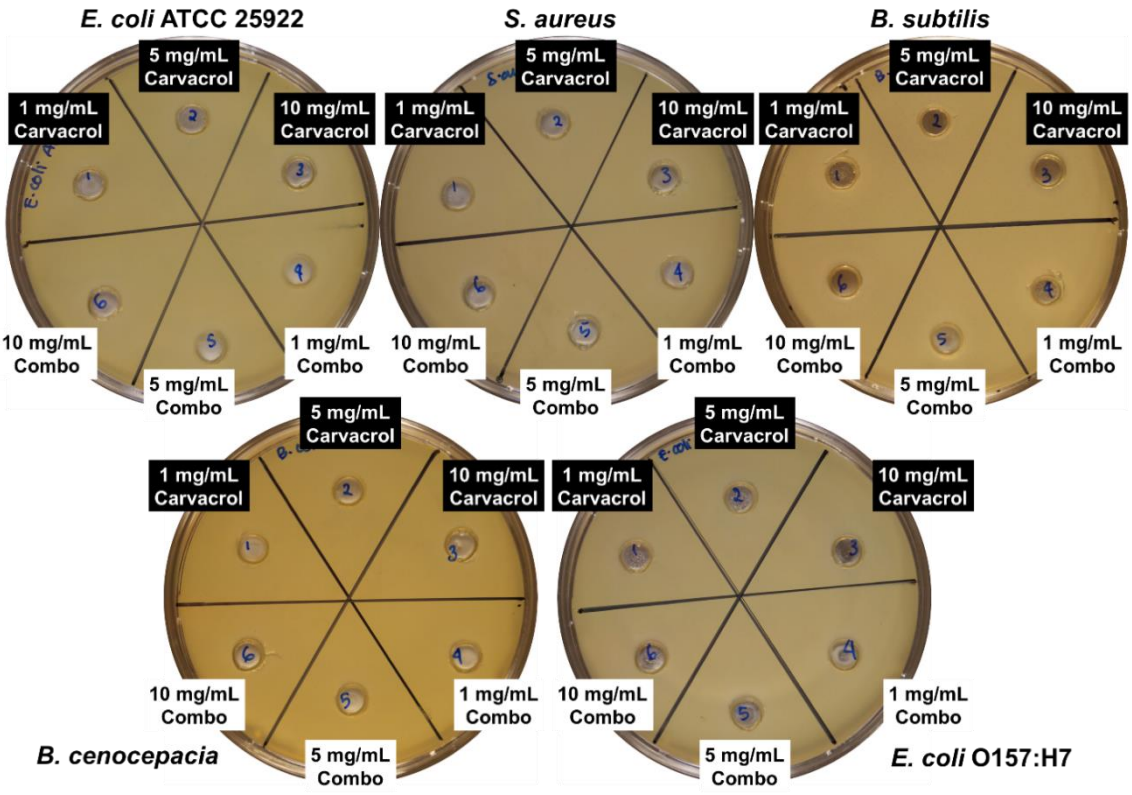

Figure A.12 Absence of antimicrobial activity for different concentrations of carvacrol and thymol/carvacrol in 70 mM Hitenol BC-20.

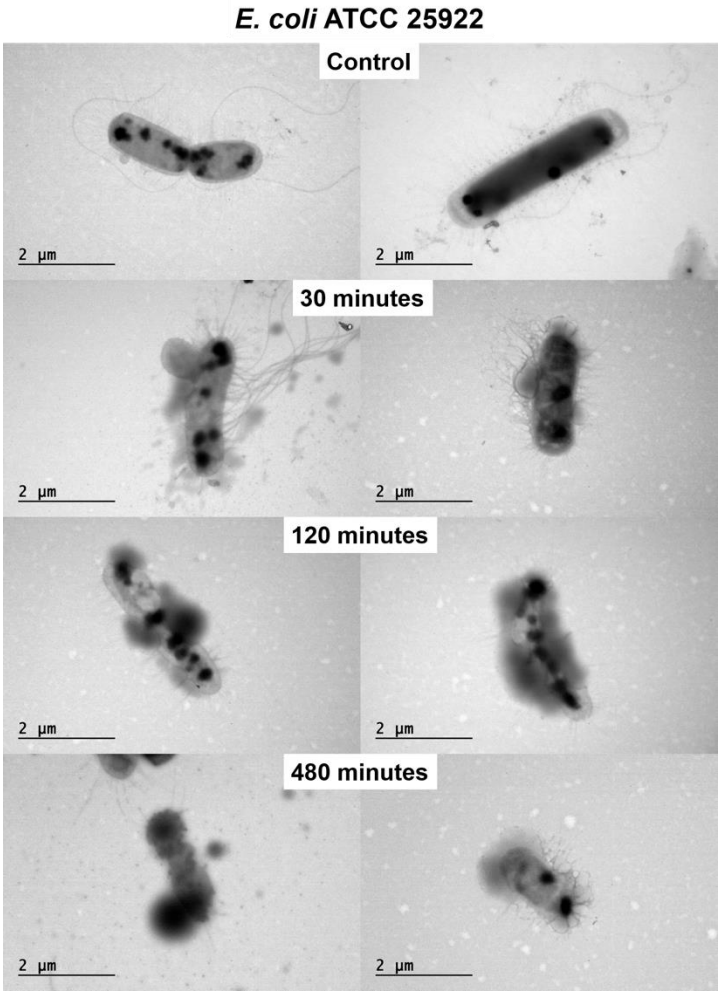

Figure A.13 Additional TEM images of *E. coli* ATCC 25922 with TC_{NPs} over time.

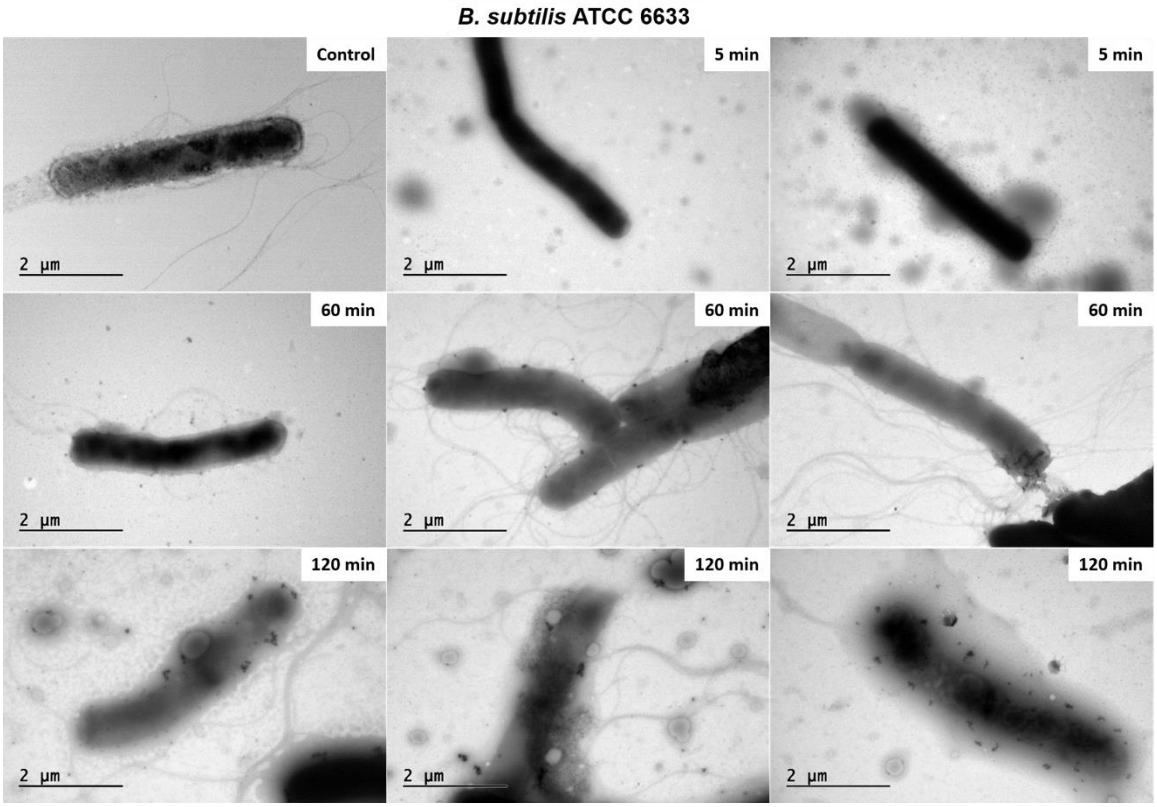

Figure A.14 Additional TEM images of *B. subtilis* ATCC 6633 with TC_{NPs} over time.

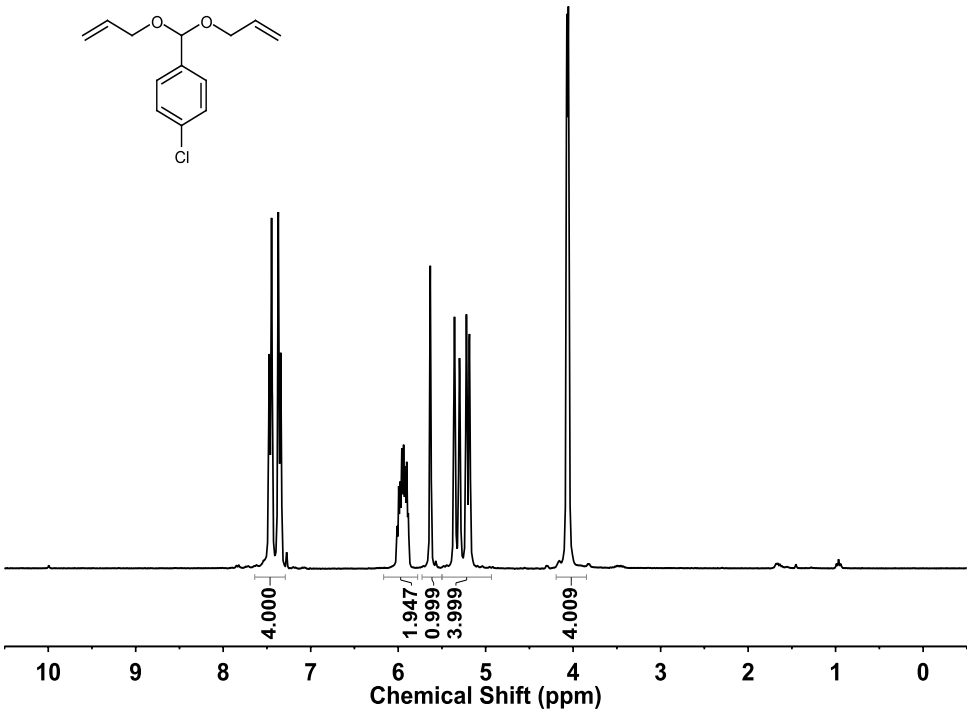

Figure B.1 ^{1}H NMR of diallyl p-chlorobenzaldehyde acetal.

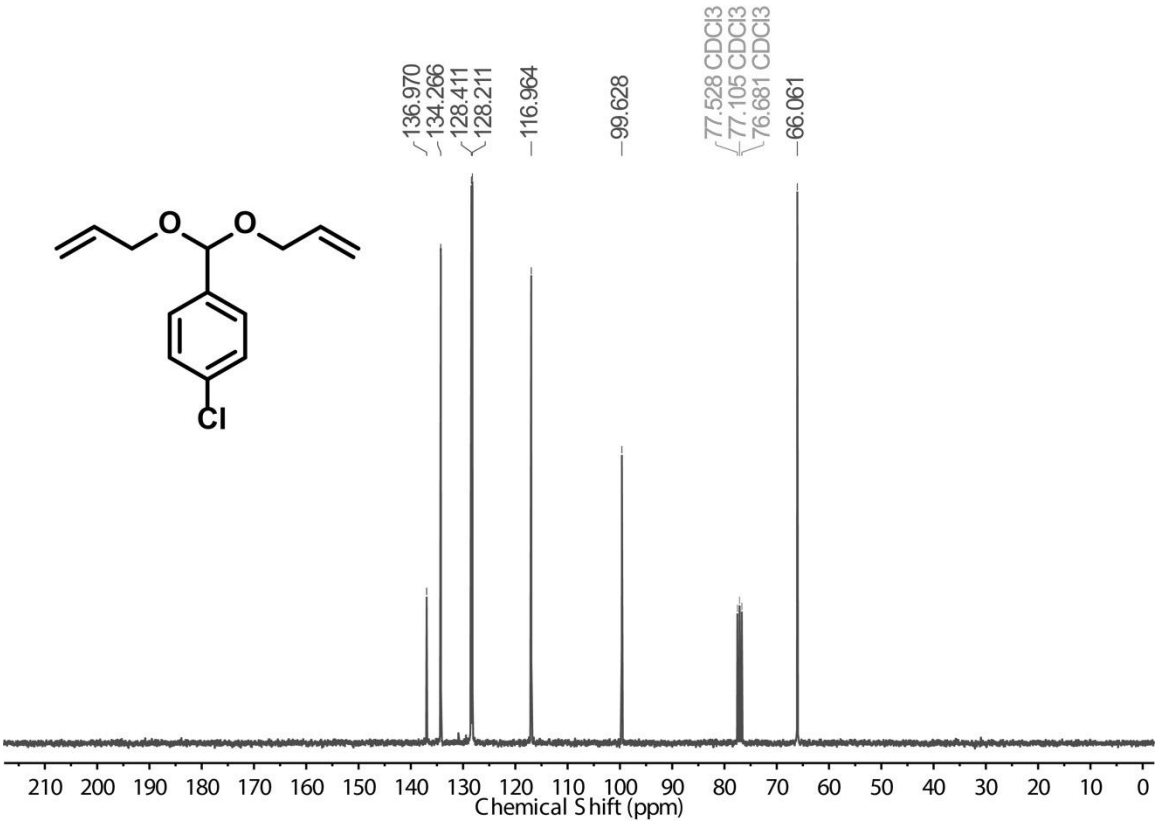

Figure B.2 ^{13}C NMR of diallyl p-chlorobenzaldehyde acetal.

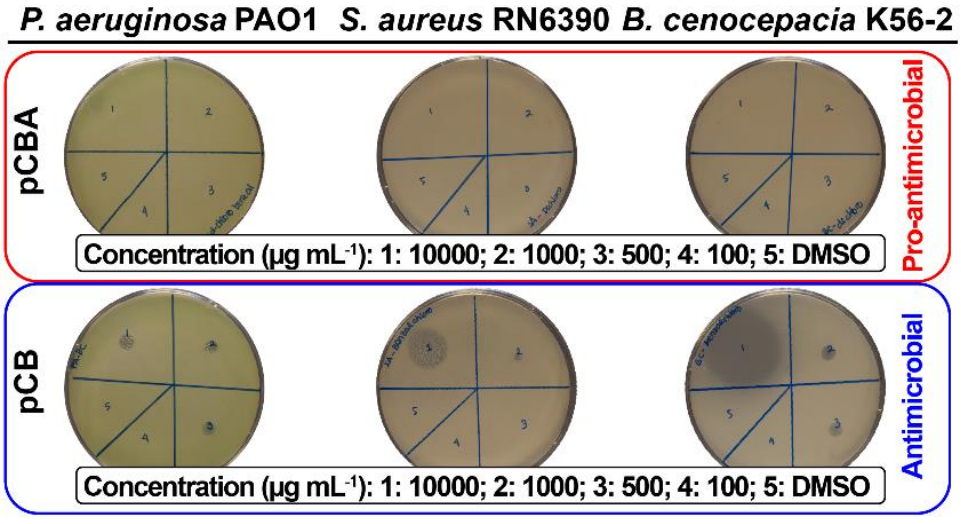

Figure B.3 Zones of inhibition for small molecule precursors within PANDA formulation.

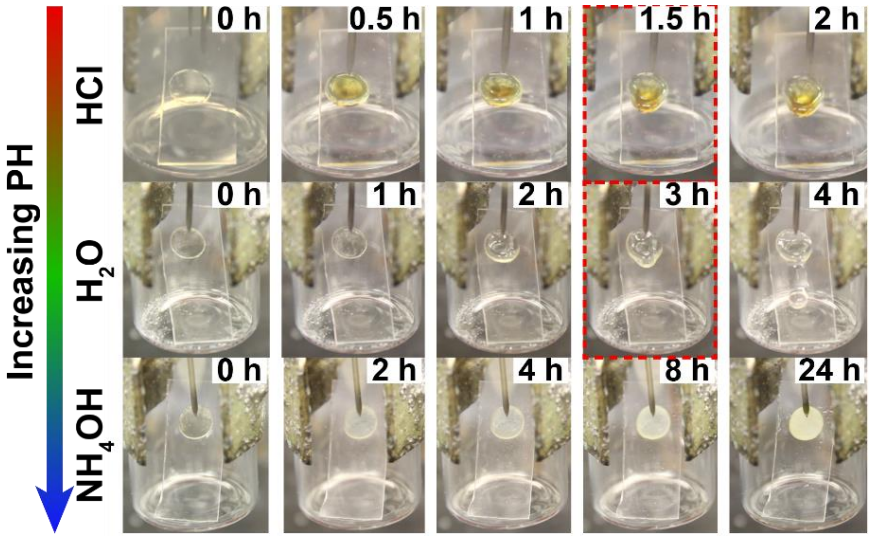

Figure B.4 PANDAs exposed to HCl vapor led to complete bulk degradation in minutes while ammonium hydroxide vapor led to retarded degradation with no flow observed within 24 h.

REFERENCES

1. O'Neil, J., Review on antimicrobial resistance. Antimicrobial resistance: tackling a crisis for the health and wealth of nations. *resistance RoA* **2014,** *1*.
2. Tenover, F. C., Mechanisms of antimicrobial resistance in bacteria. *The American journal of medicine* **2006,** *119* (6), S3-S10.
3. Yap, P. S. X.; Yiap, B. C.; Ping, H. C.; Lim, S. H. E., Essential Oils, A New Horizon in Combating Bacterial Antibiotic Resistance. *The Open Microbiology Journal* **2014,** *8*, 6-14.
4. Campbell, A. W., Autoimmunity and the Gut. *Autoimmune Diseases* **2014,** *2014*, 152428.
5. Friedman, M., Antibiotic-Resistant Bacteria: Prevalence in Food and Inactivation by Food-Compatible Compounds and Plant Extracts. *J. Agric. Food Chem.* **2015,** *63* (15), 3805-3822.
6. Hyldgaard, M.; Mygind, T.; Meyer, R. L., Essential oils in food preservation: mode of action, synergies, and interactions with food matrix components. *Front. Microbiol.* **2012,** *3*, 1-24.
7. Hyldgaard, M.; Mygind, T.; Meyer, R. L., Essential oils in food preservation: mode of action, synergies, and interactions with food matrix components. *Frontiers in microbiology* **2012,** *3*.
8. Si, W.; Gong, J.; Tsao, R.; Zhou, T.; Yu, H.; Poppe, C.; Johnson, R.; Du, Z., Antimicrobial activity of essential oils and structurally related synthetic food additives towards selected pathogenic and beneficial gut bacteria. *Journal of Applied Microbiology* **2006,** *100* (2), 296-305.
9. Sacchetti, G.; Maietti, S.; Muzzoli, M.; Scaglianti, M.; Manfredini, S.; Radice, M.; Bruni, R., Comparative evaluation of 11 essential oils of different origin as functional antioxidants, antiradicals and antimicrobials in foods. *Food chemistry* **2005,** *91* (4), 621-632.
10. Liu, C.; Liang, B.; Shi, G.; Li, Z.; Zheng, X.; Huang, Y.; Lin, L., Preparation and characteristics of nanocapsules containing essential oil for textile application. *Flavour and fragrance journal* **2015,** *30* (4), 295-301.
11. Batish, D. R.; Singh, H. P.; Kohli, R. K.; Kaur, S., Eucalyptus essential oil as a natural pesticide. *Forest Ecology and Management* **2008,** *256* (12), 2166-2174.
12. Duncan, B.; Li, X.; Landis, R. F.; Kim, S. T.; Gupta, A.; Wang, L.-S.; Ramanathan, R.; Tang, R.; Boerth, J. A.; Rotello, V. M., Nanoparticle-stabilized capsules for the treatment of bacterial biofilms. *ACS nano* **2015,** *9* (8), 7775-7782.
13. Kung, M.-L.; Lin, P.-Y.; Hsieh, C.-W.; Tai, M.-H.; Wu, D.-C.; Kuo, C.-H.; Hsieh, S.-L.; Chen, H.-T.; Hsieh, S., Bifunctional Peppermint Oil Nanoparticles for Antibacterial Activity and Fluorescence Imaging. *ACS Sustainable Chemistry & Engineering* **2014,** *2* (7), 1769-1775.
14. Kavanaugh, N. L.; Ribbeck, K., Selected Antimicrobial Essential Oils Eradicate Pseudomonas spp. and Staphylococcus aureus Biofilms. *Applied and Environmental Microbiology* **2012,** *78* (11), 4057-4061.
15. Burt, S., Essential oils: their antibacterial properties and potential applications in foods—a review. *International journal of food microbiology* **2004,** *94* (3), 223-253.

16. Nazzaro, F.; Fratianni, F.; De Martino, L.; Coppola, R.; De Feo, V., Effect of Essential Oils on Pathogenic Bacteria. *Pharmaceuticals* **2013,** *6* (12), 1451-1474.
17. Turek, C.; Stintzing, F. C., Stability of essential oils: a review. *Comprehensive Reviews in Food Science and Food Safety* **2013,** *12* (1), 40-53.
18. Ojagh, S. M.; Rezaei, M.; Razavi, S. H.; Hosseini, S. M. H., Development and evaluation of a novel biodegradable film made from chitosan and cinnamon essential oil with low affinity toward water. *Food Chemistry* **2010,** *122* (1), 161-166.
19. Bilia, A. R.; Guccione, C.; Isacchi, B.; Righeschi, C.; Firenzuoli, F.; Bergonzi, M. C., Essential oils loaded in nanosystems: a developing strategy for a successful therapeutic approach. *Evidence-Based Complementary and Alternative Medicine* **2014,** *2014*.
20. Asbahani, A. E.; Miladi, K.; Badri, W.; Sala, M.; Addi, E. H. A.; Casabianca, H.; Mousadik, A. E.; Hartmann, D.; Jilale, A.; Renaud, F. N. R.; Elaissari, A., Essential oils: From extraction to encapsulation. *Int. J. Pharm.* **2015,** *483* (1–2), 220-243.
21. Majeed, H.; Bian, Y.-Y.; Ali, B.; Jamil, A.; Majeed, U.; Khan, Q. F.; Iqbal, K. J.; Shoemaker, C. F.; Fang, Z., Essential oil encapsulations: uses, procedures, and trends. *RSC Adv.* **2015,** *5* (72), 58449-58463.
22. Liang, R.; Xu, S.; Shoemaker, C. F.; Li, Y.; Zhong, F.; Huang, Q., Physical and Antimicrobial Properties of Peppermint Oil Nanoemulsions. *Journal of Agricultural and Food Chemistry* **2012,** *60* (30), 7548-7555.
23. Gomes, C.; Moreira, R. G.; Castell-Perez, E., Poly (DL-lactide-co-glycolide) (PLGA) Nanoparticles with Entrapped trans-Cinnamaldehyde and Eugenol for Antimicrobial Delivery Applications. *Journal of Food Science* **2011,** *76* (2), N16-N24.
24. Stebbins, N. D.; Faig, J. J.; Yu, W.; Guliyev, R.; Uhrich, K. E., PolyActives: Controlled and Sustained Bioactive Release Via Hydrolytic Degradation. *Biomaterials science* **2015,** *3* (8), 1171-1187.
25. Kwon, J.; Kim, J.; Park, S.; Khang, G.; Kang, P. M.; Lee, D., Inflammation-Responsive Antioxidant Nanoparticles Based on a Polymeric Prodrug of Vanillin. *Biomacromolecules* **2013,** *14* (5), 1618-1626.
26. Ko, E.; Jeong, D.; Kim, J.; Park, S.; Khang, G.; Lee, D., Antioxidant polymeric prodrug microparticles as a therapeutic system for acute liver failure. *Biomaterials* **2014,** *35* (12), 3895-3902.
27. Carbone-Howell, A. L.; Stebbins, N. D.; Uhrich, K. E., Poly(anhydride-esters) Comprised Exclusively of Naturally Occurring Antimicrobials and EDTA: Antioxidant and Antibacterial Activities. *Biomacromolecules* **2014,** *15* (5), 1889-1895.
28. Bien-Aime, S.; Yu, W.; Uhrich, K. E., Pinosylvin-Based Polymers: Biodegradable Poly(Anhydride-Esters) for Extended Release of Antibacterial Pinosylvin. *Macromolecular Bioscience* **2016,** *16* (7), 978-983.
29. Herrmann, A., Controlled Release of Volatiles under Mild Reaction Conditions: From Nature to Everyday Products. *Angew. Chem. Int. Ed.* **2007,** *46* (31), 5836-5863.
30. Rautio, J.; Kumpulainen, H.; Heimbach, T.; Oliyai, R.; Oh, D.; Jarvinen, T.; Savolainen, J., Prodrugs: design and clinical applications. *Nat. Rev. Drug Disc.* **2008,** *7* (3), 255-270.
31. Lowe, A. B., Thiol-ene "click" reactions and recent applications in polymer and materials synthesis. *Polymer Chemistry* **2010,** *1* (1), 17-36.

32. Kade, M. J.; Burke, D. J.; Hawker, C. J., The power of thiol-ene chemistry. *J. Polym. Sci. A Polym. Chem.* **2010,** *48* (4), 743-750.
33. Hoyle, C. E.; Bowman, C. N., Thiol–Ene Click Chemistry. *Angewandte Chemie International Edition* **2010,** *49* (9), 1540-1573.
34. Lowe, A. B.; Hoyle, C. E.; Bowman, C. N., Thiol-yne click chemistry: A powerful and versatile methodology for materials synthesis. *Journal of Materials Chemistry* **2010,** *20* (23), 4745-4750.
35. Hoogenboom, R., Thiol–yne chemistry: A powerful tool for creating highly functional materials. *Angew. Chem., Int. Ed.* **2010,** *49* (20), 3415-3417.
36. Cramer, N. B.; Reddy, S. K.; Cole, M.; Hoyle, C.; Bowman, C. N., Initiation and kinetics of thiol–ene photopolymerizations without photoinitiators. *J. Polym. Sci. A Polym. Chem.* **2004,** *42* (22), 5817-5826.
37. Senyurt, A. F.; Wei, H.; Hoyle, C. E.; Piland, S. G.; Gould, T. E., Ternary Thiol− Ene/Acrylate photopolymers: effect of acrylate structure on mechanical properties. *Macromolecules* **2007,** *40* (14), 4901-4909.
38. Hoyle, C. E.; Lee, T. Y.; Roper, T., Thiol–enes: Chemistry of the past with promise for the future. *J. Polym. Sci. A Polym. Chem.* **2004,** *42* (21), 5301-5338.
39. Chiou, B.-S.; English, R. J.; Khan, S. A., Rheology and Photo-Cross-Linking of Thiol− Ene Polymers. *Macromolecules* **1996,** *29* (16), 5368-5374.
40. Chiou, B.-S.; Khan, S. A., Real-time FTIR and in situ rheological studies on the UV curing kinetics of thiol-ene polymers. *Macromolecules* **1997,** *30* (23), 7322-7328.
41. Cramer, N. B.; Bowman, C. N., Kinetics of thiol–ene and thiol–acrylate photopolymerizations with real-time fourier transform infrared. *J. Polym. Sci. A Polym. Chem.* **2001,** *39* (19), 3311-3319.
42. Cramer, N. B.; Davies, T.; O'Brien, A. K.; Bowman, C. N., Mechanism and Modeling of a Thiol− Ene Photopolymerization. *Macromolecules* **2003,** *36* (12), 4631-4636.
43. Okay, O.; Bowman, C. N., Kinetic Modeling of Thiol-Ene Reactions with Both Step and Chain Growth Aspects. *Macromolecular theory and simulations* **2005,** *14* (4), 267-277.
44. Reddy, S. K.; Cramer, N. B.; Bowman, C. N., Thiol− Vinyl Mechanisms. 1. Termination and Propagation Kinetics in Thiol− Ene Photopolymerizations. *Macromolecules* **2006,** *39* (10), 3673-3680.
45. Niu, G.; Song, L.; Zhang, H.; Cui, X.; Kashima, M.; Yang, Z.; Cao, H.; Wang, G.; Zheng, Y.; Zhu, S.; Yang, H., Application of thiol-ene photopolymerization for injectable intraocular lenses: A preliminary study. *Polymer Engineering & Science* **2010,** *50* (1), 174-182.
46. McCall, J. D.; Anseth, K. S., Thiol–ene photopolymerizations provide a facile method to encapsulate proteins and maintain their bioactivity. *Biomacromolecules* **2012,** *13* (8), 2410-2417.
47. Nair, D. P.; Podgórski, M.; Chatani, S.; Gong, T.; Xi, W.; Fenoli, C. R.; Bowman, C. N., The thiol-Michael addition click reaction: a powerful and widely used tool in materials chemistry. *Chem. Mater.* **2013,** *26* (1), 724-744.
48. Azagarsamy, M. A.; Anseth, K. S., Bioorthogonal click chemistry: an indispensable tool to create multifaceted cell culture scaffolds. ACS Publications: 2012.

49. Liu, Z.; Lin, Q.; Sun, Y.; Liu, T.; Bao, C.; Li, F.; Zhu, L., Spatiotemporally Controllable and Cytocompatible Approach Builds 3D Cell Culture Matrix by Photo-Uncaged-Thiol Michael Addition Reaction. *Advanced Materials* **2014,** *26* (23), 3912-3917.
50. Lin-Gibson, S.; Jones, R. L.; Washburn, N. R.; Horkay, F., Structure− Property Relationships of Photopolymerizable Poly (ethylene glycol) Dimethacrylate Hydrogels. *Macromolecules* **2005,** *38* (7), 2897-2902.
51. Kloxin, A. M.; Kloxin, C. J.; Bowman, C. N.; Anseth, K. S., Mechanical properties of cellularly responsive hydrogels and their experimental determination. *Advanced materials* **2010,** *22* (31), 3484-3494.
52. Andorko, J. I.; Hess, K. L.; Pineault, K. G.; Jewell, C. M., Intrinsic immunogenicity of rapidly-degradable polymers evolves during degradation. *Acta biomaterialia* **2016,** *32*, 24-34.
53. Tesar, B.; Jiang, D.; Liang, J.; Palmer, S.; Noble, P.; Goldstein, D., The role of hyaluronan degradation products as innate alloimmune agonists. *American Journal of Transplantation* **2006,** *6* (11), 2622-2635.
54. Termeer, C. C.; Hennies, J.; Voith, U.; Ahrens, T.; Weiss, J. M.; Prehm, P.; Simon, J. C., Oligosaccharides of hyaluronan are potent activators of dendritic cells. *The Journal of Immunology* **2000,** *165* (4), 1863-1870.
55. Termeer, C.; Benedix, F.; Sleeman, J.; Fieber, C.; Voith, U.; Ahrens, T.; Miyake, K.; Freudenberg, M.; Galanos, C.; Simon, J. C., Oligosaccharides of Hyaluronan activate dendritic cells via toll-like receptor 4. *Journal of Experimental Medicine* **2002,** *195* (1), 99-111.
56. Scheibner, K. A.; Lutz, M. A.; Boodoo, S.; Fenton, M. J.; Powell, J. D.; Horton, M. R., Hyaluronan fragments act as an endogenous danger signal by engaging TLR2. *The Journal of Immunology* **2006,** *177* (2), 1272-1281.
57. Carioscia, J. A.; Lu, H.; Stanbury, J. W.; Bowman, C. N., Thiol-ene oligomers as dental restorative materials. *Dental Materials* **2005,** *21* (12), 1137-1143.
58. Kim, S.; Linker, O.; Garth, K.; Carter, K. R., Degradation kinetics of acid-sensitive hydrogels. *Polymer Degradation and Stability* **2015,** *121*, 303-310.
59. Chen, N.; Dempere, L. A.; Tong, Z., Synthesis of pH-Responsive Lignin-Based Nanocapsules for Controlled Release of Hydrophobic Molecules. *ACS Sustainable Chemistry & Engineering* **2016,** *4* (10), 5204-5211.
60. Amato, D. N.; Amato, D. V.; Mavrodi, O. V.; Braasch, D. A.; Walley, S. E.; Douglas, J. R.; Mavrodi, D. V.; Patton, D. L., Destruction of Opportunistic Pathogens via Polymer Nanoparticle-Mediated Release of Plant-Based Antimicrobial Payloads. *Advanced Healthcare Materials* **2016,** *5* (9), 1094-1103.
61. de Meneses, A. C.; dos Santos, P. C. M.; Machado, T. O.; Sayer, C.; de Oliveira, D.; de Araújo, P. H. H., Poly (thioether-ester) nanoparticles entrapping clove oil for antioxidant activity improvement. *Journal of Polymer Research* **2017,** *24* (11), 202.
62. Machado, T. O.; Cardoso, P. B.; Feuser, P. E.; Sayer, C.; Araújo, P. H., Thiol-ene miniemulsion polymerization of a biobased monomer for biomedical applications. *Colloids and Surfaces B: Biointerfaces* **2017,** *159*, 509-517.
63. Durham, O. Z.; Poetz, K. L.; Shipp, D. A., Polyanhydride Nanoparticles: Thiol–Ene 'Click'Polymerizations Provide Functionalized and Cross-Linkable Nanoparticles

with Tuneable Degradation Times. *Australian Journal of Chemistry* **2017,** *70* (6), 735-742.
64. Poetz, K. L.; Mohammed, H. S.; Shipp, D. A., Surface Eroding, Semicrystalline Polyanhydrides via Thiol–Ene "Click" Photopolymerization. *Biomacromolecules* **2015,** *16* (5), 1650-1659.
65. Wang, J.; Wang, X.; Yan, G.; Fu, S.; Tang, R., pH-sensitive nanogels with ortho ester linkages prepared via thiol-ene click chemistry for efficient intracellular drug release. *Journal of colloid and interface science* **2017,** *508*, 282-290.
66. Chen, C.-K.; Wang, Q.; Jones, C. H.; Yu, Y.; Zhang, H.; Law, W.-C.; Lai, C. K.; Zeng, Q.; Prasad, P. N.; Pfeifer, B. A., Synthesis of pH-responsive chitosan nanocapsules for the controlled delivery of doxorubicin. *Langmuir* **2014,** *30* (14), 4111-4119.
67. Wang, Y.; Luo, Q.; Zhu, W.; Li, X.; Shen, Z., Reduction/pH dual-responsive nano-prodrug micelles for controlled drug delivery. *Polymer Chemistry* **2016,** *7* (15), 2665-2673.
68. Amato, D. N.; Amato, D. V.; Mavrodi, O. V.; Martin, W. B.; Swilley, S. N.; Parsons, K. H.; Mavrodi, D. V.; Patton, D. L., Pro-Antimicrobial Networks via Degradable Acetals (PANDAs) Using Thiol–Ene Photopolymerization. *ACS Macro Letters* **2017,** *6* (2), 171-175.
69. Amato, D. V.; Amato, D. N.; Blancett, L.; Mavrodi, O. V.; Martin, W. B.; Swilley, S. N.; Sandoz, M. J.; Shearer, G.; Mavrodi, D. V.; Patton, D. L., A bio-based pro-antimicrobial polymer network via degradable acetal linkages. *Acta biomaterialia* **2017**.
70. Jasinski, F.; Rannée, A. s.; Schweitzer, J.; Fischer, D.; Lobry, E.; Croutxé-Barghorn, C. l.; Schmutz, M.; Le Nouen, D.; Criqui, A.; Chemtob, A., Thiol–Ene Linear Step-Growth Photopolymerization in Miniemulsion: Fast Rates, Redox-Responsive Particles, and Semicrystalline Films. *Macromolecules* **2016,** *49* (4), 1143-1153.
71. Cardoso, P. B.; Machado, T. O.; Feuser, P. E.; Sayer, C.; Meier, M. A.; Araújo, P. H., Biocompatible Polymeric Nanoparticles From Castor Oil Derivatives via Thiol-Ene Miniemulsion Polymerization. *European Journal of Lipid Science and Technology*.
72. Poetz, K. L.; Durham, O. Z.; Shipp, D. A., Polyanhydride nanoparticles by 'click'thiol–ene polymerization. *Polymer Chemistry* **2015,** *6* (30), 5464-5469.
73. Türünç, O.; Meier, M. A., Thiol-ene vs. ADMET: a complementary approach to fatty acid-based biodegradable polymers. *Green Chemistry* **2011,** *13* (2), 314-320.
74. Vandenbergh, J.; Ramakers, G.; van Lokeren, L.; van Assche, G.; Junkers, T., Synthesis of degradable multi-segmented polymers via Michael-addition thiol–ene step-growth polymerization. *Rsc Advances* **2015,** *5* (100), 81920-81932.
75. Cardoso, P. B.; Machado, T. O.; Feuser, P. E.; Sayer, C.; Meier, M. A. R.; Araújo, P. H. H., Biocompatible Polymeric Nanoparticles From Castor Oil Derivatives via Thiol-Ene Miniemulsion Polymerization. *European Journal of Lipid Science and Technology* **2018,** *120* (1), 1700212-n/a.
76. Kharkar, P. M.; Rehmann, M. S.; Skeens, K. M.; Maverakis, E.; Kloxin, A. M., Thiol–ene click hydrogels for therapeutic delivery. *ACS biomaterials science & engineering* **2016,** *2* (2), 165-179.

77. Li, Q.; Zhou, H.; Hoyle, C. E., The effect of thiol and ene structures on thiol–ene networks: Photopolymerization, physical, mechanical and optical properties. *Polymer* **2009,** *50* (10), 2237-2245.
78. Liao, Z.; Xue, D.; Li, H.; Shi, L., Fragrance-Containing Microcapsules Based on Interfacial Thiol-Ene Polymerization. *Journal of Applied Polymer Science* **2016,** *133* (36).
79. Rutherglen, B. G.; McBath, R. A.; Huang, Y. L.; Shipp, D. A., Polyanhydride networks from thiol− ene polymerizations. *Macromolecules* **2010,** *43* (24), 10297-10303.
80. Anseth, K. S.; Shastri, V. R.; Langer, R., Photopolymerizable degradable polyanhydrides with osteocompatibility. *Nature biotechnology* **1999,** *17* (2), 156-159.
81. Kim, B. S.; Hrkach, J. S.; Langer, R., Synthesis and characterization of novel degradable photocrosslinked poly (ether-anhydride) networks. *J. Polym. Sci. A Polym. Chem.* **2000,** *38* (8), 1277-1282.
82. Kwisnek, L.; Goetz, J.; Meyers, K. P.; Heinz, S. R.; Wiggins, J. S.; Nazarenko, S., PEG Containing Thiol–Ene Network Membranes for CO2 Separation: Effect of Cross-Linking on Thermal, Mechanical, and Gas Transport Properties. *Macromolecules* **2014,** *47* (10), 3243-3253.
83. de Oliveira, F. C.; Olvera, D.; Sawkins, M. J.; Cryan, S.-A.; Kimmins, S. D.; da Silva, T. E.; Kelly, D. J.; Duffy, G. P.; Kearney, C.; Heise, A., Direct UV-Triggered Thiol–ene Cross-Linking of Electrospun Polyester Fibers from Unsaturated Poly (macrolactone) s and Their Drug Loading by Solvent Swelling. *Biomacromolecules* **2017,** *18* (12), 4292-4298.
84. Stebbins, N. D.; Faig, J. J.; Yu, W.; Guliyev, R.; Uhrich, K. E., Polyactives: controlled and sustained bioactive release via hydrolytic degradation. *Biomater. Sci.* **2015,** *3* (8), 1171-1187.
85. http://www.cdc.gov/drugresistance/threat-report-2013/.
86. Mahenthiralingam, E.; Baldwin, A.; Dowson, C. G., Burkholderia cepacia complex bacteria: opportunistic pathogens with important natural biology. *J. Appl. Microbiol.* **2008,** *104* (6), 1539-1551.
87. Holden, M.; Seth-Smith, H.; Crossman, L.; Sebaihia, M.; Bentley, S.; Cerdeño-Tárraga, A.; Thomson, N.; Bason, N.; Quail, M.; Sharp, S.; Cherevach, I.; Churcher, C.; Goodhead, I.; Hauser, H.; Holroyd, N.; Mungall, K.; Scott, P.; Walker, D.; White, B.; Rose, H.; Iversen, P.; Mil-Homens, D.; Rocha, E.; Fialho, A.; Baldwin, A.; Dowson, C.; Barrell, B.; Govan, J.; Vandamme, P.; Hart, C. A.; Mahenthiralingam, E.; Parkhill, J., The Genome of Burkholderia cenocepacia J2315, an Epidemic Pathogen of Cystic Fibrosis Patients. *J Bacteriol.* **2009,** *191* (1), 261-277.
88. Drevinek, P.; Mahenthiralingam, E., Burkholderia cenocepacia in cystic fibrosis: epidemiology and molecular mechanisms of virulence. *Clin. Microbiol. Infect.* **2010,** *16* (7), 821-830.
89. Bakkali, F.; Averbeck, S.; Averbeck, D.; Waomar, M., Biological effects of essential oils - A review. *Food Chem. Toxicol.* **2008,** *46* (2), 446-475.
90. Burt, S., Essential oils: their antibacterial properties and potential applications in foods - a review. *Int. J. Food Microbiol.* **2004,** *94* (3), 223-253.

91. Hyldgaard, M.; Mygind, T.; Meyer, R. L., Essential oils in food preservation: mode of action, synergies, and interactions with food matrix components. *Front. Microbiol.* **2012,** *3*.
92. Sacchetti, G.; Maietti, S.; Muzzoli, M.; Scaglianti, M.; Manfredini, S.; Radice, M.; Bruni, R., Comparative evaluation of 11 essential oils of different origin as functional antioxidants, antiradicals and antimicrobials in foods. *Food Chem.* **2005,** *91* (4), 621-632.
93. Liu, C.; Liang, B.; Shi, G.; Li, Z.; Zheng, X.; Huang, Y.; Lin, L., Preparation and characteristics of nanocapsules containing essential oil for textile application. *Flavour Frag. J.* **2015,** *30* (4), 295-301.
94. Batish, D. R.; Singh, H. P.; Kohli, S. K.; Kaur, S., Eucalyptus essential oil as a natural pesticide. *Forest Ecol. Manag.* **2008,** *256* (12), 2166-2174.
95. Kung, M.-L.; Lin, P.-Y.; Hsieh, C.-W.; Tai, M.-H.; Wu, D.-C.; Kuo, C.-H.; Hsieh, S.-L.; Chen, H.-T.; Hsieh, S., Bifunctional Peppermint Oil Nanoparticles for Antibacterial Activity and Fluorescence Imaging. *ACS Sustainable Chem. Eng.* **2014,** *2* (7), 1769-1775.
96. Helander, I. M.; Alakomi, H. L.; Latva-Kala, K.; Mattila-Sandholm, T.; Pol, I.; Smid, E. J.; Gorris, L. G. M.; von Wright, A., Characterization of the action of selected essential oil components on gram-negative bacteria. *J. Agric. Food Chem.* **1998,** *46* (9), 3590-3595.
97. Lambert, R. J. W.; Skandamis, P. N.; Coote, P. J.; Nychas, G. J. E., A study of the minimum inhibitory concentration and mode of action of oregano essential oil, thymol and carvacrol. *J. Appl. Microbiol.* **2001,** *91* (3), 453-462.
98. Maida, I.; Lo Nostro, A.; Pesavento, G.; Barnabei, M.; Calonico, C.; Perrin, E.; Chiellini, C.; Fondi, M.; Mengoni, A.; Maggini, V.; Vannacci, A.; Gallo, E.; Bilia, A. R.; Flamini, G.; Gori, L.; Firenzuoli, F.; Fani, R., Exploring the Anti-Burkholderia cepacia Complex Activity of Essential Oils: A Preliminary Analysis. *J. Evid. Based. Complementary. Altern. Med.* **2014,** *2014*, 10.
99. Sherry, M.; Charcosset, C.; Fessi, H.; Greige-Gerges, H., Essential oils encapsulated in liposomes: a review. *J. Liposome Res.* **2013,** *23* (4), 268-275.
100. McClements, D. J., *Nanoparticle- and microparticle-based delivery systems : encapsulation, protection and release of active compounds*. CRC Press: Boca Raton, 2015.
101. Lee, S.-M.; Nguyen, S. T., Smart Nanoscale Drug Delivery Platforms from Stimuli-Responsive Polymers and Liposomes. *Macromolecules* **2013,** *46* (23), 9169-9180.
102. Ikoba, U.; Peng, H.; Li, H.; Miller, C.; Yu, C.; Wang, Q., Nanocarriers in therapy of infectious and inflammatory diseases. *Nanoscale* **2015,** *7* (10), 4291-4305.
103. He, W.; Gu, X.; Liu, S., Surfactant-Free One-Step Synthesis of Dual-Functional Polyurea Microcapsules: Contact Infection Control and Drug Delivery. *Adv. Funct. Mater.* **2012,** *22* (19), 4023-4031.
104. Noimark, S.; Weiner, J.; Noor, N.; Allan, E.; Williams, C. K.; Shaffer, M. S. P.; Parkin, I. P., Dual-Mechanism Antimicrobial Polymer–ZnO Nanoparticle and Crystal Violet-Encapsulated Silicone. *Adv. Funct. Mater.* **2015,** *25* (9), 1367-1373.
105. Woranuch, S.; Yoksan, R., Eugenol-loaded chitosan nanoparticles: II. Application in bio-based plastics for active packaging. *Carbohyd. Polym.* **2013,** *96* (2), 586-592.

106. Iannitelli, A.; Grande, R.; Di Stefano, A.; Di Giulio, M.; Sozio, P.; Bessa, L. J.; Laserra, S.; Paolini, C.; Protasi, F.; Cellini, L., Potential Antibacterial Activity of Carvacrol-Loaded Poly(DL-lactide-co-glycolide) (PLGA) Nanoparticles against Microbial Biofilm. *Int. J. Nanomed.* **2011,** *12* (8), 5039-5051.
107. Wattanasatcha, A.; Rengpipat, S.; Wanichwecharungruang, S., Thymol nanospheres as an effective anti-bacterial agent. *Int. J. Pharm.* **2012,** *434* (1–2), 360-365.
108. da Rosa, C. G.; de Oliveira Brisola Maciel, M. V.; de Carvalho, S. M.; de Melo, A. P. Z.; Jummes, B.; da Silva, T.; Martelli, S. M.; Villetti, M. A.; Bertoldi, F. C.; Barreto, P. L. M., Characterization and evaluation of physicochemical and antimicrobial properties of zein nanoparticles loaded with phenolics monoterpenes. *Colloid Surface A* **2015,** *481*, 337-344.
109. Keawchaoon, L.; Yoksan, R., Preparation, characterization and in vitro release study of carvacrol-loaded chitosan nanoparticles. *Colloid. Surface B* **2011,** *84* (1), 163-171.
110. Asua, J. M., Miniemulsion polymerization. *Prog. Polym. Sci.* **2002,** *27* (7), 1283-1346.
111. Landfester, K., Miniemulsion Polymerization and the Structure of Polymer and Hybrid Nanoparticles. *Angew. Chem. Int. Ed.* **2009,** *48* (25), 4488-4507.
112. Landfester, K.; Musyanovych, A.; Mailänder, V., From polymeric particles to multifunctional nanocapsules for biomedical applications using the miniemulsion process. *J. Polym. Sci. Part A: Polym. Chem.* **2010,** *48* (3), 493-515.
113. Amato, D. V.; Amato, D. N.; Flynt, A. S.; Patton, D. L., Functional, sub-100 nm polymer nanoparticles via thiol-ene miniemulsion photopolymerization. *Polym. Chem.* **2015,** *6* (31), 5625-5632.
114. Durham, O. Z.; Krishnan, S.; Shipp, D. A., Polymer Microspheres Prepared by Water-Borne Thiol–Ene Suspension Photopolymerization. *ACS Macro Lett.* **2012,** *1* (9), 1134-1137.
115. Wang, C.; Chatani, S.; Podgorski, M.; Bowman, C. N., Thiol-Michael Addition Miniemulsion Polymerizations: Functional Nanoparticles and Reactive Latex Films. *Polym. Chem.* **2015,** *6*, 3758-3763.
116. Jasinski, F.; Lobry, E.; Tarablsi, B.; Chemtob, A.; Croutxé-Barghorn, C.; Le Nouen, D.; Criqui, A., Light-Mediated Thiol–Ene Polymerization in Miniemulsion: A Fast Route to Semicrystalline Polysulfide Nanoparticles. *ACS Macro Lett.* **2014,** *3* (9), 958-962.
117. Amato, D. N.; Amato, D. V.; Narayanan, J.; Donovan, B. R.; Douglas, J. R.; Walley, S. E.; Flynt, A. S.; Patton, D. L., Functional, composite polythioether nanoparticles via thiol-alkyne photopolymerization in miniemulsion. *Chem. Commun.* **2015,** *51* (54), 10910-10913.
118. Durham, O. Z.; Norton, H. R.; Shipp, D. A., Functional polymer particles via thiol-ene and thiol-yne suspension "click" polymerization. *Rsc Adv.* **2015,** *5* (82), 66757-66766.
119. Brown, J. C.; Pusey, P. N.; Dietz, R., Photon correlation study of polydisperse samples of polystyrene in cyclohexane. *J. Chem. Phys.* **1975,** *62* (3), 1136-1144.

120. Novick, R. P.; Ross, H. F.; Projan, S. J.; Kornblum, J.; Kreiswirth, B.; Moghazeh, S., Synthesis of staphylococcal virulence factors is controlled by a regulatory RNA molecule. *The EMBO Journal* **1993,** *12* (10), 3967-3975.
121. Mahenthiralingam, E.; Bischof, J.; Byrne, S. K.; Radomski, C.; Davies, J. E.; Av-Gay, Y.; Vandamme, P., DNA-based diagnostic approaches for identification of Burkholderia cepacia complex, Burkholderia vietnamiensis, Burkholderia multivorans, Burkholderia stabilis, and Burkholderia cepacia genomovars I and III. *J. Clin. Microbiol.* **2000,** *38* (9), 3165-3173.
122. Wiegand, I.; Hilpert, K.; Hancock, R. E. W., Agar and broth dilution methods to determine the minimal inhibitory concentration (MIC) of antimicrobial substances. *Nat. Protocols* **2008,** *3* (2), 163-175.
123. Landa, B. B.; Mavrodi, D. M.; Thomashow, L. S.; Weller, D. M., Interactions between strains of 2, 4-diacetylphloroglucinol-producing Pseudomonas fluorescens in the rhizosphere of wheat. *Phytopathology* **2003,** *93* (8), 982-994.
124. Sparks, B. J.; Hoff, E. F. T.; Hayes, L. P.; Patton, D. L., Mussel-Inspired Thiol-Ene Polymer Networks: Influencing Network Properties and Adhesion with Catechol Functionality. *Chem. Mater.* **2012,** *24* (18), 3633-3642.
125. Donovan, B. R.; Cobb, J. S.; Hoff, E. F. T.; Patton, D. L., Thiol-ene adhesives from clove oil derivatives. *RSC Adv.* **2014,** *4* (106), 61927-61935.
126. Flory, P. J., Molecular theory of rubber elasticity. *Polymer* **1979,** *20* (11), 1317-1320.
127. Chen, H.; Davidson, P. M.; Zhong, Q., Impacts of sample preparation methods on solubility and antilisterial characteristics of essential oil components in milk. *Appl. Environ. Microb.* **2014,** *80* (3), 907-916.
128. Cosentino, S.; Tuberoso, C. I. G.; Pisano, B.; Satta, M.; Mascia, V.; Arzedi, E.; Palmas, F., In-vitro antimicrobial activity and chemical composition of Sardinian Thymus essential oils. *Lett. Appl. Microbiol.* **1999,** *29* (2), 130-135.
129. Radovic-Moreno, A. F.; Lu, T. K.; Puscasu, V. A.; Yoon, C. J.; Langer, R.; Farokhzad, O. C., Surface Charge-Switching Polymeric Nanoparticles for Bacterial Cell Wall-Targeted Delivery of Antibiotics. *ACS Nano* **2012,** *6* (5), 4279-4287.
130. Rose, H.; Baldwin, A.; Dowson, C. G.; Mahenthiralingam, E., Biocide susceptibility of the Burkholderia cepacia complex. *J. Antimicrob. Chemo.* **2009**.
131. O'Neil, J., *Antimicrobial Resistance: Tackling a Crisis for the Health and Wealth of Nations*. 2016.
132. Burt, S., Essential oils: their antibacterial properties and potential applications in foods—a review. *Int. J. Food Microbiol.* **2004,** *94* (3), 223-253.
133. Nielsen, P. V.; Rios, R., Inhibition of fungal growth on bread by volatile components from spices and herbs, and the possible application in active packaging, with special emphasis on mustard essential oil. *Int. J. Food Microbiol.* **2000,** *60* (2–3), 219-229.
134. El Asbahani, A.; Miladi, K.; Badri, W.; Sala, M.; Addi, E.; Casabianca, H.; El Mousadik, A.; Hartmann, D.; Jilale, A.; Renaud, F.; Elaissari, A., Essential Oils: From Extraction to Encapsulation. *Int. J. Pharm.* **2015,** *483* (1–2), 220.

135. Sánchez-González, L.; Vargas, M.; González-Martínez, C.; Chiralt, A.; Cháfer, M., Use of Essential Oils in Bioactive Edible Coatings: A Review. *Food Eng. Rev.* **2011,** *3* (1), 1-16.
136. Majeed, H.; Bian, Y.-Y.; Ali, B.; Jamil, A.; Majeed, U.; Khan, Q.; Iqbal, K.; Shoemaker, C.; Fang, Z., Essential oil encapsulations: uses, procedures, and trends. *RSC Adv.* **2015,** *5* (72), 58449-58463.
137. Bien-Aime, S.; Yu, W.; Uhrich, K. E., Pinosylvin-Based Polymers: Biodegradable Poly(Anhydride-Esters) for Extended Release of Antibacterial Pinosylvin. *Macromol. Biosci.* **2016,** *16* (7), 978-983.
138. Ouimet, M. A.; Griffin, J.; Carbone-Howell, A. L.; Wu, W.-H.; Stebbins, N. D.; Di, R.; Uhrich, K. E., Biodegradable ferulic acid-containing poly (anhydride-ester): degradation products with controlled release and sustained antioxidant activity. *Biomacromolecules* **2013,** *14* (3), 854-861.
139. Guo, S.; Nakagawa, Y.; Barhoumi, A.; Wang, W.; Zhan, C.; Tong, R.; Santamaria, C.; Kohane, D. S., Extended Release of Native Drug Conjugated in Polyketal Microparticles. *J. Am. Chem. Soc.* **2016,** *138* (19), 6127-6130.
140. Lv, L.; Guo, Y.; Shen, Y.; Liu, J.; Zhang, W.; Zhou, D.; Guo, S., Intracellularly Degradable, Self-Assembled Amphiphilic Block Copolycurcumin Nanoparticles for Efficient In Vivo Cancer Chemotherapy. *Adv. Healthcare Mater.* **2015,** *4* (10), 1496-1501.
141. Kim, B.; Lee, E.; Kim, Y.; Park, S.; Khang, G.; Lee, D., Dual Acid-Responsive Micelle-Forming Anticancer Polymers as New Anticancer Therapeutics. *Adv. Funct. Mater.* **2013,** *23* (40), 5091-5097.
142. Burkoth, A.; Burdick, J.; Anseth, K., Surface and bulk modifications to photocrosslinked polyanhydrides to control degradation behavior. *J. Biomed. Mater. Res.* **2000,** *51* (3), 352-359.
143. Rydholm, A. E.; Reddy, S. K.; Anseth, K. S.; Bowman, C. N., Controlling Network Structure in Degradable Thiol−Acrylate Biomaterials to Tune Mass Loss Behavior. *Biomacromolecules* **2006,** *7* (10), 2827-2836.
144. Chandorkar, Y.; Bhagat, R. K.; Madras, G.; Basu, B., Cross-Linked, Biodegradable, Cytocompatible Salicylic Acid Based Polyesters for Localized, Sustained Delivery of Salicylic Acid: An In Vitro Study. *Biomacromolecules* **2014,** *15* (3), 863-875.
145. Dasgupta, Q.; Madras, G.; Chatterjee, K., Controlled Release of Usnic Acid from Biodegradable Polyesters to Inhibit Biofilm Formation. *ACS Biomater. Sci. Eng.* **2016**.
146. Dasgupta, Q.; Chatterjee, K.; Madras, G., Controlled Release of Salicylic Acid from Biodegradable Cross-Linked Polyesters. *Mol. Pharm.* **2015,** *12* (9), 3479-3489.
147. Dasgupta, Q.; Madras, G.; Chatterjee, K., Controlled release kinetics of p-aminosalicylic acid from biodegradable crosslinked polyesters for enhanced anti-mycobacterial activity. *Acta Biomater.* **2016,** *30*, 168-176.
148. Lu, L.; Peter, S. J.; D. Lyman, M.; Lai, H.-L.; Leite, S. M.; Tamada, J. A.; Uyama, S.; Vacanti, J. P.; Robert, L.; Mikos, A. G., In vitro and in vivo degradation of porous poly(dl-lactic-co-glycolic acid) foams. *Biomaterials* **2000,** *21* (18), 1837-1845.
149. Binauld, S.; Stenzel, M. H., Acid-degradable polymers for drug delivery: a decade of innovation. *Chem. Commun.* **2013,** *49* (21), 2082-2102.

150. Murthy, N.; Thng, Y. X.; Schuck, S.; Xu, M. C.; Fréchet, J. M. J., A Novel Strategy for Encapsulation and Release of Proteins: Hydrogels and Microgels with Acid-Labile Acetal Cross-Linkers. *J. Am. Chem. Soc.* **2002,** *124* (42), 12398-12399.
151. Kim, S.; Linker, O.; Garth, K.; Carter, K. R., Degradation kinetics of acid-sensitive hydrogels. *Polym. Degrad. Stab.* **2015,** *121*, 303-310.
152. Hoyle, C. E.; Bowman, C. N., Thiol–Ene Click Chemistry. *Angew. Chemie Int. Ed.* **2010,** *49* (9), 1540-1573.
153. Yarlagadda, V.; Samaddar, S.; Paramanandham, K.; Shome, B. R.; Haldar, J., Membrane Disruption and Enhanced Inhibition of Cell-Wall Biosynthesis: A Synergistic Approach to Tackle Vancomycin-Resistant Bacteria. *Angew. Chem. Int. Ed.* **2015,** *54* (46), 13644-13649.
154. Riss, T. L.; Moravec, R. A.; Niles, A. L.; Benink, H. A.; Worzella, T. J.; Minor, L., Cell viability assays. In *Assay Guidance Manual*, Sittampalam, G. S., Coussens N.P., Nelson H., Ed. Bethesda (MD): 2015.
155. Friedman, M.; Henika, P.; Mandrell, R., Antibacterial activities of phenolic benzaldehydes and benzoic acids against Campylobacter jejuni, Escherichia coli, Listeria monocytogenes, and Salmonella enterica. *J. Food Protect.* **2003,** *66* (10), 1811-1821.
156. Pelttari, E.; Karhumaki, E.; Langshaw, J.; Perakyla, H.; Elo, H., Antimicrobial Properties of Substituted Salicylaldehydes and Related Compounds. *Z. Naturforsch. C* **2007,** *62* (7–8), 487.
157. Shreaz, S.; Bhatia, R.; Khan, N.; Imran Ahmad, S.; Muralidhar, S.; Basir, S.; Manzoor, N.; Khan, L., Interesting anticandidal effects of anisic aldehydes on growth and proton-pumping-ATPase-targeted activity. *Microb. Pathogenesis* **2011,** *51* (4), 277-284.
158. Xie, R.; Tu, M.; Elder, T., Substituent Effect of Phenolic Aldehyde Inhibition on Alcoholic Fermentation by Saccharomyces cerevisiae. *Energy Fuels* **2016,** *30* (4), 3078-3084.
159. Fife, T. H.; Jao, L. K., Substituent Effects in Acetal Hydrolysis. *J. Org. Chem.* **1965,** *30* (5), 1492-1495.
160. Ulery, B.; Nair, L.; Laurencin, C., Biomedical Applications of Biodegradable Polymers. *J. Polym. Sci. B Polym. Phys.* **2011,** *49* (12), 832-864.
161. Heller, J., Poly (ortho esters). In *Biopolymers I*, Langer, R. S.; Peppas, N. A., Eds. Springer Berlin Heidelberg: Berlin, Heidelberg, 1993; pp 41-92.
162. Metters, A.; Hubbell, J., Network Formation and Degradation Behavior of Hydrogels Formed by Michael-Type Addition Reactions. *Biomacromolecules* **2005,** *6* (1), 290-301.
163. Rydholm, A. E.; Bowman, C. N.; Anseth, K. S., Degradable Thiol-Acrylate Photopolymers: Polymerization and Degradation Behavior of an in Situ Forming Biomaterial. *Biomaterials* **2005,** *26*, 4495.
164. Randall, G. C.; Doyle, P. S., Permeation-driven flow in poly(dimethylsiloxane) microfluidic devices. *Proc. Natl. Acad. Sci. U. S. A.* **2005,** *102* (31), 10813-10818.
165. Kantarcioğlu, A.; Celkan, T.; Yücel, A.; Mikami, Y.; Kurugoglu, S.; Mitani, H.; Altas, K., Fatal Trichoderma harzianum infection in a leukemic pediatric patient. *Medical Mycology* **2009,** *47* (2), 207-215.
166. Pfaller, M.; Diekema, D.; Gibbs, D.; Newell, V.; Ellis, D.; Tullio, V.; Rodloff, A.; Fu, W.; Ling, T., Results from the ARTEMIS DISK Global Antifungal Surveillance

Study, 1997 to 2007: a 10.5-Year Analysis of Susceptibilities of Candida Species to Fluconazole and Voriconazole as Determined by CLSI Standardized Disk Diffusion. *J. Clin. Microbiol.* **2010,** *48* (4), 1366-1377.
167. Masters, J. R. W., Human cancer cell lines: fact and fantasy. *Nat. Rev. Mol. Cell Biol.* **2000,** *1* (3), 233-236.
168. White, T. C.; Marr, K. A.; Bowden, R. A., Clinical, Cellular, and Molecular Factors That Contribute to Antifungal Drug Resistance. *Clinical Microbiology Reviews* **1998,** *11* (2), 382-402.
169. Armstrong-James, D.; Meintjes, G.; Brown, G. D., A neglected epidemic: fungal infections in HIV/AIDS. *Trends in Microbiology* **2014,** *22* (3), 120-127.
170. Ribeiro, M.; Monteiro, F. J.; Ferraz, M. P., Infection of orthopedic implants with emphasis on bacterial adhesion process and techniques used in studying bacterial-material interactions. *Biomatter* **2012,** *2* (4), 176-194.
171. Cianflone, N. F. C., Salmonellosis and the GI Tract: More than Just Peanut Butter. *Current gastroenterology reports* **2008,** *10* (4), 424-431.
172. Gutierrez, J. A.; Crowder, T.; Rinaldo-Matthis, A.; Ho, M.-C.; Almo, S. C.; Schramm, V. L., Transition state analogs of 5[prime]-methylthioadenosine nucleosidase disrupt quorum sensing. *Nat Chem Biol* **2009,** *5* (4), 251-257.
173. Stone, L. K.; Baym, M.; Lieberman, T. D.; Chait, R.; Clardy, J.; Kishony, R., Compounds that select against the tetracycline-resistance efflux pump. *Nat Chem Biol* **2016,** *12* (11), 902-904.
174. Baym, M.; Stone, L. K.; Kishony, R., Multidrug evolutionary strategies to reverse antibiotic resistance. *Science* **2016,** *351* (6268).
175. Wright, G. D., Antibiotic Adjuvants: Rescuing Antibiotics from Resistance. *Trends in Microbiology* **2016,** *24* (11), 862-871.
176. Yoshida, M.; Reyes, S. G.; Tsuda, S.; Horinouchi, T.; Furusawa, C.; Cronin, L., Time-programmable drug dosing allows the manipulation, suppression and reversal of antibiotic drug resistance in vitro. *Nature Communications* **2017,** *8*, 15589.
177. Yarlagadda, V.; Samaddar, S.; Paramanandham, K.; Shome, B. R.; Haldar, J., Membrane Disruption and Enhanced Inhibition of Cell-Wall Biosynthesis: A Synergistic Approach to Tackle Vancomycin-Resistant Bacteria. *Angewandte Chemie International Edition* **2015,** *54* (46), 13644-13649.
178. Yarlagadda, V.; Sarkar, P.; Samaddar, S.; Haldar, J., A Vancomycin Derivative with a Pyrophosphate-Binding Group: A Strategy to Combat Vancomycin-Resistant Bacteria. *Angewandte Chemie* **2016,** *128* (27), 7967-7971.
179. Wattamwar, P. P.; Mo, Y.; Wan, R.; Palli, R.; Zhang, Q.; Dziubla, T. D., Antioxidant activity of degradable polymer poly (trolox ester) to suppress oxidative stress injury in the cells. *Advanced Functional Materials* **2010,** *20* (1), 147-154.
180. Rosario-Meléndez, R.; Yu, W.; Uhrich, K. E., Biodegradable Polyesters Containing Ibuprofen and Naproxen As Pendant Groups. *Biomacromolecules* **2013,** *14* (10), 3542-3548.
181. Carbone-Howell, A. L.; Stebbins, N. D.; Uhrich, K. E., Poly (anhydride-esters) comprised exclusively of naturally occurring antimicrobials and EDTA: Antioxidant and antibacterial activities. *Biomacromolecules* **2014,** *15* (5), 1889-1895.

182. Rosenberg, L.; Carbone, A.; Römling, U.; Uhrich, K.; Chikindas, M., Salicylic acid-based poly (anhydride esters) for control of biofilm formation in Salmonella enterica serovar Typhimurium. *Letters in applied microbiology* **2008,** *46* (5), 593-599.
183. Ouimet, M. A.; Stebbins, N. D.; Uhrich, K. E., Biodegradable Coumaric Acid-Based Poly (anhydride-ester) Synthesis and Subsequent Controlled Release. *Macromolecular rapid communications* **2013,** *34* (15), 1231-1236.
184. Johnson, M. L.; Uhrich, K. E., Concurrent release of admixed antimicrobials and salicylic acid from salicylate-based poly (anhydride-esters). *Journal of Biomedical Materials Research Part A* **2009,** *91* (3), 671-678.
185. Carbone-Howell, A.; Ouimet, M.; Uhrich, K., Biodegradable, Bioactive-Based Poly (anhydride-esters) for Personal Care and Cosmetic Applications. In *Polymers for Personal Care and Cosmetics*, ACS Publications: 2013; pp 145-155.
186. Prudencio, A.; Faig, J. J.; Song, M.; Uhrich, K. E., Phenolic Acid-based Poly (anhydride-esters) as Antioxidant Biomaterials. *Macromolecular bioscience* **2016,** *16* (2), 214-222.
187. Stebbins, N. D.; Yu, W.; Uhrich, K. E., Linear, Mannitol-Based Poly (anhydride-esters) with High Ibuprofen Loading and Anti-Inflammatory Activity. *Biomacromolecules* **2015,** *16* (11), 3632-3639.
188. Prudencio, A.; Stebbins, N. D.; Johnson, M.; Song, M.; Langowski, B. A.; Uhrich, K. E., Polymeric prodrugs of ampicillin as antibacterial coatings. *Journal of Bioactive and Compatible Polymers* **2014,** *29* (3), 208-220.
189. Noel, A.; Borguet, Y. P.; Raymond, J. E.; Wooley, K. L., Poly(carbonate–amide)s Derived from Bio-Based Resources: Poly(ferulic acid-co-tyrosine). *Macromolecules* **2014,** *47* (9), 2974-2983.
190. Faig, J. J.; Moretti, A.; Joseph, L. B.; Zhang, Y.; Nova, M. J.; Smith, K.; Uhrich, K. E., Biodegradable Kojic Acid-Based Polymers: Controlled Delivery of Bioactives for Melanogenesis Inhibition. *Biomacromolecules* **2017,** *18* (2), 363-373.
191. Guo, S.; Nakagawa, Y.; Barhoumi, A.; Wang, W.; Zhan, C.; Tong, R.; Santamaria, C.; Kohane, D. S., Extended Release of Native Drug Conjugated in Polyketal Microparticles. *Journal of the American Chemical Society* **2016,** *138* (19), 6127-6130.
192. van Lith, R.; Gregory, E. K.; Yang, J.; Kibbe, M. R.; Ameer, G. A., Engineering biodegradable polyester elastomers with antioxidant properties to attenuate oxidative stress in tissues. *Biomaterials* **2014,** *35* (28), 8113-8122.
193. Dasgupta, Q.; Madras, G.; Chatterjee, K., Controlled release kinetics of p-aminosalicylic acid from biodegradable crosslinked polyesters for enhanced anti-mycobacterial activity. *Acta Biomaterialia* **2016,** *30*, 168-176.
194. Wattamwar, P. P.; Biswal, D.; Cochran, D. B.; Lyvers, A. C.; Eitel, R. E.; Anderson, K. W.; Hilt, J. Z.; Dziubla, T. D., Synthesis and characterization of poly(antioxidant β-amino esters) for controlled release of polyphenolic antioxidants. *Acta Biomaterialia* **2012,** *8* (7), 2529-2537.
195. Liu, B.; Thayumanavan, S., Substituent Effects on the pH Sensitivity of Acetals and Ketals and Their Correlation with Encapsulation Stability in Polymeric Nanogels. *Journal of the American Chemical Society* **2017,** *139* (6), 2306-2317.
196. Tsunoda, T.; Suzuki, M.; Noyori, R., A facile procedure for acetalization under aprotic conditions. *Tetrahedron letters* **1980,** *21* (14), 1357-1358.

197. Jett, B. D.; Hatter, K. L.; Huycke, M. M.; Gilmore, M. S., Simplified agar plate method for quantifying viable bacteria. *Biotechniques* **1997,** *23* (4), 648-650.
198. Worsham, P.; Goldman, W., Quantitative plating of Histoplasma capsulatum without addition of conditioned medium or siderophores. *Journal of Medical and Veterinary Mycology* **1988,** *26* (3), 137-143.
199. ISO, I., 10993–5: 2009 Biological Evaluation of Medical Devices–Part 5: Tests for in Vitro Cytotoxicity. *International Organization for Standardization, Geneva* **2009**.
200. Hopfenberg, H. B., Controlled Release from Erodible Slabs, Cylinders, and Spheres. In *Controlled Release Polymeric Formulations*, AMERICAN CHEMICAL SOCIETY: 1976; Vol. 33, pp 26-32.
201. Fife, T. H.; Jao, L. K., Substituent Effects in Acetal Hydrolysis. *The Journal of Organic Chemistry* **1965,** *30* (5), 1492-1495.
202. Garripelli, V. K.; Kim, J. K.; Namgung, R.; Kim, W. J.; Repka, M. A.; Jo, S., A novel thermosensitive polymer with pH-dependent degradation for drug delivery. *Acta Biomaterialia* **2010,** *6* (2), 477-485.
203. Mayaud, L.; Carricajo, A.; Zhiri, A.; Aubert, G., Comparison of bacteriostatic and bactericidal activity of 13 essential oils against strains with varying sensitivity to antibiotics. *Letters in Applied Microbiology* **2008,** *47* (3), 167-173.
204. Smith, P.; Stewart; Fyfe, Antimicrobial properties of plant essential oils and essences against five important food-borne pathogens. *Letters in Applied Microbiology* **1998,** *26* (2), 118-122.
205. Lobritz, M. A.; Belenky, P.; Porter, C. B. M.; Gutierrez, A.; Yang, J. H.; Schwarz, E. G.; Dwyer, D. J.; Khalil, A. S.; Collins, J. J., Antibiotic efficacy is linked to bacterial cellular respiration. *Proceedings of the National Academy of Sciences* **2015,** *112* (27), 8173-8180.
206. Berney, M.; Hammes, F.; Bosshard, F.; Weilenmann, H.-U.; Egli, T., Assessment and interpretation of bacterial viability by using the LIVE/DEAD BacLight Kit in combination with flow cytometry. *Applied and environmental microbiology* **2007,** *73* (10), 3283-3290.
207. Chen, X.; Zhang, X.; Meng, R.; Zhao, Z.; Liu, Z.; Zhao, X.; Shi, C.; Guo, N., Efficacy of a combination of nisin and p-Anisaldehyde against Listeria monocytogenes. *Food Control* **2016,** *66*, 100-106.
208. Shi, C.; Zhao, X.; Meng, R.; Liu, Z.; Zhang, G.; Guo, N., Synergistic antimicrobial effects of nisin and p-Anisaldehyde on Staphylococcus aureus in pasteurized milk. *LWT - Food Science and Technology* **2017,** *84* (Supplement C), 222-230.
209. Yu, L.; Guo, N.; Yang, Y.; Wu, X.; Meng, R.; Fan, J.; Ge, F.; Wang, X.; Liu, J.; Deng, X., Microarray analysis of p-anisaldehyde-induced transcriptome of Saccharomyces cerevisiae. *Journal of industrial microbiology & biotechnology* **2010,** *37* (3), 313-322.
210. Natsch, A.; Gfeller, H.; Haupt, T.; Brunner, G., Chemical Reactivity and Skin Sensitization Potential for Benzaldehydes: Can Schiff Base Formation Explain Everything? *Chemical Research in Toxicology* **2012,** *25* (10), 2203-2215.
211. Kauffman, C. A., Histoplasmosis: a Clinical and Laboratory Update. *Clinical Microbiology Reviews* **2007,** *20* (1), 115-132.